NASA CR-54710
GDC DBE 65-026

FACILITY FORM 602

N67 10759 (ACCESSION NUMBER)
(THRU)
115 (PAGES)
1 (CODE)
CR-54710 (NASA CR OR TMX OR AD NUMBER)
28 (CATEGORY)

EXPERIMENTAL AND EVALUATION STUDIES OF A COAXIAL PLASMA GUN ACCELERATOR

By
A. V. Larson, L. Liebing, and R. Dethlefsen
Space Science Laboratory

Prepared for
NATIONAL AERONAUTICS AND SPACE ADMINISTRATION

CONTRACT NAS 3-7111

GPO PRICE $ _____

CFSTI PRICE(S) $ _____

Hard copy (HC) 3.00

Microfiche (MF) .75

ff 653 July 65

GENERAL DYNAMICS
Convair Division

NOTICE

This report was prepared as an account of Government sponsored work. Neither the United States, nor the National Aeronautics and Space Administration (NASA), nor any person acting on behalf of NASA:

A.) Makes any warranty or representation, expressed or implied, with respect to the accuracy, completeness, or usefulness of the information contained in this report, or that the use of any information, apparatus, method, or process disclosed in this report may not infringe privately owned rights; or

B.) Assumes any liabilities with respect to the use of, or for damages resulting from the use of any information, apparatus, method or process disclosed in this report.

As used above, "person acting on behalf of NASA" includes any employee or contractor of NASA, or employee of such contractor, to the extent that such employee or contractor of NASA, or employee of such contractor prepares, disseminates, or provides access to, any information pursuant to his employment or contract with NASA, or his employment with such contractor.

Requests for copies of this report should be referred to

National Aeronautics and Space Administration
Office of Scientific and Technical Information
Attention: AFSS-A
Washington, D.C. 20546

NASA CR-54710
GDC-DBE-65-026

FINAL REPORT

EXPERIMENTAL AND EVALUATION STUDIES OF A COAXIAL PLASMA GUN ACCELERATOR

BY

A. V. Larson, L. Liebing, and R. Dethlefsen
Space Sceince Laboratory

prepared for

NATIONAL AERONAUTICS AND SPACE ADMINISTRATION

July 1966

CONTRACT NAS 3-7111

Project Manager
NASA Lewis Research Center
Cleveland, Ohio
Spacecraft Technology Division
Mr. Peter Ramins

GENERAL DYNAMICS
CONVAIR DIVISION
San Diego, California

TABLE OF CONTENTS

	PAGE
LIST OF TABLES AND FIGURES	iv
1.0 FOREWORD	1
2.0 INTRODUCTION	2
3.0 REVIEW OF PREVIOUS WORK	3
4.0 COAXIAL THRUSTORS	7
4.1 Introduction	7
4.2 Thrustor Experiments, Radial Propellant Injection	7
4.2.1 Nature of Discharge	8
4.2.2 Thrustor Performance	20
4.2.3 Faster Propellant Injection	25
4.3 Thrustor Experiments, Axial Propellant Injection	33
4.3.1 Apparatus and Performance	33
4.3.2 Comparison with Other Experiments	38
4.4 Summary and Conclusions	42
5.0 PULSED ARC THRUSTOR	44
5.1 Introduction	44
5.2 Experiments	45
5.3 Summary and Conclusions	61
6.0 PROPELLANT INJECTORS	62
6.1 Fast Gas Valves	62
6.2 Metallic Vapor Injectors	66
6.2.1 Choice of Metal	66
6.2.2 Injection Schemes	67
6.2.3 Experiments	72

TABLE OF CONTENTS (CONT'D)

		PAGE
7.0	POWER	84
	7.1 Introduction	84
	7.2 Power Sources	86
	7.3 Power Conditioning	87
8.0	DIAGNOSTICS	90
	8.1 Thrust Stand	90
	8.1.1 Description	90
	8.1.2 Typical Operation	93
	8.2 Mass Flow Apparatus	94
	8.3 A Fast-Acting Calorimeter	97
	8.4 Velocity Probe	98
9.0	APPENDIX	102
10.0	REFERENCES	105
11.0	ACKNOWLEDGEMENTS	107
12.0	DISTRIBUTION LIST	108

LIST OF TABLES AND FIGURES

TABLE NO.		PAGE
I:	DATA FROM THRUSTOR EXPERIMENTS, RADIAL PROPELLANT INJECTION, NITROGEN (CURVES 1-7) AND XENON (CURVES 8-12) PROPELLANTS, SECTION 4.2.2.	22
II:	DATA FROM THRUSTOR EXPERIMENTS, FASTER RADIAL PROPELLANT INJECTION AT THE INSULATORS, NITROGEN PROPELLANT, SECTION 4.2.3.	31
III:	DATA FROM THRUSTOR EXPERIMENTS, SECTION 4.2.3 DOWNSTREAM RADIAL PROPELLANT INJECTION, NITROGEN PROPELLANT	32
IV:	DATA FROM THRUSTOR EXPERIMENTS, AXIAL PROPELLANT INJECTION, XENON PROPELLANT, SECTION 4.3.	36
V:	EXPERIMENTAL RESULTS WITH VACUUM SPARK INJECTOR SECTION 6.2.3	82

FIG. NO.		
1:	VOLTAGE SWITCHED THRUSTOR.	9
2:	PHOTOGRAPH OF THRUSTOR AND CAPACITOR	10
3:	GAS DENSITY DISTRIBUTIONS AT DIFFERENT TIMES AFTER GAS VALVE TRIGGER.	11
4:	PROPELLANT LOAD VS TIME.	12
5:	OSCILLOGRAMS OF $B_\theta(z,t)$ AT MID-RADII, DISTANCE FROM INSULATOR, Z = 0, 2, 4, 6, 8 CM, CAPACITOR VOLTAGE 1.0 kV. .	14
6:	OSCILLOGRAMS OF $B_\theta(z,t)$ AT MID-RADII, CAPACITOR VOLTAGE 2.0 kV, PLENUM 60 P.S.I., FIRING DELAY 200 μSEC.	15
7:	PHOTOGRAPHS OF THE DISCHARGE CAPACITOR VOLTAGE 1.0 kV, PLENUM 12 P.S.I.	16
8:	OSCILLOGRAMS OF THE THRUSTOR VOLTAGE AND CURRENT, FIRING DELAY 200 μSEC	17
9:	CALORIMETRIC EFFICIENCY VS FIRING DELAY, C = 181 μF, GUN OF FIG. 1, NITROGEN PROPELLANT.	18
10:	FARADAY CUP OSCILLOGRAMS FLIGHT DISTANCE ~ 87 CM, GUN VOLTAGE 1.0 kV, PLENUM 12 P.S.I.	19
11:	BARREL CONFIGURATIONS.	21

LIST OF TABLES AND FIGURES (CONT'D)

FIG. NO.		PAGE
12:	THRUST EFFICIENCY VS I_{SP}	24
13:	ION FLUX PER UNIT AREA PER SHOT VS ANGLE FROM THRUSTOR AXIS	26
14:	FERROMAGNETIC CORE VALVE	27
15:	GAS OUTPUT OF THE FERROMAGNETIC CORE VALVE	28
16:	GAS DENSITY DISTRIBUTIONS	30
17:	OUTLINE OF THE ACCELERATOR WITH AXIAL INJECTION AND SPARKER TRIGGERS	34
18:	GAS DENSITY DISTRIBUTION	35
19:	FARADAY CUP SIGNALS FOR RUN 91, TABLE IV (FLIGHT DISTANCE 4m)	37
20:	ION FLUX PER UNIT AREA PER SHOT VS ANGLE FROM THRUSTOR AXIS	39
21:	OUTLINE OF THE G. E. ACCELERATOR	40
22:	COMPARISON OF PERFORMANCE (G. E. DATA FROM FIG. II-11 OF REF. 15) (CONVAIR DATA FROM TABLE IV)	41
23:	SCHEMATIC OF THE PULSED ARC THRUSTOR	46
24:	MASS FLOW RATE CALIBRATION, HELIUM PROPELLANT	47
25:	BIAS FIELD	49
26:	CURRENT AND VOLTAGE OSCILLOGRAMS FOR THE PULSED ARC THRUSTOR, HELIUM PROPELLANT, 55 P.S.I., BANK VOLTAGE 400 VOLTS	50
27:	ENERGY ANALYZER OSCILLOGRAMS HELIUM PROPELLANT	51
28:	VELOCITY PROBE OSCILLOGRAMS	53
29:	ION VELOCITY DISTRIBUTION DERIVED FROM VELOCITY PROBE DATA	54
30:	VELOCITY PROBE OSCILLOGRAM	55
31:	ION VELOCITY DISTRIBUTION	56
32:	DIAGRAM SHOWING THE POSITION OF THE PROBES AND THE MEASUREMENTS OF B_θ AND j_θ	58

LIST OF TABLES AND FIGURES (CONT'D)

FIG. NO.		PAGE
33:	OSCILLOGRAMS OF ARC CURRENT, CURRENT DENSITY, AND MAGNETIC FIELD.	59
34:	SOLENOID-COCKED, SPRING-ACTUATED VALVE	64
35:	METAL PROPELLANT INJECTOR.	70
36:	METAL PROPELLANT INJECTOR.	70
37:	LITHIUM WIRE EXTRUDER.	73
38:	DETAILS OF LITHIUM WIRE EXTRUDER	74
39:	MERCURY INJECTOR	76
40:	SPREADING OF THE EJECTED MERCURY JET (AS DETERMINED BY CRYOGENIC CONDENSATION).	77
41:	MOMENTUM TRANSFERRED FROM PLASMA JET TO BALLISTIC PENDULUM AS FUNCTION OF CAPACITOR CHARGING VOLTAGE	77
42:	OSCILLOGRAMS OF CURRENT DENSITY: UPPER BEAM AND CAPACITOR DISCHARGE CURRENT: LOWER BEAM	79
43:	COAXIAL SOURCE OF METAL PLASMA BURSTS.	81
44:	CONCEPTUAL PROPULSION SYSTEM	85
45:	CAPACITOR CHARGING SCHEMES	88
46:	SCHEMATIC OF THE THRUST STAND SYSTEM	91
47:	THRUST BALANCE CALIBRATION	95
48:	TYPICAL IMPULSE RECORDS.	96
49:	FAST ACTING CALORIMETER OSCILLOGRAMS (a) CALIBRATION (b) WITH THRUSTOR.	99

1.0 FOREWORD

This report is presented in partial fulfillment of contract NAS 3-7111. It contains a description of the work carried out during the fifth year of an experimental program to evaluate the pulsed coaxial plasma gun as a thrustor for space vehicles. The research of the preceeding four years is summarized in the final reports of the previous contracts.[1-4]

2.0 INTRODUCTION

A wide variety of plasma accelerators can be classified as coaxial. Three types have been investigated in our research and development program. All are pulsed, receiving power from capacitor banks, and in each, the current passes through the plasma via electrode structures. For mass economy, it is also necessary to pulse the propellant flow. The magnitude of the discharge current is such that the dominant accelerating force is the j x B force.

Our devices can be further classified, apart from geometrical details, by the method of the propellant injection, the duration of the discharge, and the behavior of the current distribution. In the first device, which we continue to call the coaxial gun, the current distribution moves along the coaxial electrodes and, acting like a piston, expells plasma. The discharge pulse is typically 1-10 μsec long, and is matched to the arrival of the current at the exit of the accelerator. This device has been studied extensively, for a variety of propellant distributions using radial injection. (See Sections 3 and 4).

In the second device, the discharge is typically 1 msec long, and the current distribution remains stationary. The propellant pulse and power pulse maintain a quasi-steady-state condition for most of the discharge, and it is found, that the properties of the discharge and the exhaust do likewise. This device, the Pulsed Arc Gun, is essentially a pulsed MPD arc. Basic studies and performance measurements on this device are reported in Section 5. Original measurements on the current density and the magnetic fields in such devices have been made. A unique tool for measuring the velocity distributions of the ions in the exhaust has been used.

The third accelerator type was originated in another laboratory. It, like the coaxial gun, has a short pulse. It features unique methods for propellant injection and for triggering the discharge. The nature of the discharge has not yet been probed. Our experience with such an acceleration is given in Section 4.3.

Initial work directed toward realistic spaceflight propellant injectors, as opposed to laboratory injectors, is given in Section 6. The use of pulsed, metal feed systems is considered, and exploratory experiments are described.

Section 7 contains a preliminary look at power conditioning. Section 8 describes the new diagnostic tools which were used this year.

3.0 REVIEW OF PREVIOUS WORK

At the beginning of this program the coaxial gun was chosen for development because it is simple in concept, it offers the possibility of extreme reliability, and it is a device in which the plasma is always tightly coupled to the magnetic field as distinct from inductive guns. The original design was based on the model of a current sheet accelerating a constant mass of gas.[1] A gun with a short barrel length and a correspondingly short electrical period was used in order to limit the time available for the growth of instabilities at the interface between the magnetic field and the plasma. It was believed that these constraints would also minimize the electrode erosion. The gun was operated in the gas-triggered mode because the lifetime of high current switches is too short for practical missions, and because scaling laws indicated that an extremely low source inductance ($\sim 10^{-9}$ H) was necessary for efficient operation.

In the first year a major effort was spent in developing diagnostic methods to measure the electric and magnetic fields in the gun.[5] Detailed measurements of the azimuthal magnetic field and the axial electric field were made from which the ion density distribution was deduced under the assumptions that the electrons were the main current carriers and that there was no radial plasma motion. The conclusion drawn from these measurements was that an ionization wave propagated in the accelerator, imparting some forward momentum to the ions but insufficient to cause significant mass accumulation in the current sheet. Our later research showed that one assumption above is not valid, that ion current is in fact important, and that the plasma is either brought to the velocity of the current sheet, or driven into the electrodes.

The field probes showed that there was no appreciable acceleration of the plasma in one of the early guns. The scaling laws showed that of eight possible system parameters, the capacitor was the only good choice to vary. We predicted quantitatively the increase in performance to be expected by increasing C from 1 μF to 5 μF. Again the probes proved valuable in suggesting that a fixed energy loss might occur early in the discharge, which could be minimized relatively, by again increasing C.

Other conclusions in the first year were: it was possible to transfer the energy of the magnetic field into directed plasma kinetic energy; the relaxation oscillator mode (no moving parts - gaseous propellants) would probably not be feasible at repetition rates less than 100 per second under gun conditions in use; ballistic pendulums were being used erroneously in this field;[6] and finally, that the identification of a moving current distribution or a moving luminous front with an actual motion of the plasma is very hazardous.

The energy-storage capacitance increase from 1 to 5 μF was done toward the end of the first year, and the parasitic inductance was minimized in order to improve the energy transfer to the accelerator. Soon afterwards we found that the current sheet, which was initially azimuthally symmetric,

would collapse into a spoke after it had moved a few centimeters along the barrels.[7] After several months of investigation we found that this instability would not occur if the barrels were uniformly filled with gas when the gun fired. In this work we first applied to plasma propulsion the fast-acting ionization gauge technique of Marshall.

The E and B field mapping was then continued, current and voltage measurements were made, the equivalent electric circuit was described and an energy inventory was taken. About 65% of the stored energy was delivered to the accelerator but the overall thermal efficiency was only about 25%. The energy-storage capacitance was increased to 10 μF and the source inductance was lowered to about 1 nH, the practical limit in this type of accelerator. The efficiency of energy transfer from capacitor to the accelerator increased as expected, but there was no significant improvement in the overall efficiency. Another increase in capacitance was deemed desirable, thereby increasing the electrical period so that the current sheet would be moving on the rising portion of the current waveform.

Additional results of the second year were: it is impossible to measure resistive losses by voltage measurements at the muzzle; the assumption that the electrons carry all the current is untenable. The latter was a direct result of a diagnostic program to measure the ion velocity in the exhaust.[8,9] The electrostatic cylindrical analyzer of Eubank was adapted as a diagnostic tool. It was later shown that such analyzers were being improperly used in plasma exhausts by us and other groups.[8] The conclusion that ions were important current carriers, however, was established firmly in our later experiments with E probes and Faraday cups.

The experiments on current carriers are important to the question of the acceleration process and to the phenomena at the electrode surface. The experiments led to Lovberg's concept of ion current[9a] which results from the ionization process followed by the separation of the particles in each electron-ion pair formed in a magnetic field.

During the third year, a capacitor development program was started to reduce the size, weight, and cost of the capacitor, while at the same time doubling the capacitance. In the course of this work a lightweight, low loss, low impedance distributed parameter pulse line was developed. A pulse line is particularly useful in this application because the amplitude and period of the current can be controlled independently, and in addition the current and voltage waveforms are in phase. An accurate energy inventory[9b] was taken with the pulse line and found to be consistent with circuit theory. The inventory showed that ohmic losses were small, that 88% of the stored energy could be transferred to the accelerator and that this was shared approximately equally between work done on the current sheet and magnetic field energy, as expected, up to the time of maximum magnetic energy. Thereafter, some of the magnetic energy was withdrawn into the capacitor and some went into additional work on the current sheet. The thermal efficiency of the accelerator was found to be dependent on the matching between the length of the accelerator and the pulse time. The highest efficiency obtained was 45% at an average exhaust velocity of 7 cm/μsec.

At this time it was apparent that the overall efficiency of the accelerator was not being limited by poor energy transfer from the pulse line to the current sheet. The poor efficiency was attributed to the fact that the current sheet was found to move at constant velocity into a gas of uniform density. In this situation energy supplied to the plasma is equally partitioned between directed kinetic energy and internal energy. Our theoretical estimates showed that the internal energy would be lost in radiation in typical accelerators in a time scale comparable to the acceleration period.[10] Consequently, the efficiency of the device, when operated in this mode, could not be greater than about 50%.

At the beginning of the fourth year the relationship between the current sheet velocity, the gun current and the pulse-line impedance was investigated, in a gun with a uniform gas fill, for a variety of propellants. It was found that the sheet speed varied linearly with current and was relatively insensitive to density, in accordance with a simple snowplow model. The exhaust velocity was approximately equal to the sheet speed provided that the current had not dropped substantially when the plasma reached the end of the gun. With this mode of operation thermal efficiencies in the range 35-45% were obtained in the specific impulse range 2,000-10,000 seconds for a wide variety of propellants.

Because of the estimated theoretical limit of 50% on efficiency, and the experimental observation that over a wide range of parameters the measured efficiency was $\leq$ 45%, no more experiments were planned with the gun operating with a uniform gas fill. There did remain the possibility of inhibiting the loss in radiation by use of propellants of greater atomic mass and lesser number density with the hope of recovering the internal energy by means of a proper nozzle. Also, one could hope to establish a preionized gas fill so that the ions might bounce off the current sheet. Another alternative was to tailor the energy source so that a constant velocity current sheet would not occur.

We tried, instead, to circumvent the 50% efficiency limit by two methods: one, essentially the slug-model approach again in which the mass is entrained in the moving current sheet early in the acceleration cycle and then vigorously accelerated; and in the other the plasma is accelerated by a stationary current sheet as in steady-state accelerators. The former approach required that spoke instabilities be inhibited. The latter was a new concept in pulsed accelerators; it is essentially a pulsed arc, and the device has been designated a pulsed arc gun. A strong effort was applied to the pulsed arc gun for about one year.[11] The results and our present opinion of the device are given in a later section. In September 1965, the pulsed arc gun program was interrupted in order to pursue the performance evaluation of the coaxial thrustor.

One further significant accomplishment in the fourth year was in the continued development of energy-storage capacitors.[12] Over one million discharges were achieved at energy densities of 80 joules/lb and 4 joules/in.^{3} with a charging voltage at 4 kV. These energy densities are considerably higher than the minimum required for practical missions; we are confident that neither capacitor weight nor lifetime will be the limiting factor in the performance of pulsed plasma thrustors. Also, we

gained further experience in analysis by examining the energy-storage requirements for pulsed arc guns which operate at a few hundred volts.

In the conventional coaxial gun program, several experiments were performed using a gas-triggered gun with a single set of gas ports near the breech. The current sheet propagated much the same as in the uniform-fill experiments until it approached the region where the gas density dropped. At this point the character of the current sheet changed: the leading edge of the current sheet accelerated while the trailing portion did not. We were generally dissatisfied with the amount of parametric control available over the gas distribution, but encouraged by a lack of spoke instabilities. A more versatile thrustor was built which is described in the next section.

4.0 COAXIAL THRUSTORS

4.1 Introduction

The previous section shows that most of our thrustor development has centered upon the coaxial rail gun in which the plasma is accelerated by the stroke of a magnetic field "piston". For this type thrustor, theoretical considerations[13,14] have shown the superiority of a pre-discharge propellant distribution (the slug model) which is localized in a compact volume at the start of the stroke. Our earlier experiments with slug acceleration were interrupted because the discharge collapsed into inefficient instabilities. Extensive work on gas-triggered thrustors with uniform mass loads led to calorimetric efficiencies near 50% over a wide range of plasma outputs. Analysis indicated that energy lost through radiation would probably limit performance to that level.

In this period, experiments with non-uniform propellant distributions were renewed with two goals, to avoid instabilities and to demonstrate improved dynamic efficiency due to proper propellant loading. The experiments fall into three classes. The first experiments dealt with the nature of the propellant distribution and the nature of the discharge, in particular, its stability. The thrustor performance was judged by means of the calorimetric efficiency. In the second group of experiments, the overall thrustor efficiency and the specific impulse were determined from measurements of thrust, mass flow rate, and power. A large number of parametric changes were made in the thrustor design and the mode of operation in order to improve the thrustor performance. In the third phase of the program, the constraint to follow the slug-model, rail-type thrustor was relaxed. The propellant loading was changed from a radial injection at the insulator, to axial injection at various locations along the axis of the electrodes. A parametric program of thrust efficiencies and specific impulse measurements was then accomplished.

4.2 Thrustor Experiments, Radial Propellant Injection

The objective of the following experiments was to study the performance of a thrustor with a non-uniform propellant distribution. The propellant distribution within the barrels was measured as a function of time and correlated with the instant of the thrustor discharge. To enchance the control over the propellant input, the time delay between the gas injection and the thrustor discharge was programmed. Also, a fast-acting gas valve was built into the thrustor. The delay of the discharge was accomplished by operating the thrustor in a voltage-switched mode. The voltage switch is not practical for a space mission but is convenient for these studies. Practical means for triggering the thrustor do exist.

The electrode configuration, gas valve assembly, and voltage switch are shown in Figure 1, and a photograph of the thrustor and a capacitor is shown in Figure 2. The anode and the back flange are connected to the capacitor. The cathode is held at anode potential by a 2200 Ω bleeder resistor until the spark gap fires. The gap is triggered by a surface ignitor in the face of one electrode. An electromagnetically-driven eddy-current type gas valve opens the propellant plenum. The energy is stored in a pulse line, with 181 μF capacitance, 5.6 mΩ impedance, and a pulse time of 2.2 μsec.

In the following experiments, the propellant was nitrogen. The propellant distribution was measured with a fast-acting ionization gauge. The neutral gas density was measured at three radii at one centimeter intervals along the axis. The data taken near the inner and outer barrels are shown in Figure 3. A non-uniform gas distribution exists over the gas ports at early times and then broadens into a nearly uniform distribution. The propellant inventory per shot is shown in Figure 4. The propellant first appears at the ports 80 μsec after the gas valve is triggered, and 400 μsec later, 90% of the propellant has left the plenum. The flow into the plenum is restricted so that the plenum empties during the valve cycle.

The 6AH6 ionization gauge is non-linear at high densities. In order to map the propellant distribution close to the gas ports, it is necessary to reduce the plenum pressure below that necessary for thrustor firing. The data in Figures 3 and 4 were taken at a plenum pressure of 60 Torr; the thrustor experiments, however, were run at plenum pressures of 600 Torr to 4 atm. At plenum pressures above 60 Torr, the mass loading became relatively heavier at the outer barrels near the insulator. The latter was observed by always locating the gauge such that its response remained linear. The conclusion is made that a non-uniform gas distribution exists for several hundred microseconds. At the barrel exit, the gauge output was proportional to plenum pressure up to at least 600 Torr, and it was possible at 600 Torr to substantiate the propellant inventory of Figure 4.

4.2.1 Nature of Discharge

The thrustor could be fired in the range 80 μsec $< t <$ 500 μsec where the firing delay, t, is referenced to the instant of the gas valve trigger. Thus the voltage-switched thrustor could be operated with a variety of non-uniform propellant distributions. Instability in the current sheet was generally found to occur only for t less than 125 μsec. By shorting the spark gap, or switching very early, the gun was found to be propellant-triggered near t = 100 μsec. An instability was evidenced by loss of axial symmetry in the magnetic field distributions and in the luminosity of the discharge.

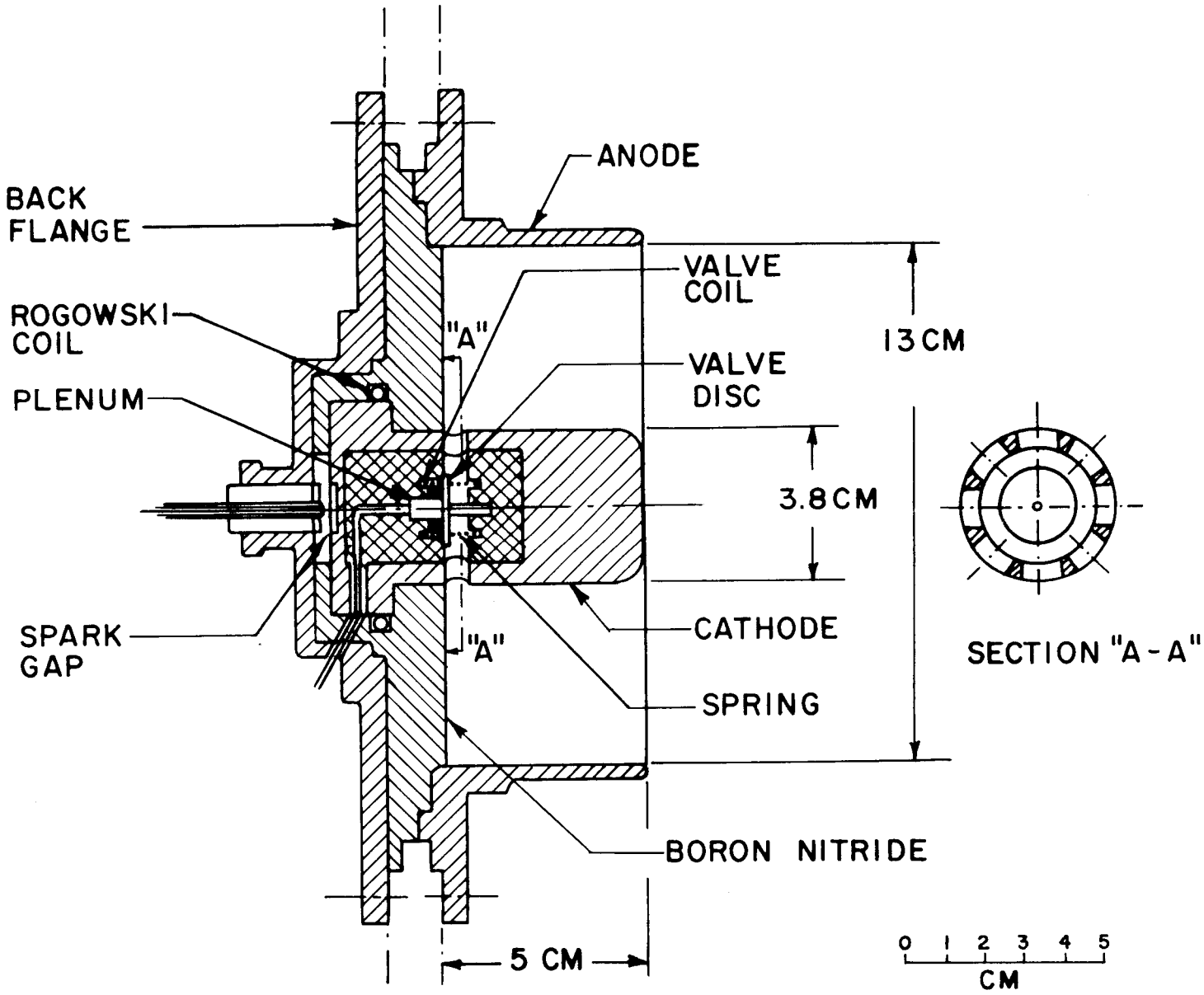

FIG. 1 : VOLTAGE SWITCHED THRUSTOR

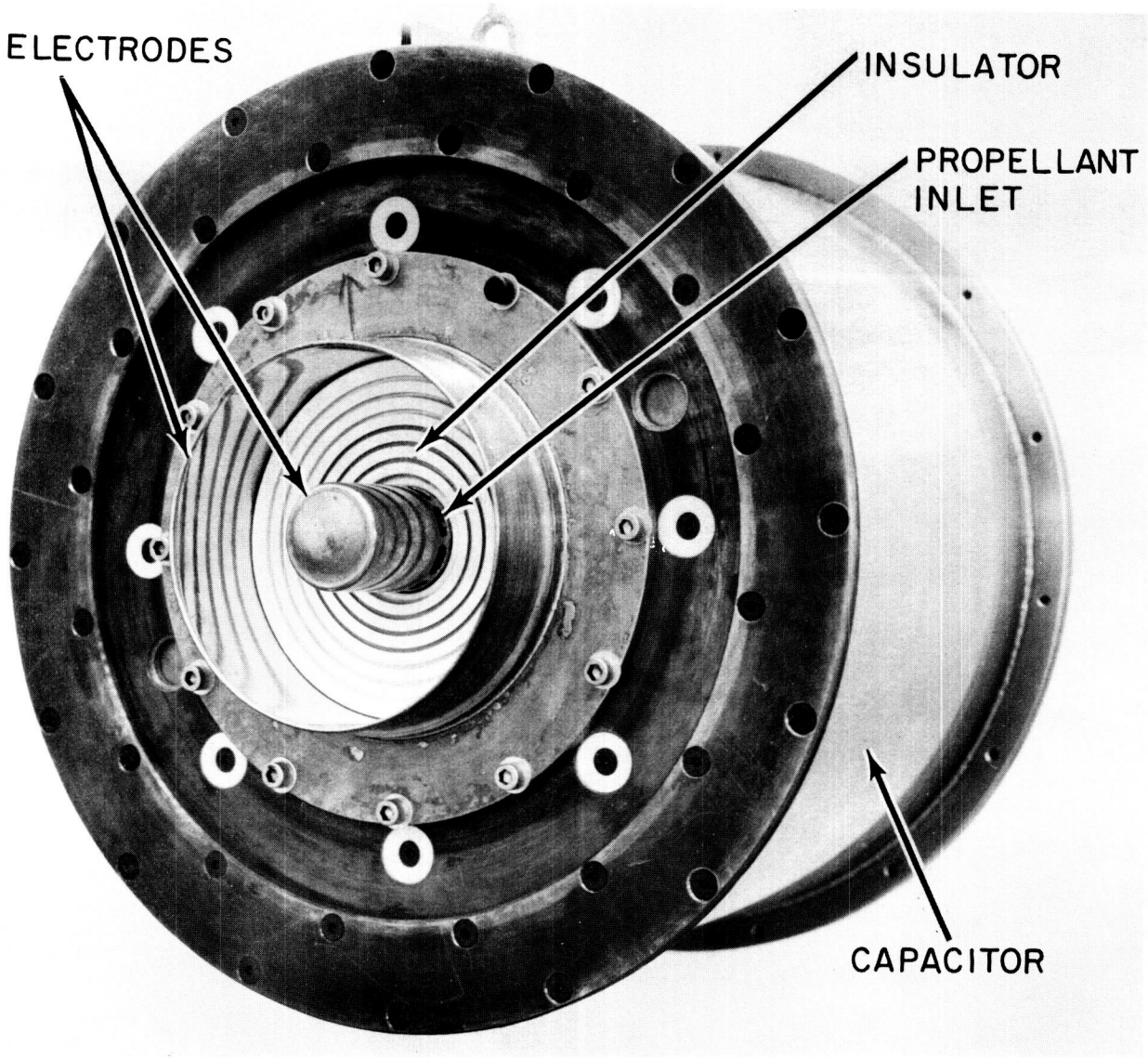

FIG. 2 : PHOTOGRAPH OF THRUSTOR AND CAPACITOR

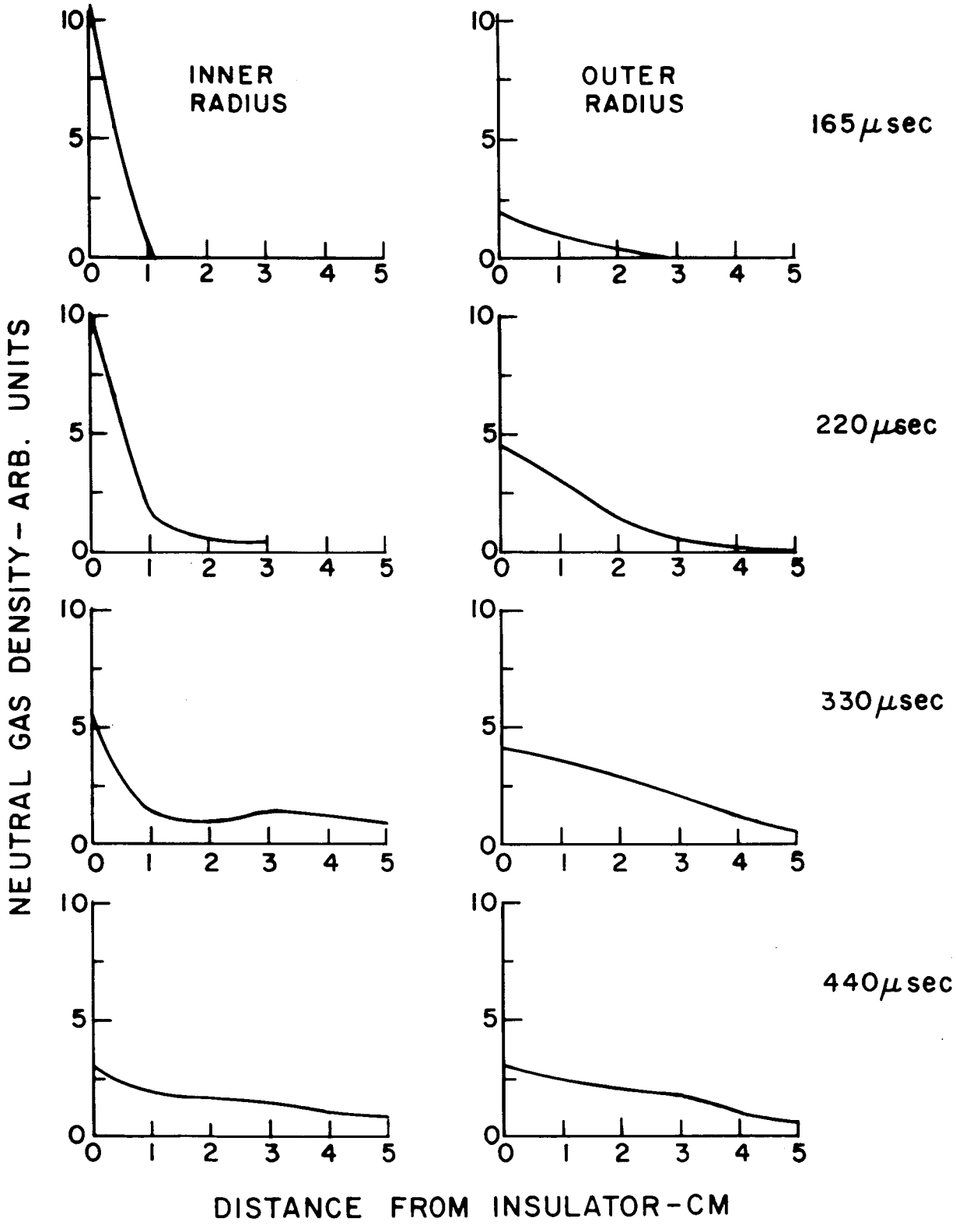

FIG. 3 : GAS DENSITY DISTRIBUTIONS AT DIFFERENT TIMES AFTER GAS VALVE TRIGGER

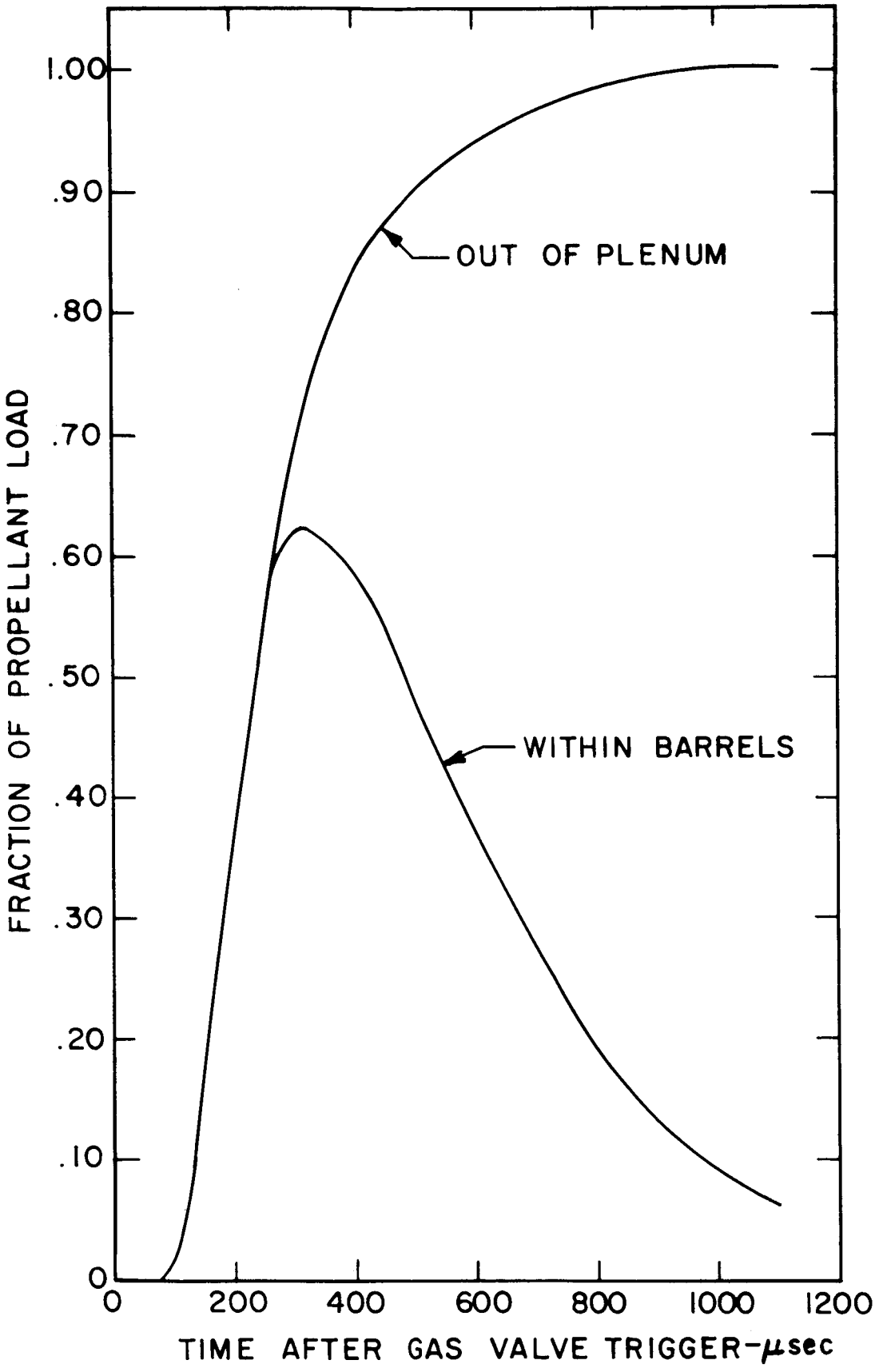

FIG. 4 : PROPELLANT LOAD VS TIME

The data which follow demonstrate the axial symmetry and the general nature of the thrustor discharge. Currents to the tank walls were negligible. The azimuthal magnetic field, B_θ, was measured simultaneously by two probes located a distance, z, from the insulator and on diametrically opposite sides of the cathode. The oscillograms, in Figure 5, give superpositions of the integrated probe signals, proportional to $B_\theta(t)$, taken at 2 cm intervals in the axial (z) direction for various delays. The length of the barrels was 5 cm. Similar oscillograms are presented in Figure 6 under the condition of higher capacitor voltage and higher plenum pressure. The first photograph shows again that the current sheet propagates in a stable and symmetric fashion over twice the barrel length; the second photograph, taken at a high gain, demonstrates the existence of the current sheet up to a distance of 30 cm. A second current sheet of smaller amplitude is also seen in both photographs.

Photographs showing the time integrated luminosity profiles in the discharge are given in Figure 7. The measurements of the thrustor voltage and current, see Figure 8, show that the discharge is nearly critically damped. The steps in the voltage waveform indicate the pulse-line type behavior of the capacitor.

Since the voltage-switched thrustor could operate on non-uniform propellant distributions without instabilities, other measurements were started. A re-entrant calorimeter of 58 cm diameter was placed 25 cm from the muzzle. The calorimeter was electrically isolated: its presence did not affect the voltage, current, or the luminosity profile of the thrustor. Calorimetric efficiency, defined as the energy in the calorimeter divided by the energy in the capacitor, was measured at different firing delays, capacitor voltages and plenum pressures. The results are given in Figure 9. Peak calorimetric efficiencies of 65% were observed at firing delays of 200 to 250 μsec. The energy lost in the spark gap was measured to be about 10%. By replacing the spark gap trigger with an efficient trigger, we would expect to achieve calorimetric efficiencies of 70%.

The drop in efficiency at longer firing delays is consistent with a measured decrease in the number of exhaust ions and a decrease in the ion velocity. The properties of the exhaust were measured by a Faraday cup placed on axis 87 cm from the muzzle of the thrustor. Typical results are given in Figure 10. The signal in the upper beam is proportional to the ion current per unit area. Time of flight is used to estimate the average ion velocity. The signal in the lower beam varies as the ion flux per shot per unit area. The relative oscilloscope gains are given in arbitrary units of each beam. The decrease in the average velocity and in the number of ions as the firing delay increased was found to be more severe for higher plenum pressures. Although these observations were taken on axis, earlier measurements off axis gave similar results.

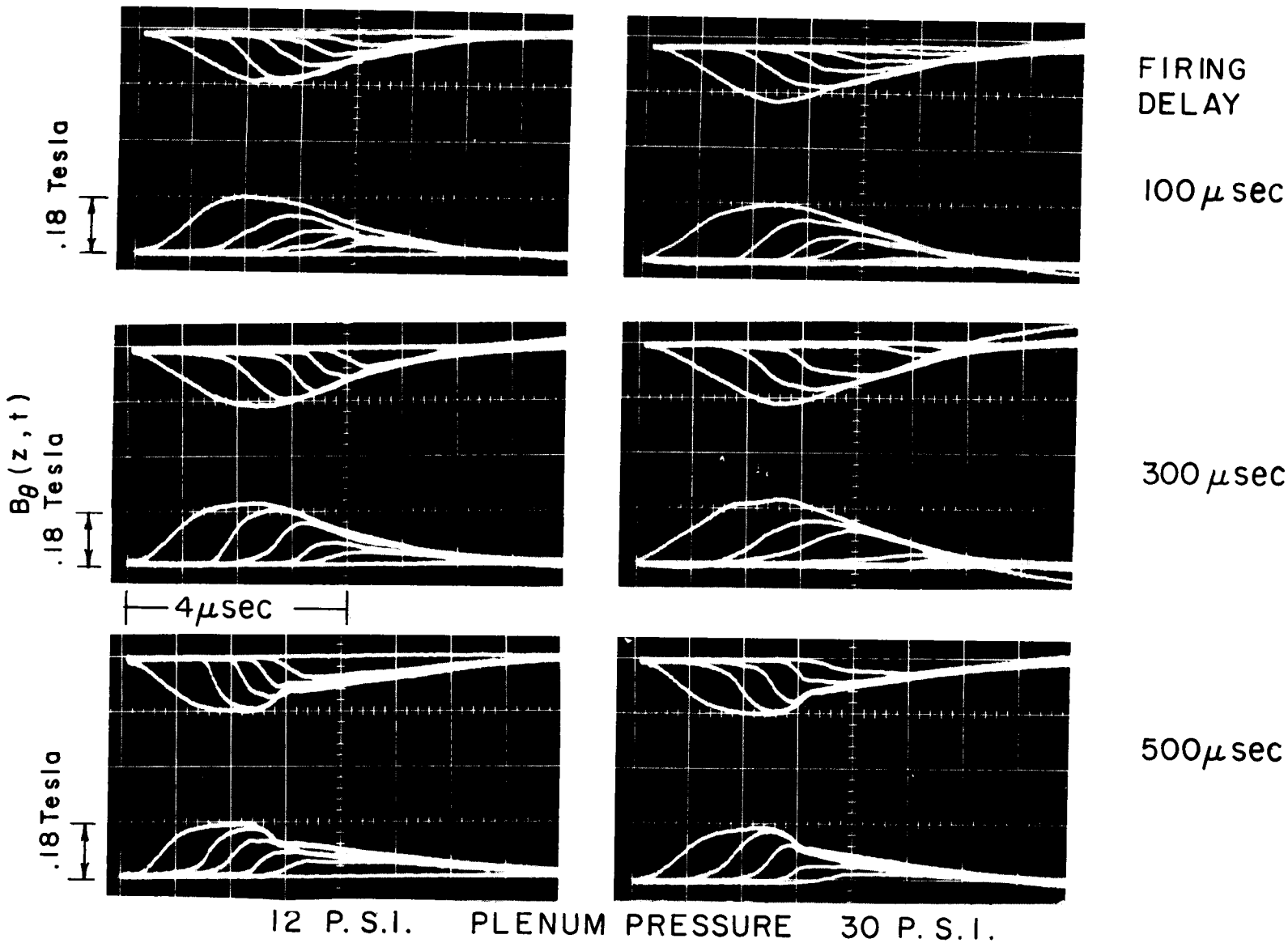

FIG. 5 : OSCILLOGRAMS OF $B_\theta(z,t)$ AT MID-RADII
DISTANCE FROM INSULATOR, Z = 0,2,4,6,8 cm
CAPACITOR VOLTAGE 1.0 kV

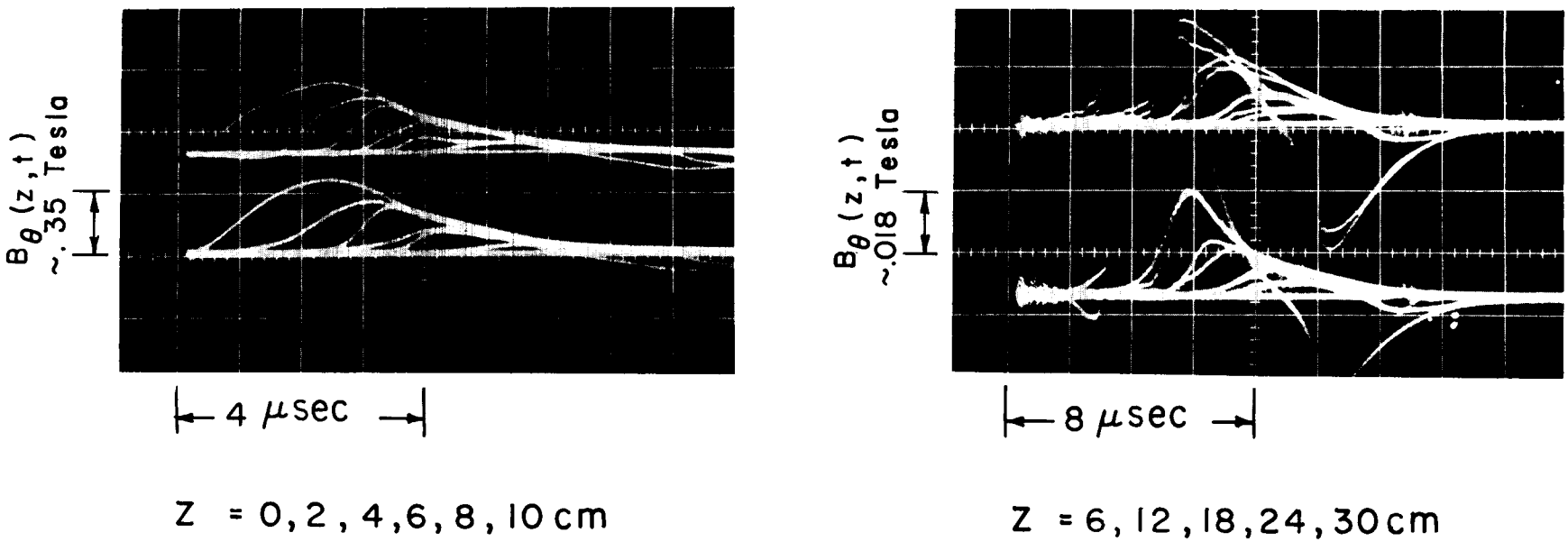

FIG. 6 : OSCILLOGRAMS OF $B_\theta(z,t)$ AT MID-RADII
CAPACITOR VOLTAGE 2.0 kV, PLENUM 60 P.S.I.
FIRING DELAY 200 μsec

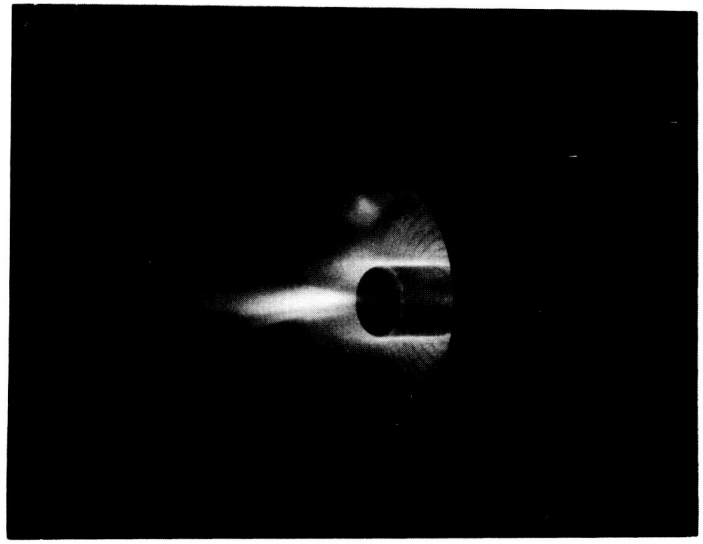

200μsec

FIRING DELAY

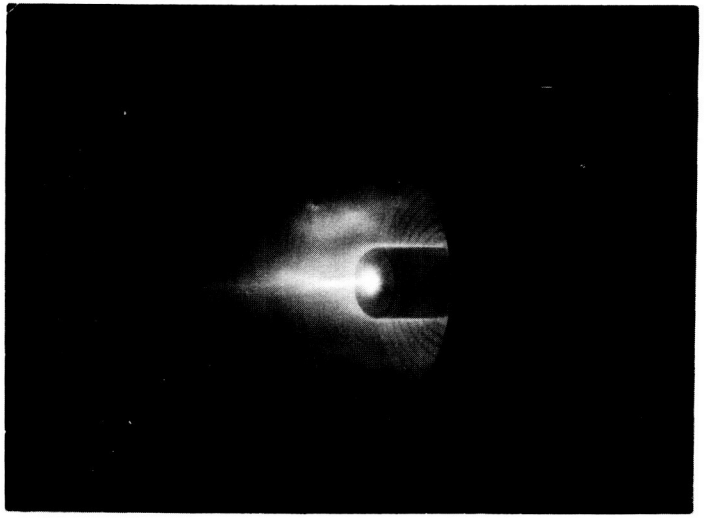

400μsec

FIG. 7 : PHOTOGRAPHS OF THE DISCHARGE
CAPACITOR VOLTAGE 1.0 kV PLENUM 12 P.S.I.

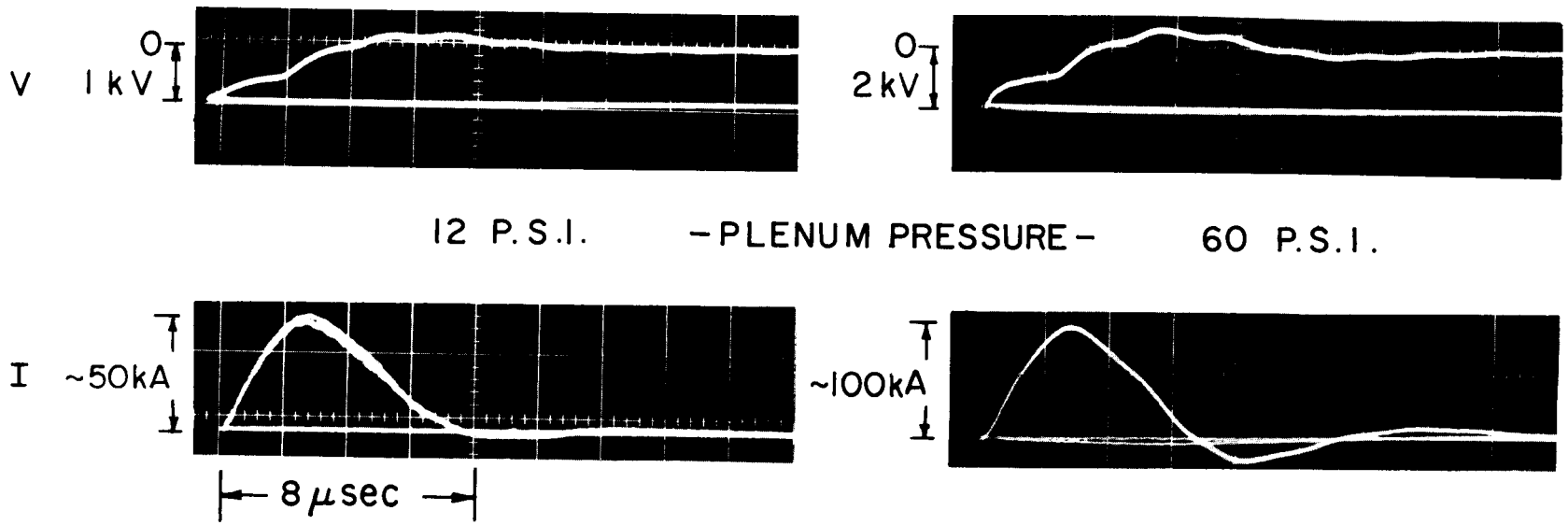

FIG. 8 : OSCILLOGRAMS OF THE THRUSTOR VOLTAGE AND CURRENT
FIRING DELAY 200 μsec

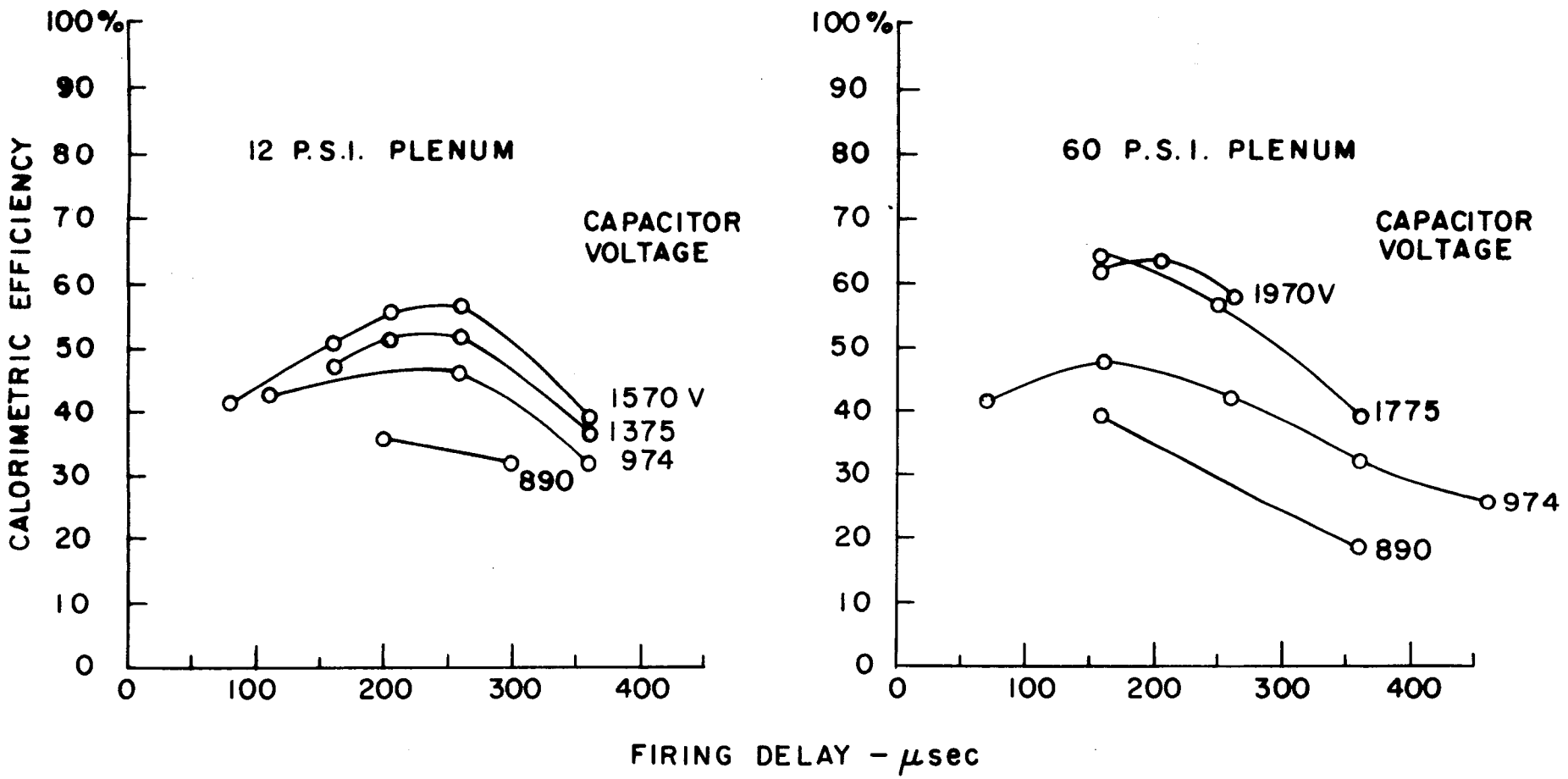

FIG. 9 : CALORIMETRIC EFFICIENCY VS. FIRING DELAY
C = 181 μF , GUN OF FIG. 1, NITROGEN PROPELLANT

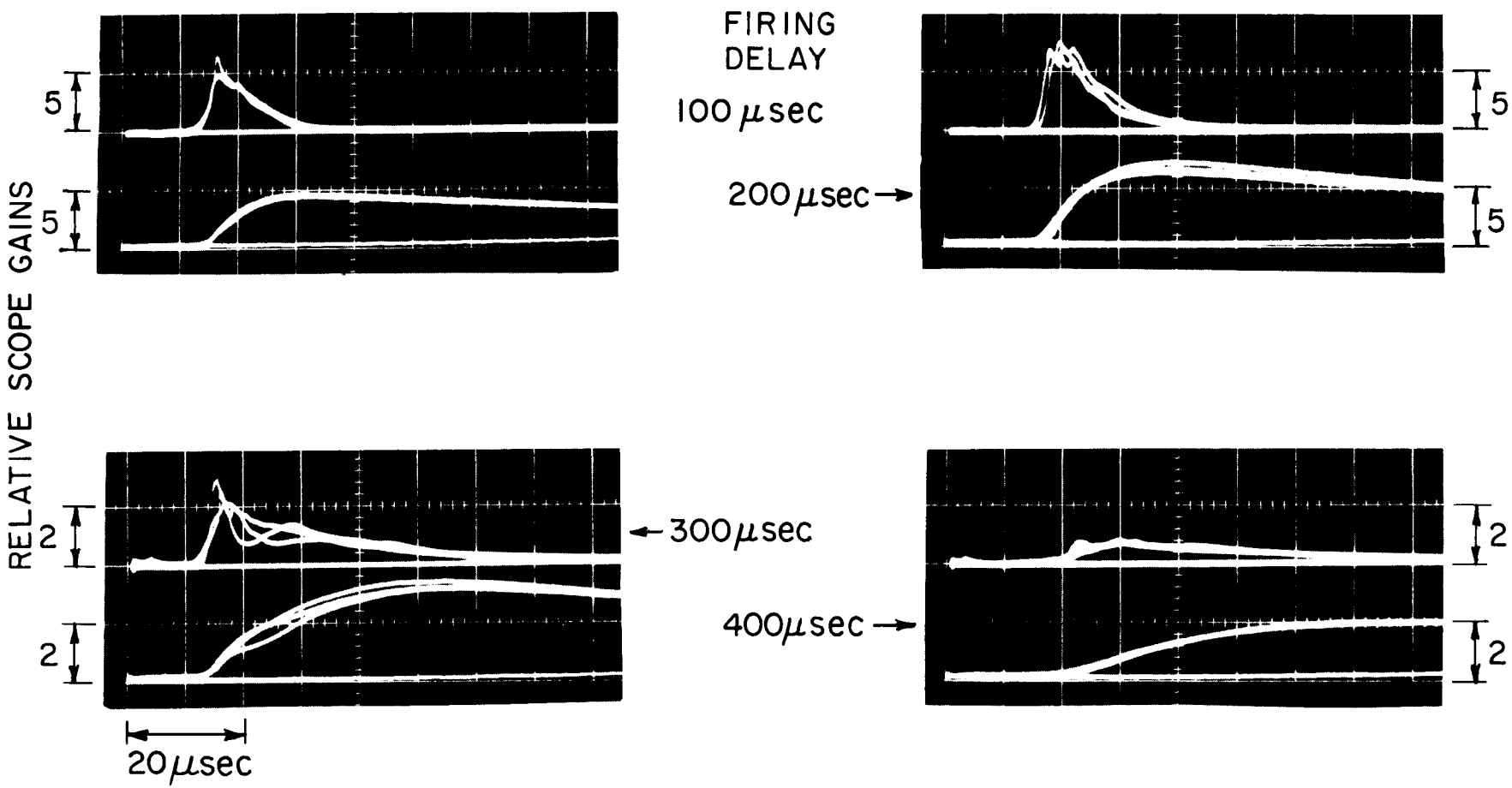

FIG. 10 : FARADAY CUP OSCILLOGRAMS
FLIGHT DISTANCE ~ 87 cm, GUN VOLTAGE 1.0 kV PLENUM 12 P.S.I.
LOWER TRACE IS THE INTEGRAL OF THE UPPER TRACE
(PLATEAU DROOP IS AN EFFECT OF THE RC INTEGRATOR)

4.2.2 Thrustor Performance

Because of the high calorimetric efficiency, it was meaningful to start thrust efficiency measurements. The thrustor circuitry, including a new 140 μF capacitor was constructed to fit onto the thrust stand inside the vacuum chamber. The thrustor impulse per shot, the mass injected per shot, and the energy stored in the capacitor per shot were measured. From these, the thrust efficiency, $T^2/2\dot{m}P$, and the specific impulse, $T/g\dot{m}$, were determined. The discharge repetition rate was nominally 0.1 sec^{-1}.

The thrust balance is described in Section 8.1.1. For all measurements in this report, the thrust balance was operated as described in Section 8.1.2. The total mass per shot injected into the gun was determined by means of a pressure and volume measurement. The device for a volumetric measurement of the injected gas is described in Section 8.2. The accuracy of the $\dot{m}$ measurement is 5%. The electrical energy which was stored in the capacitor was determined by the charging voltage and the gun-capacitance (140 μF).

Measurements were performed with nitrogen and xenon as propellants. The stored energy was varied between 160 and 700 joules, and the injected mass per shot between .02 and .4 mg for the nitrogen runs and between .07 and 2 mg for the xenon runs. The measured impulse level was between 150 and 1000 dyne-sec for nitrogen and between 300 and 1200 dyne-sec for xenon. The specific impulse for nitrogen varied between 750 and 15000 sec and between 350 and 8000 sec for xenon.

At each particular plenum pressure and capacitor voltage the delay time between gas injection and gun switching was varied until the maximum thrust value was found. At this optimum delay time the thrust efficiency and specific impulse were determined.

In the first series of measurements, the barrel arrangements shown in Figure 11 were used. Experimental results are presented in Table I and again in Figure 12 for two of the gun models. Figure 12 shows the thrust efficiency as a function of the specific impulse. The lines connect the data taken at different capacitor voltages, but nearly the same injected mass. The solid lines connect data taken with the barrels shown in Figure 11(a) (also Figure 1). The dashed lines connect data taken with the inner barrel of Figure 11(a) and the outer barrel of Figure 11(d). Similar results were obtained with the other geometries of Figure 11.

The background pressure in the tank was less than 10^{-6} Torr. At this low pressure there does not exist a gas reentrainment problem during the shot. Between shots, however, gas can be adsorbed at the surface of cathode, anode, and back insulator. The problem of propellant addition from these walls was investigated because the first shots of a series, after several minutes down-time, showed a higher thrust than the later shots. This levelled off to a stable plateau value after about 20 shots had been fired at a repetition rate of 1 shot every 10 sec or faster.

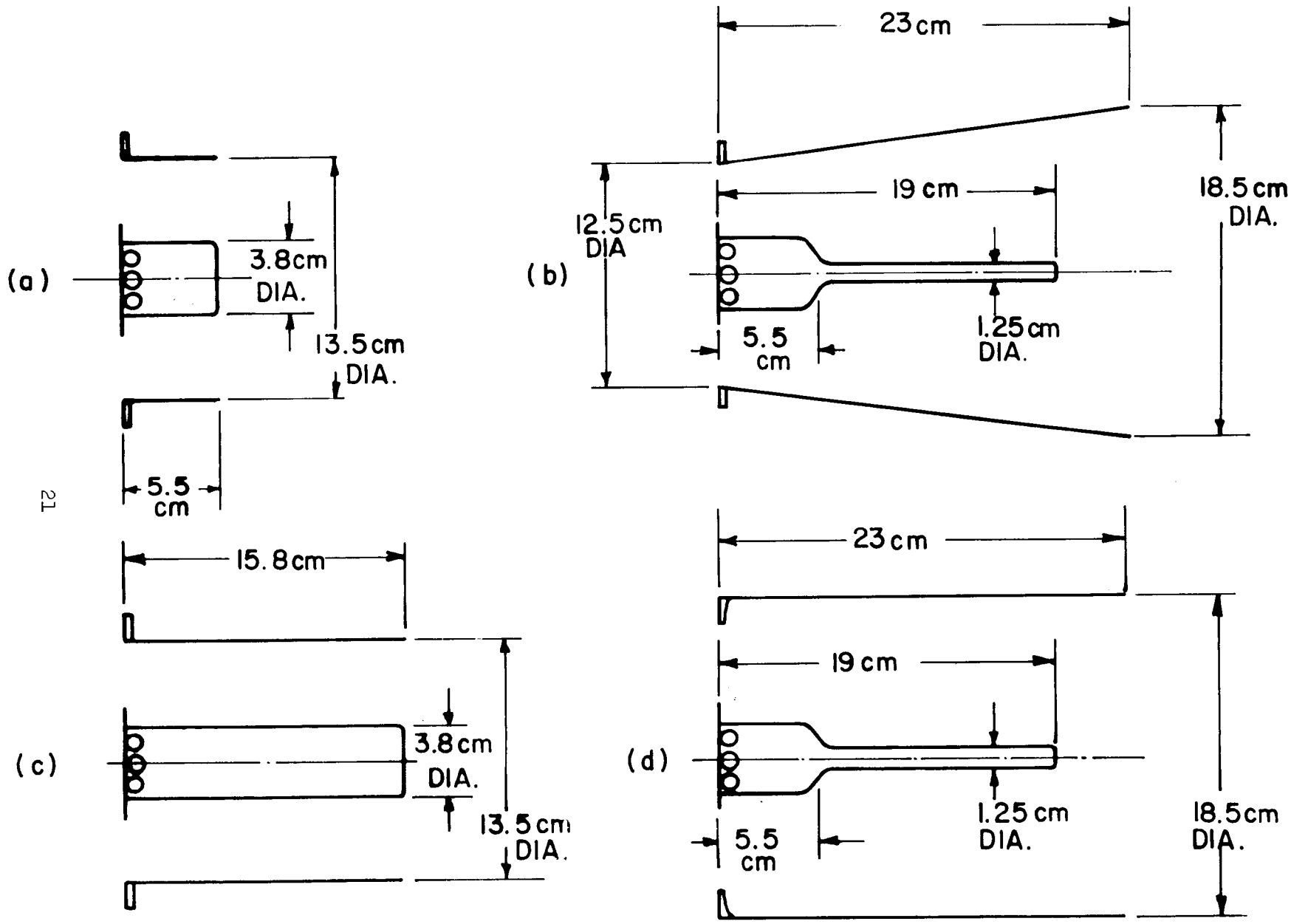

FIG. 11 : BARREL CONFIGURATIONS

TABLE I

DATA FROM THRUSTOR EXPERIMENTS, RADIAL PROPELLANT INJECTION, NITROGEN (CURVES 1-7) AND XENON (CURVES 8-12) PROPELLANTS, SECTION 4.2.2

Curve of Fig. 12	Run No.	Thrust Efficiency η %	I_{sp} (sec)	Delay Time (μsec)	Impulse per Shot (dyne sec)	Mass per Shot (10^{-5} g)	Energy per Shot (10^7 ergs)	Kilovolt
1	46f	13	1100	300	380	34.8	158	1.5
1	46e	17	1650	300	580	34.8	280	2.0
1	46d	18	2150	300	750	34.8	438	2.5
1	49	24	3130	300	1019	32.5	665	3.08
2	36	8	750	250	310	40.7	158	1.5
2	30	12	1300	250	500	38.0	280	2.0
2	37	11	1650	250	575	34.8	438	2.5
3	47	15	2500	300	574	22.5	473	2.6
3	48	19	3480	300	727	20.9	665	3.08
4	34	23	5000	250	145	2.9	158	1.5
4	32	21	6400	250	185	2.9	280	2.0
4	33	42	13000	250	327	2.9	438	2.5
5	46a	23	2400	250	300	12.4	158	1.5
5	46b	22	3100	250	390	12.6	280	2.0
5	46c	30	4800	250	540	11.3	438	2.5
6	35	13	1850	250	222	12.0	158	1.5
6	29	14	2630	250	305	11.6	280	2.0
6	38	27	4500	250	525	11.6	438	2.5
7	46i	24	5200	300	150	2.9	158	1.5
7	46h	36	8300	300	240	2.9	280	2.0
7	46g	56	1300	250	380	2.9	438	2.5
8	43	8	560	400	800	147.0	280	2.0
8	44	6	585	400	850	145.0	438	2.5
9	45c	6	350	500	525	149.0	158	1.5
9	45b	6	460	300	695	149.0	280	2.0

Table I is continued on the next page.

TABLE I

(Cont'd)

Curve of Fig. 12	Run No.	Thrust Efficiency $\eta\%$	I_{sp} (sec)	Delay Time (μsec)	Impulse per Shot (dyne sec)	Mass per Shot (10^{-5} g)	Energy per Shot (10^7 ergs)	Kilovolt
9	45a	11	810	500	1210	149.0	438	2.5
10	40b	15	1400	400	600	44.0	280	2.0
10	42	16	1800	400	780	43.5	438	2.5
11	45f	9	710	450	385	54.3	158	1.5
11	45E	11	1060	450	575	54.3	280	2.0
11	45d	13	1500	500	805	54.3	438	2.5
12	45i	21	2360	500	283	12.0	158	1.5
12	45h	28	3600	500	435	12.0	280	2.0
12	45g	28	4500	400	543	12.0	438	2.5

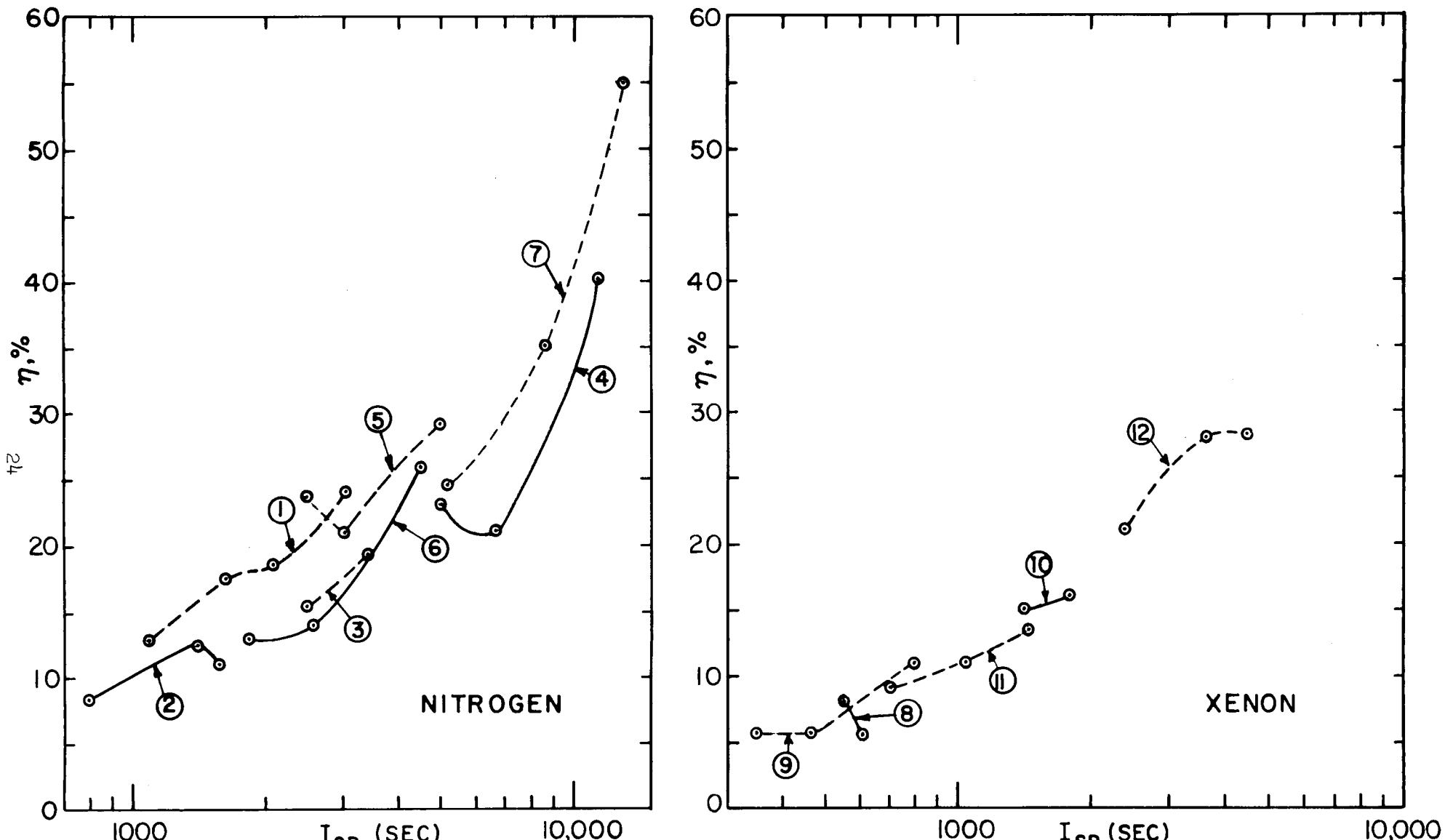

FIG. 12 : THRUST EFFICIENCY vs. I_{SP}

Experiments were done with baked-out insulators and barrels which were preheated immediately before a shot, to 600°C for several minutes, by quickly removable coils. The impulse of the initial shots in a test series diminished considerably, but the plateau values were unchanged. These plateau values are presented in Figure 12.

In this work the boron nitride insulator was found to outgas about 10^{19} particles per second during the preheating process. It was replaced by a glazed aluminum oxide insulator, which is impervious to water vapors. The erosion rate in this thrustor was not measured, but is expected to be small, based upon visual observations after 10^5 shots and measurements in a variety of similar devices operating at 1-2 kV, 10^4 amps, and having discharge times of a few μsec.[15]

Faraday cups were mounted one meter from the thrustor on a rotating arm. The ion flux per unit area per shot was measured as a function of angle from 0° to 90° relative to the thrustor axis. A typical run is shown in Figure 13. The confinement of the beam is relatively good for pulsed plasma thrustors.

4.2.3 Faster Propellant Injection

A comparison of the propellant inventory for nitrogen (Figure 4) and the optimum delay times for maximum thrust (Table I), shows that less than 60% of the propellant was used in the accelerating process. This direct efficiency loss could be charged to the slowness of the valve and its less-than-optimum location and port arrangement (Figure 1). Since the thrustor performance was otherwise generally good, a program for better propellant injection was undertaken.

The ferromagnetic core valve described in Section 6.1 had already been built and tested. It was incorporated into the gun as shown in Figure 14. The cathode was attached to the face of the valve body by three thin radial copper fins, thus allowing an optimal open structure for the gas ports.

In comparison to the previous eddy-current type valve, the valve in Figure 14 opens faster because of the better use of the electromagnetic forces, and closes faster by the aid of the pressure force acting at the back of the diaphragm as the reservoir empties. The operation of the valve for nitrogen and xenon is demonstrated in Figure 15. For these measurements, the cathode was removed, and a CK 5702 ionization gauge was placed as close as possible (.5 cm) to the valve output. The valve opens or closes in about 100 μsec and the total open-time is less than 250 μsec. The delay time between triggering the valve circuit (time zero in Figure 15) and the appearance of the gas in front of the valve was 180 μsec.

Since the neutral gas spreads out into the interelectrode region with essentially its sound velocity, it will have travelled a distance of only 7.5 cm in the case of nitrogen and 3.4 cm in the case of xenon before the valve has closed completely. This fact in connection with the open structure of the gas ports should allow a close approximation of the slug model propellant distribution.

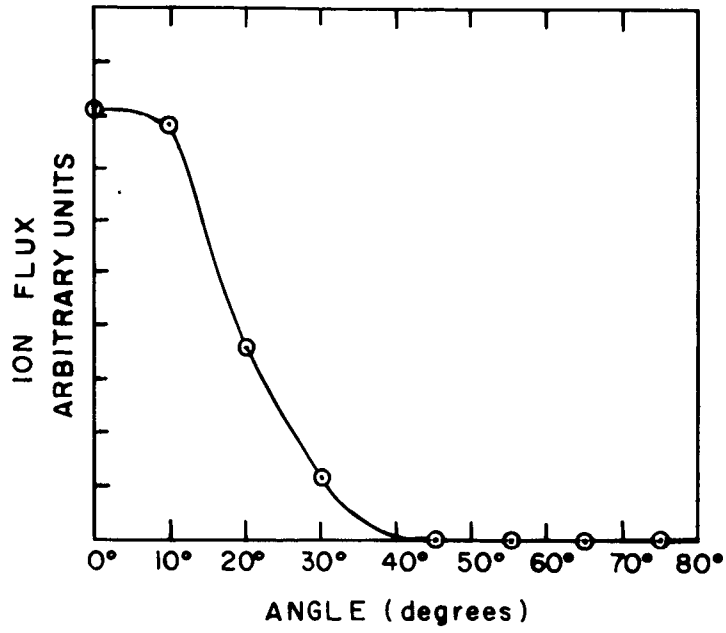

FIG. 13 : ION FLUX PER UNIT AREA PER SHOT vs. ANGLE FROM THRUSTOR AXIS.

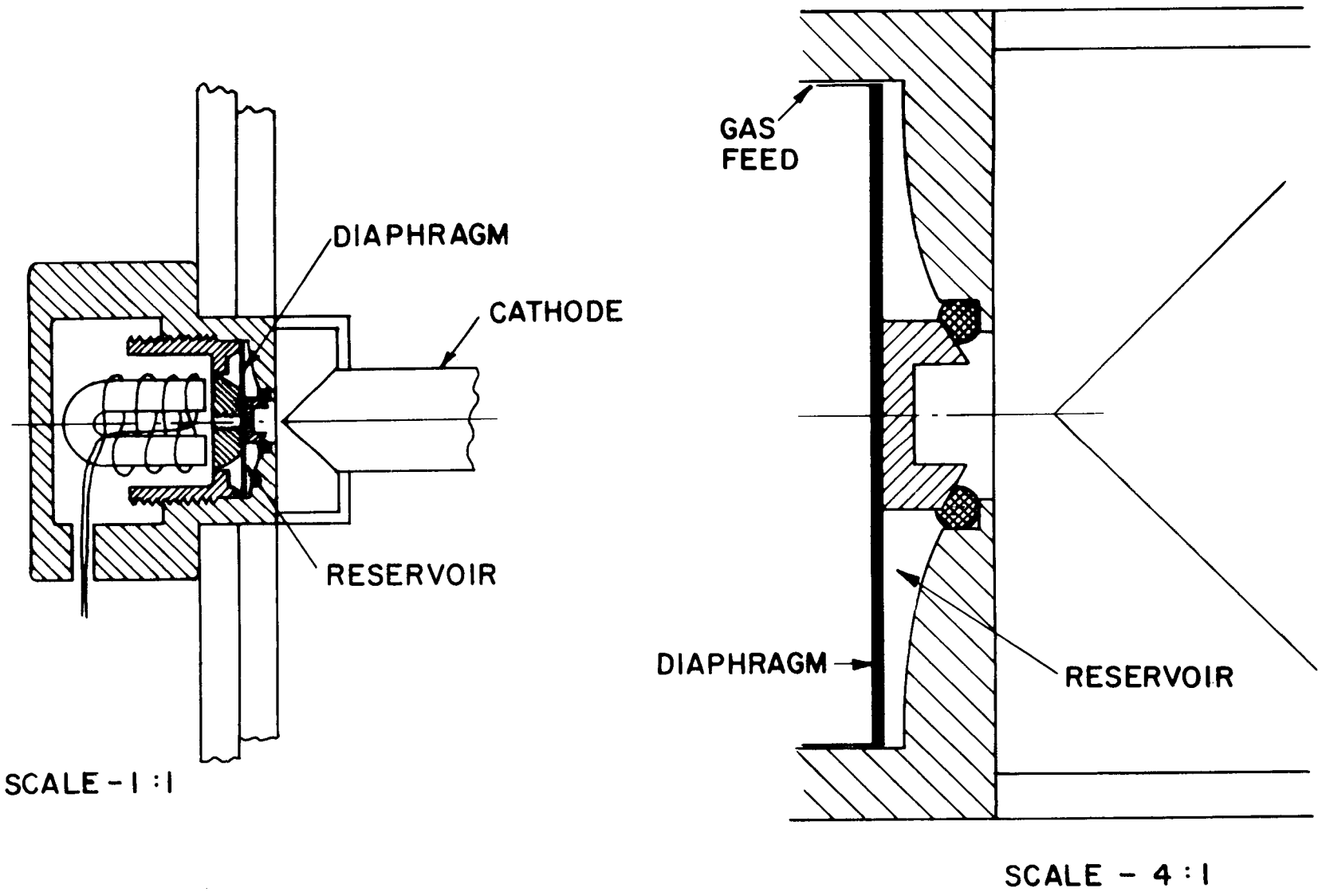

FIG. 14 : FERROMAGNETIC CORE VALVE

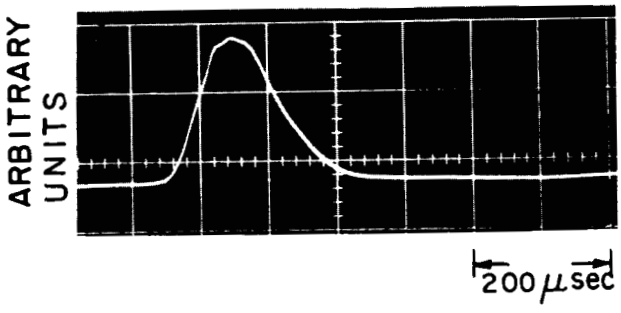

NITROGEN
(2 at.)

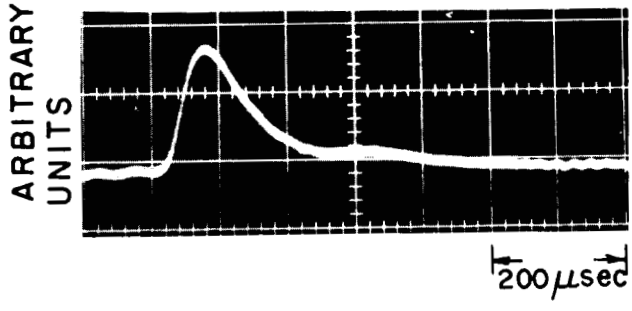

XENON
(.5 at)

FIG. 15 : GAS OUTPUT OF THE FERROMAGNETIC CORE VALVE

Density measurements of the neutral gas were taken with the CK 5702 fast ionization gauge technique. The CK 5702 is smaller than the 6AH6 used previously (Figures 3 and 4) and has a greater range of linearity.[15] The measurements with nitrogen are shown in Figure 16, where the propellant distribution is plotted on a full-scale drawing of the interelectrode region. The black points between cathode and anode represent the various locations of the fast ionization gauge. The curves above these points give the neutral gas densities (in arbitrary units) at 300, 400, and 500 μsec after the valve circuit has been triggered. Note that the amplitude units of these curves are not the same: the raw data has been multiplied by 1/9, 1/4, and 1 for the 300, 400, and 500 μsec curves, respectively.

The slug model seems to be best approximated at a delay time of 400 μsec. At this time the gas is still concentrated in the first third of the anode length, and the valve has already closed. Note that the location of the gas ports is extended in front of the insulator by 2 cm. This was done in order to avoid a pressure build up at the insulator which could have moved the slug further downstream. The density distribution shows, however, that an extension of 1 cm would have been sufficient. It also suggests that the back insulator might be contoured as indicated by the dotted line without disturbing the distribution.

Thrust efficiency measurements were made with nitrogen as the propellant. The mass loading and energy per shot was varied. The measurements are listed in Table II. The delay time is again the optimum interval between the triggering of the valve circuit and the breakdown of the discharge.

The result of these measurements is that the thrust efficiency is a little lower compared to the data taken with the slower valve (Figure 12). The optimal delay time here was such that in some runs (delay time ≥ 400 μsec) the valve had closed completely before the gun fired, in other runs (delay time = 300 μsec) the valve was still in the closing process. Thus even though most of the propellant was available to the discharge, the performance did not improve.

In anticipation of the experiments to be reported in the next section, the ferromagnetic core valve assembly was constructed in such a way that the location of the radial gas injection point could be moved stepwise downstream. This was simply done by incorporating extension rings between the valve and the cathode flange of the capacitor. The location of the valve with respect to the gas ports did not change. Measurements were performed for one set of operational conditions, using nitrogen as propellant. The measurements are presented in Table III. L means the distance between the insulator of the gun and the gas injection point. The results show a trend toward lower efficiency if the valve is moved downstream.

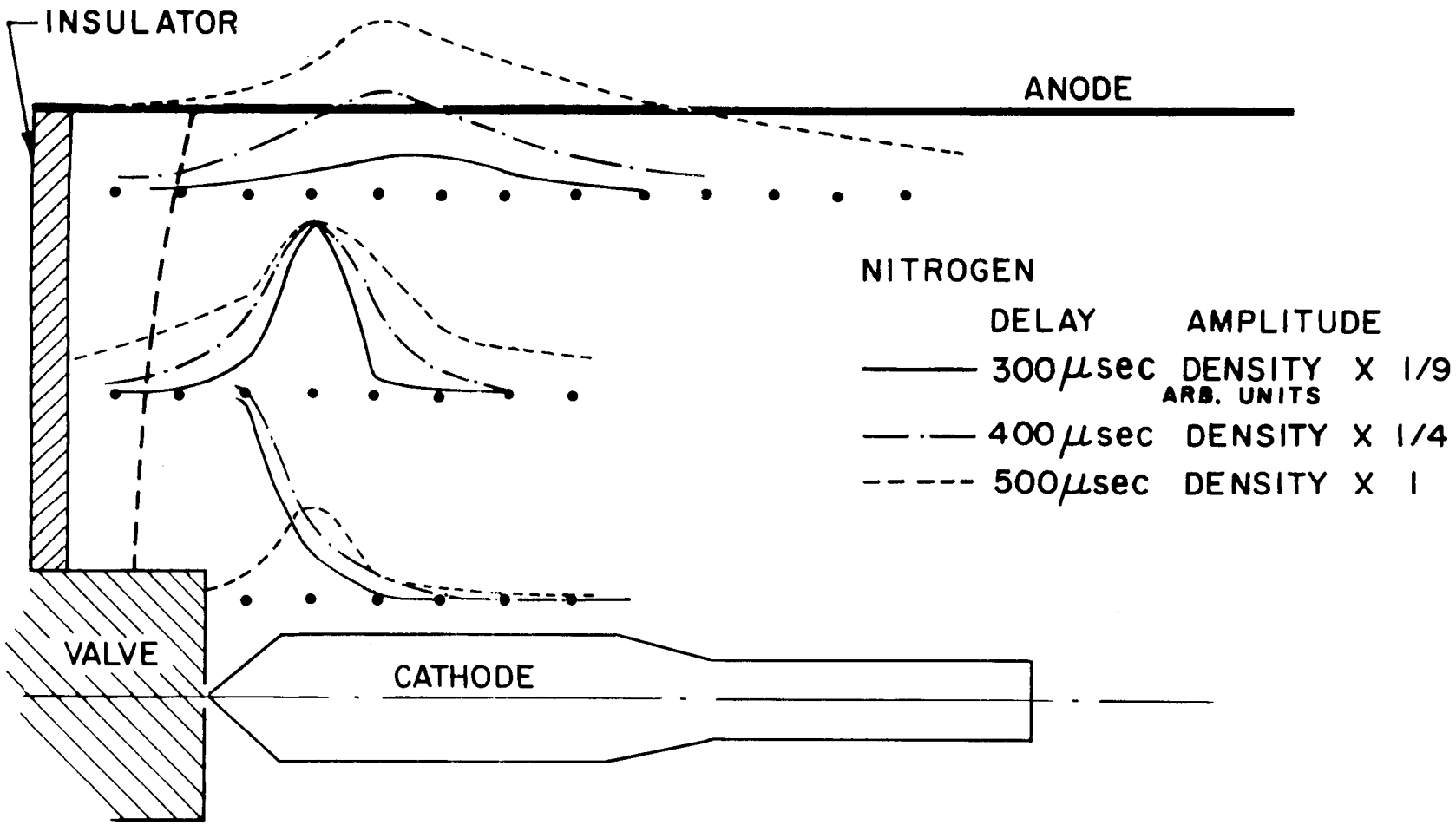

FIG. 16 : GAS DENSITY DISTRIBUTIONS
(ELECTRODES SHOWN FULL SCALE)

TABLE II

DATA FROM THRUSTOR EXPERIMENTS, FASTER RADIAL PROPELLANT INJECTION AT THE INSULATOR, NITROGEN PROPELLANT, SECTION 4.2.3

Run No.	Thrust Efficiency η %	I_{sp} (sec)	Delay Time (μsec)	Impulse per shot (dyne sec)	Mass per shot (10^{-5} g)	Energy per shot (10^{7} ergs)	Kilovolt
67	7	1700	300	120	6.96	158	1.5
97A	7	2000	300	110	5.50	158	1.5
98A	10	2300	300	137	5.90	158	1.5
98B	13	3500	300	210	5.90	280	2.0
97B	13	3700	300	202	5.50	280	2.0
72	17	2740	450	191	6.96	158	1.5
68	18	4900	300	331	6.96	438	2.5
71	20	3970	300	277	6.96	280	2.0
97C	19	5450	300	300	5.50	438	2.5
74	20	5600	400	204	3.65	280	2.0
73	28	8000	400	306	3.80	438	2.5

TABLE III

DATA FROM THRUSTOR EXPERIMENTS, SECTION 4.2.3
DOWNSTREAM RADIAL PROPELLANT INJECTION,
NITROGEN PROPELLANT

Run No.	Thrust Efficiency η%	I_{sp} (sec)	Delay Time (μsec)	Impulse per shot (dyne sec)	Mass per shot (10^{-5} g)	Energy per shot (10^7 ergs)	Kilovolt	L(cm)
68	18	4900	300	331	6.96	438	2.5	2.0
69	10	3600	300	249	6.96	438	2.5	9.5
70	9	3800	325	219	5.80	438	2.5	16.5

4.3 Thrustor Experiments, Axial Propellant Injection

4.3.1 Apparatus and Performance

Significant improvements in the efficiency of pulsed plasma accelerators have been reported by the General Electric Company.[15] The increase in performance has been attributed in large part to a particular mode of propellant injection and engine ignition. The propellant is injected axially, at some distance from the insulator, and after nearly complete injection, the engine is ignited by auxiliary electrical sparkers.

In contrast, our accelerator development program has featured radial propellant injection, at the insulator, and engine ignition by controlled electric fields. Other parameters in the two programs, such as gun geometry, capacitance, and voltage have been similar.

In the final phase of this contract, and then under Convair support, we have sought confirmation of the advantage of the axial-injection, sparker-triggered mode. This could be done simply by changing the barrel geometry, and the mode of operation of our device.

The new configuration is outlined in Figure 17. The gas valve is the ferromagnetic core valve of Figure 14, operating as shown in Figure 15. The auxiliary sparkers are needed because, with axial injection, the gun does not fire at the voltages and mass loads of interest. The sparker electrodes are installed through the back insulator, and are powered by a 26 kV, 6 joule pulse. The discharge could be triggered at a variable delay with respect to the gas valve trigger pulse.

In all experiments on this device, the propellant was xenon. The experiments were conducted in the manner described in Section 4.2.2. The neutral gas distribution is plotted in Figure 18 for a delay time of 850 μsec which is close to the delay time for optimum thrust. At this delay time, the valve has long been closed, and almost all the propellant is available to the discharge. The gas spreads out into the interelectrode region at an angle of 45° with respect to the axis.

The data from the thrust efficiency measurements are given in Table IV. The average exhaust velocities of the ions are approximate, and were taken from Faraday cup signals. In general, the performance is comparable to or lower than experienced with the radial injection thrustors.

In addition to the performance measurements, some data on the exhaust are presented. A typical Faraday cup signal taken at 4 m downstream is shown in Figure 19. This signal belongs to run No. 91, Table IV, and represents the exhaust from the low gun voltage and medium-mass loading conditions. Upper and lower beams show the same signal, but on a

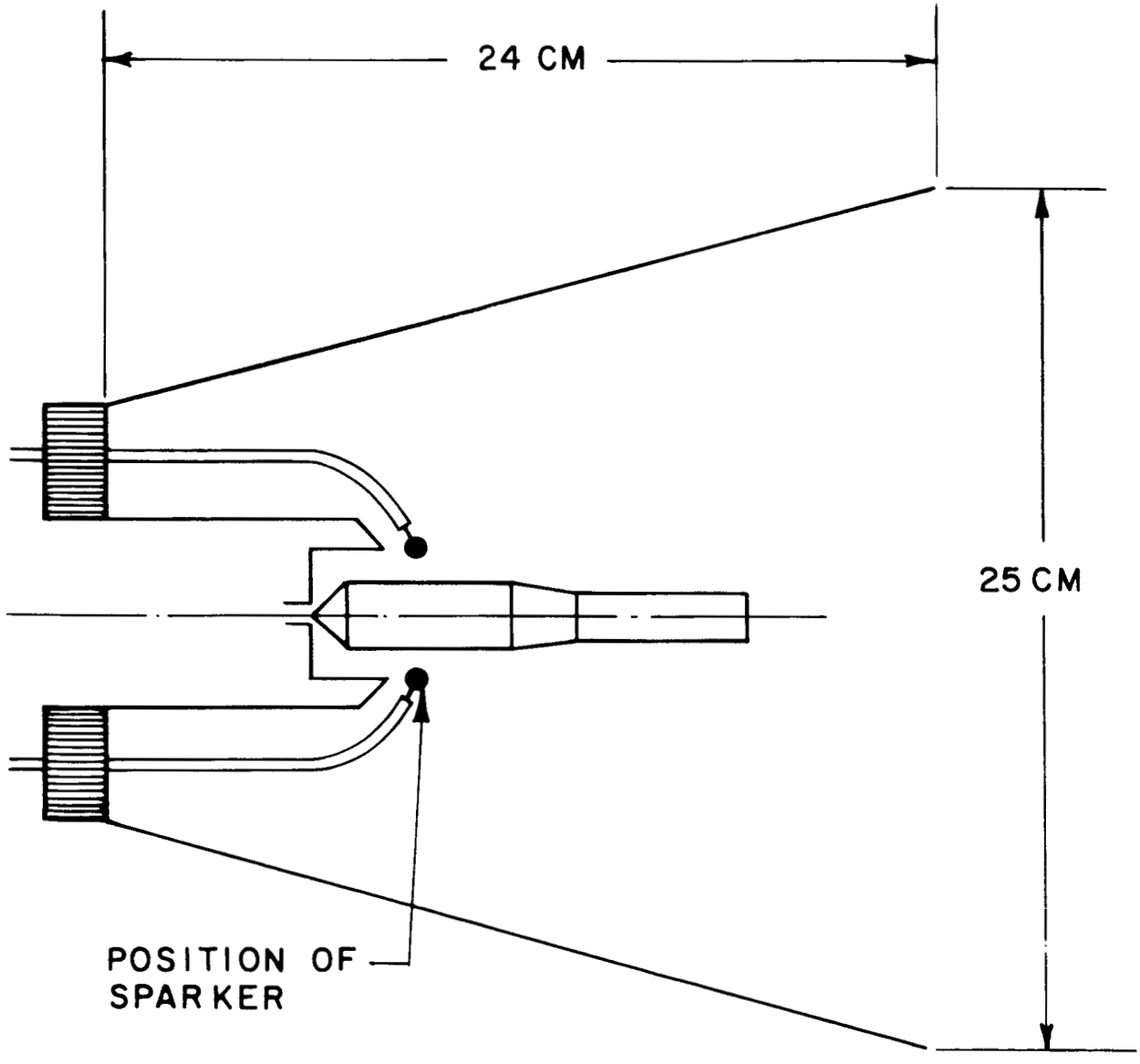

FIG. 17 : OUTLINE OF THE ACCELERATOR WITH AXIAL INJECTION AND SPARKER TRIGGERS

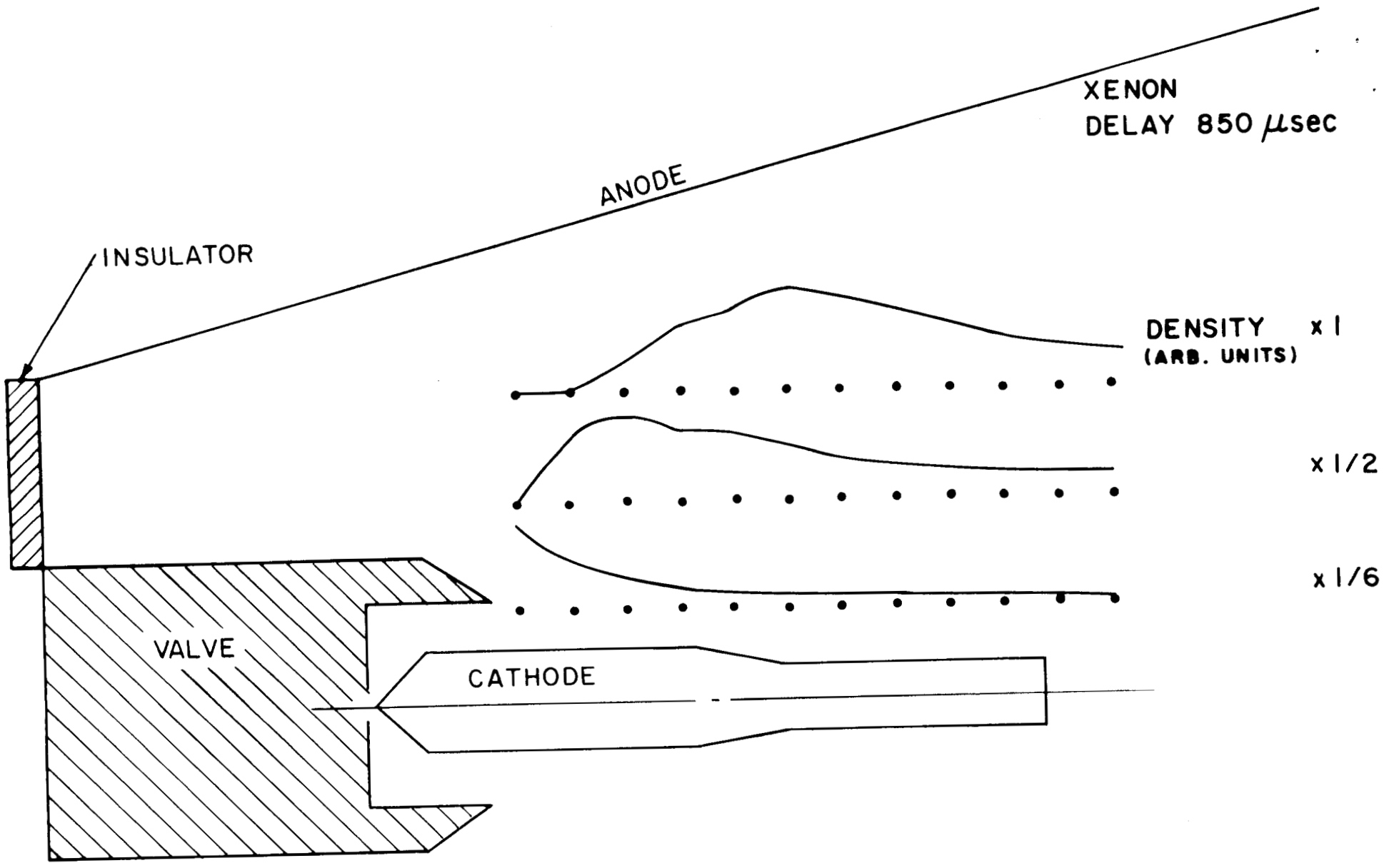

FIG. 18 : GAS DENSITY DISTRIBUTION
(ELECTRODES SHOWN FULL SCALE)

TABLE IV

DATA FROM THRUSTOR EXPERIMENTS, AXIAL PROPELLANT INJECTION, XENON PROPELLANT, SECTION 4.3

Run No.	Thrust Efficiency η%	I_{sp}(sec)	Delay Time (μsec)	Impulse per shot (dyne sec)	Mass per shot (10^{-5} g)	Energy per shot (10^{7} ergs)	Kilovolt	Exhaust Velocity cm/μsec
80	7	1400	850	68	4.7	70	1.0	-
86	8	1800	850	53	2.9	63	.95	-
91	8	1400	850	73	5.2	63	.95	3
87	11	2200	850	65	2.9	63	.95	-
88	12	2900	850	86	2.9	109	1.25	13
83	12	2100	850	72	3.5	63	.95	4
75	13	2100	700	204	9.8	158	1.5	-
92	13	2800	850	146	5.18	158	1.5	5
82	13	3000	850	100	3.48	109	1.25	5
78	14	2500	800	173	6.9	158	1.5	-
84	14	3000	850	103	3.5	109	1.25	4
89	14	3900	850	115	2.92	158	1.50	8
85	16	3800	850	132	3.5	158	1.50	5
79	16	4300	850	202	4.7	280	2.0	-
93	17	4300	850	222	5.18	280	2.0	7
77	18	4100	700	396	9.8	438	2.5	-
81	18	4900	850	205	4.2	280	2.0	-
90	18	5900	850	173	2.92	280	2.0	8
76	20	3400	700	333	9.8	280	2.0	-

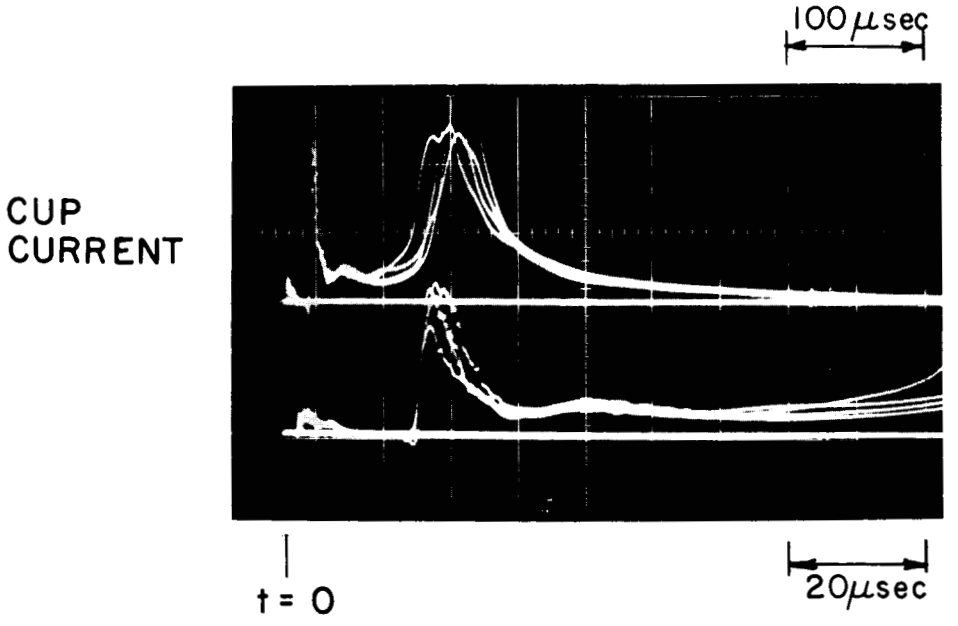

FIG. 19 : FARADAY CUP SIGNALS FOR RUN 91, TABLE IV (FLIGHT DISTANCE 4 m)

different time scale (50 μsec/cm and 10 μsec/cm). The scope was triggered with a pulse from the discharging gun capacitor. The corresponding transients are seen at the beginning of the signal (between 0 and 10 μsec). When the plasma arrives, a large amplitude peak can be seen which is expanded in the lower beam. The meaning of this peak has not been investigated yet. The average plasma velocity is about 3 cm/μsec.

The plasma beam spread was measured with the rotatable Faraday cup for two different mass loadings and three different capacitor voltages (Figure 20). The radius of the rotation arm was 80 cm with the gun being placed in the center.

4.3.2 Comparison with Other Experiments

For the preceeding experiments, we designed the hardware to duplicate the G. E. engine[15] as closely as possible in the time available. The G. E. engine is shown in Figure 21 and is to be compared with our device in Figure 17. The geometries are quite similar, except for the location of the insulator. The gun capacitances are identical within 3% and the terminal connections are both coaxial and minimal in inductance. Xenon is used as propellant in both guns, and the same technique is used for measuring propellant distribution. We find that about 90% of the propellant loading is available to the discharge at a firing delay of about 850 μsec which is optimum with respect to thrust. The main propellant stream is about 45° from the gun axis. Similar conditions are reported by G. E.[15]

In the first experiments, we used three sparkers connected in series at a place corresponding to that in the G. E. gun. At lower $\dot{m}$, two sparkers were used, as shown in Figure 17. The different arrangement gave better reliability in the firing of the gun, but there were no changes in performance.

The performance, measured at Philadelphia, of the G. E. engine and the performance, measured at San Diego, of the Convair engine are compared in Figure 22. The data for Figure 22 are taken from Table IV of this report and Figure II-11 of the report in Reference 15. The lines, labelled by voltage values, connect runs taken at the same voltage. The data points are labelled by mass injection values, mg/sec (G. E.) and mg/shot (Convair). Taking into account the G. E. repetition rate of ten shots/sec, it is seen that in some of the runs, the same capacitor voltage and mass injected per shot were used in both laboratories. By comparing the overall trends, it is obvious that the G. E. results have not be reproduced.

The effect of repetition rate is not likely to be serious over the range of interest. G. E. [15] and Convair (Section 4.2.2) both report changes in performance if the interval between shots is tens of seconds.

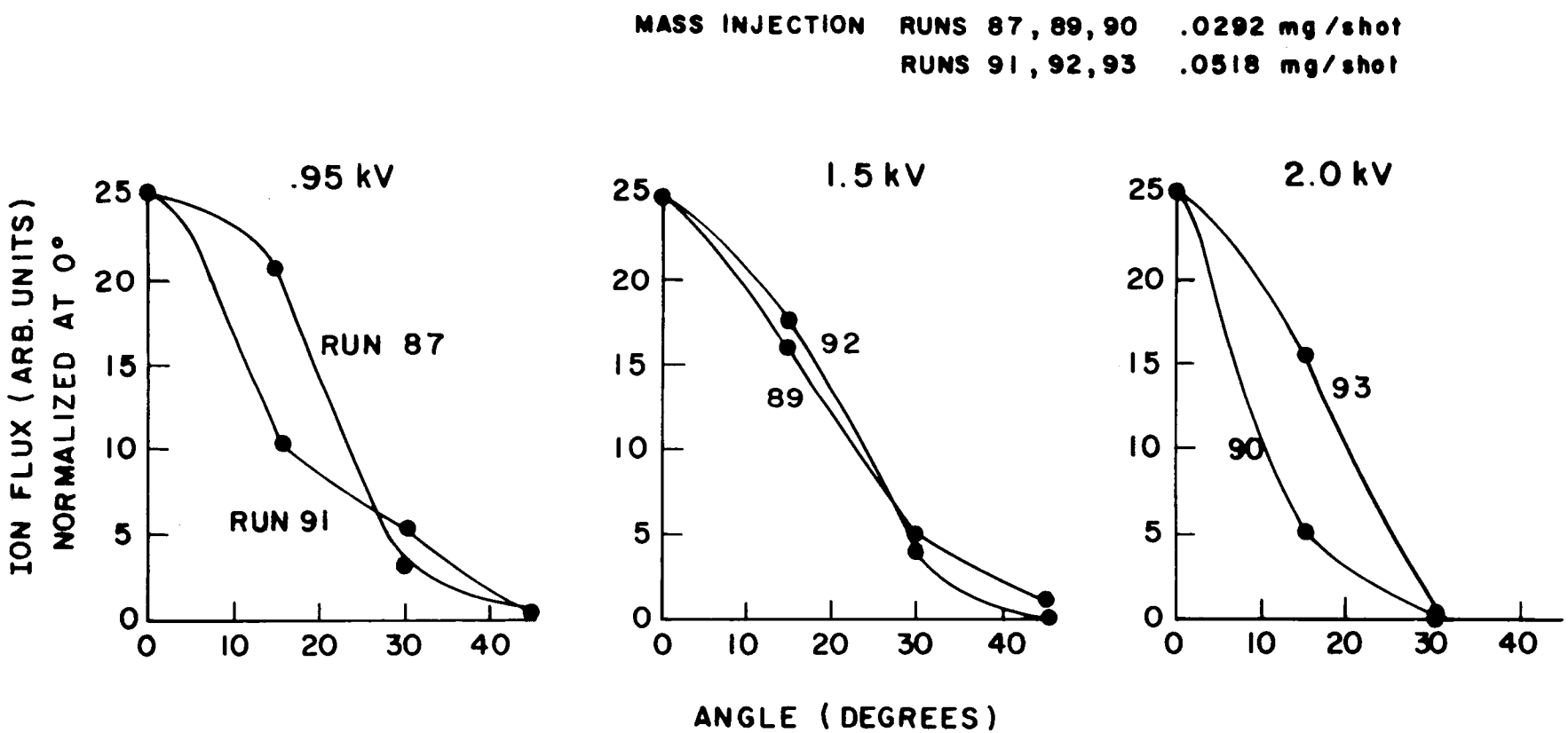

FIG. 20 : ION FLUX PER UNIT AREA PER SHOT vs ANGLE FROM THRUSTOR AXIS

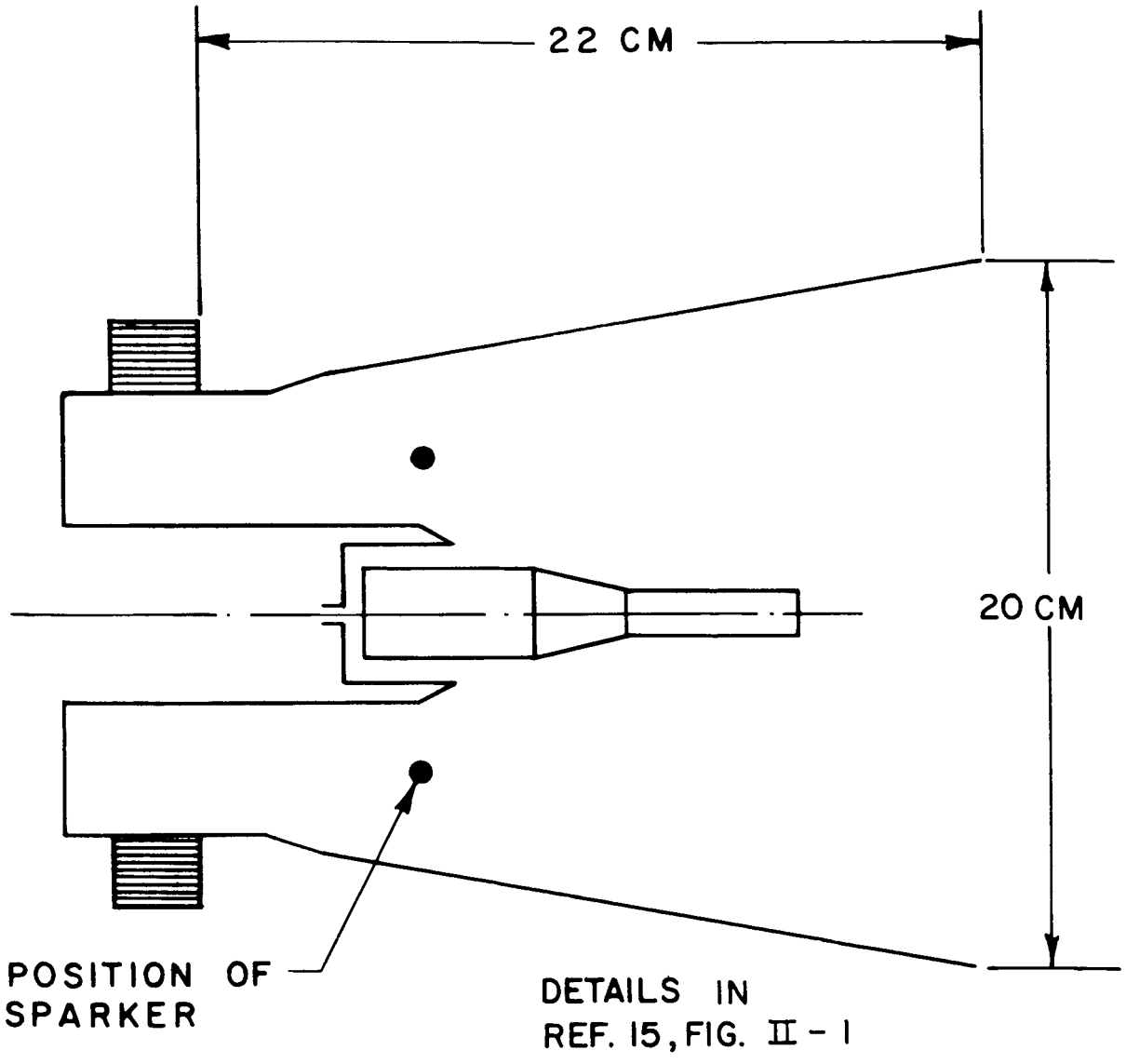

FIG. 21 : OUTLINE OF THE G.E. ACCELERATOR

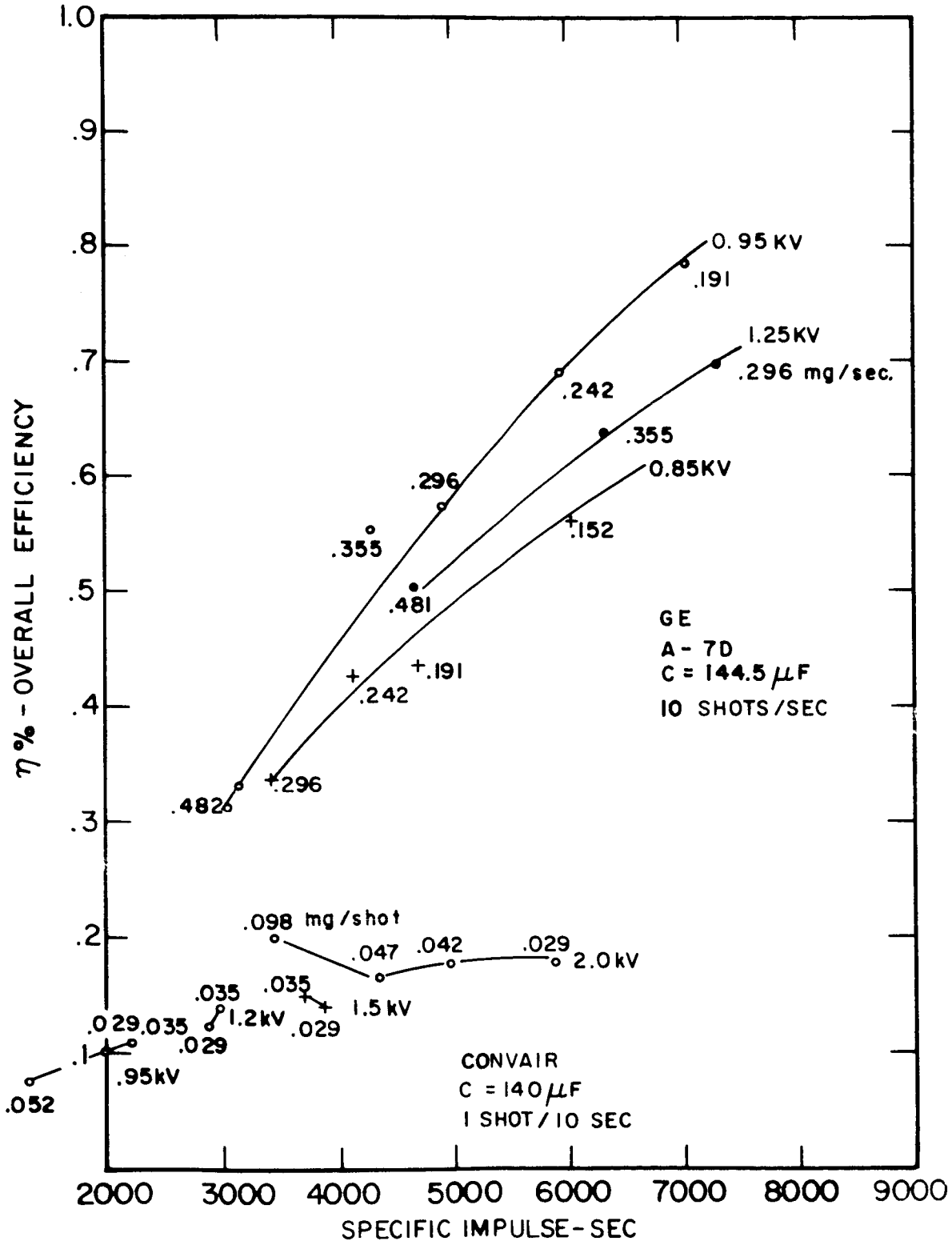

FIG. 22 : COMPARISON OF PERFORMANCE
(GE. DATA FROM FIG. II-11 OF REF. 15)
(CONVAIR DATA FROM TABLE IV)

Neither group has yet checked the effect over the complete range of 10 sec^{-1} to .1 sec^{-1}, which is not directly simple because of the necessity for changes in the instrumentation. G. E. reports no difference between 10 sec^{-1} and 1 sec^{-1}. We observe no effect in the interval between .3 sec^{-1} and .05 sec^{-1}, and only a minor change in performance if the repetition rate is .02 sec^{-1}.

Faraday Cups have been used in the exhaust of both thrustors to measure the flux of ions. The relative amplitudes of the ion current versus flight time are similar in both laboratories for runs taken under approximately the same conditions. Thus the average velocities of the ions are comparable. The angular spread about the thrustor axis of the ionic component of the beam is somewhat less at the G. E. laboratories.

Experiments which could give other possible diagnostic comparisons have not yet been conducted.

One of two alternative conclusions is possible:

EITHER (1) an error in thrust, mass flow rate, or power measurements has been made in one of the laboratories

OR (2) the two devices are truly quite different in operating characteristics.

If alternative (1) is true, then the identification of the specific measurement error would probably strengthen the whole technology of thrustor measurements.

If alternative (2) is true, then the remarkable difference in performance of the devices in Figures 17 and 21 would have resulted from a detail of construction which in itself would be important to discover and understand.

4.4 Summary and Conclusions

The conclusions to be drawn from these measurements are:

1. The firing of the voltage-switched thrustor can be timed over a range of several hundred μsec after propellant injection.

2. At the earliest firing time, equivalent to the propellant-triggered mode, very little of the propellant is in the barrels and is located principally at the insulator. Spoke instabilities then occur.

3. The thrustor will fire in an axially symmetric, stable manner over an interval in which the neutral gas distribution changes from the slug-model approximation to a nearly uniform distribution.

4. The capacitor discharge is approximately critically damped.

5. The calorimetric efficiency, referenced to the stored energy, increases with capacitor voltage and is rather insensitive to plenum pressure. The peak calorimetric efficiencies of 65%-70% occur for propellant distributions which are approximations to the slug-model.

6. The average exhaust velocity and the number of ions in the exhaust are greater for firing delays at which the slug-model approximation is valid.

7. After extensive parametric studies, the overall efficiency of the coaxial gun with radial propellant injection can be classified as typically 20-30% at an I_{sp} of 5000 seconds.

8. In the experiments with the axial injection - electrically triggered accelerator, the efficiency was found to be typically 10-20% at an I_{sp} of 5000 seconds.

9. The average axial velocity of the ions in the exhaust is greater than the average velocity calculated from the specific impulse by as much as a factor of two.

5.0 PULSED ARC THRUSTOR

5.1 Introduction

A pulsed version of the MPD arc was originated by this group about two years ago, and the initial experiments with it have been published.[11] The essential feature is a stationary current sheet through which propellant is fed and accelerated. The pulse length in this quasi-stationary process is readily variable and typically has a value of 10^{-3} sec. These characteristics distinguish the pulsed arc thrustor from the conventional coaxial plasma thrustor (where the pulse time, 1-10 μsec, is determined by the transit time of a current sheet moving over the length of the electrode). The objectives of the experiments to be described were:

(a) to determine the performance potential of the pulsed arc device as a thrustor and

(b) to perform diagnostic measurements leading to an understanding of the acceleration process in the stationary current-sheet mode. These measurements were also expected to contribute to the understanding of the continuous MPD arc but which are more difficult to perform in a steady-state discharge.

The apparatus consists of coaxial electrodes, a pulsed gas valve and a lumped parameter LC discharge line as power supply.

Earlier experiments were performed with an electrode geometry similar to the MPD arcs.[11] The performance as judged from calorimetric and other exhaust measurements was the same or lower than that reported for the continuous MPD arc.

A relatively large amount of erosion was observed at the cathode which could not be eliminated by shaping the cathode in different ways (hollow, conical) or by chosing different cathode materials such as copper, tungsten, or thoriated tungsten. Also the geometry was not convenient for probing the discharge.

Several modifications were made:

(a) The cathode diameter was increased to try to reduce erosion.

(b) A faster gas valve was installed and the valve-gas-port arrangement was modified so that the injected mass flow into the thrustor was constant for most of the discharge and could be calibrated in a simple way. This calibration allowed a comparison of the eroded mass with the gas input.

(c) The interelectrode space was increased to allow access for probes.

It was found that with nitrogen and argon as propellant, the gun current and voltage, the ion energy and ion density in the exhaust were independent of the mass flow rate. With helium as a propellant these parameters turned out to be a function of the mass flow rate. Therefore, helium seemed to carry greater promise for optimizing the thrustor, from the point of view of investigating phenomena that are sensitive to propellant flow, thus helium was chosen as propellant for all experiments reported in the following.

5.2 Experiments

The experiments were performed in a stainless steel vacuum tank of about 1 x 1 x 2 m in dimensions. The gun was located close to one end of the tank but completely insulated from the tank wall. Tank currents were reduced to less than 10% of the arc current by placing an insulating skirt around the anode and by insulating the end dome of the vacuum tank. The background pressure was in the order of 10^{-6} Torr.

A scale drawing of the electrode and insulator arrangement in the new pulsed arc thrustor is shown in Figure 23. The copper electrodes are connected to a capacitor bank which operates as a pulse line with 90 mΩ impedance and 650 μsec pulse duration.

A magnetic bias field is provided to make the discharge symmetric. This field also induces azimuthal Hall currents. The bias field coil is connected to an electrolytic capacitor bank which has a pulse duration long compared with the discharge time of the gun. The average bias field strength in the gun could be varied from zero to 5 kGauss.

An ignitor electrode is situated in the anode - cathode interspace, connected by a small 0.01 μF capacitor to the cathode and charged to about 3 kV. This ignites the discharge as soon as neutral gas appears in the interelectrode space. A fast-opening valve (eddy-current type), described in Section 6.1 injects the gas into the discharge chamber. The gas is fed through six sonic orifices which control and meter the flow rate. These orifices are located close to the anode.

The low back pressure in the discharge chamber has no effect on the mass flow rate. The gas flow could, therefore, be calibrated by recording the pressure rise in the vacuum tank of known volume. The mass flow rate calibration was made by sealing the vacuum chamber and then determining the rate of pressure rise with a McLeod gauge when a constant pressure was applied to the plenum chamber of the valve. This calibration is shown in Figure 24. The volume of the valve plenum was chosen large enough so that its pressure stayed practically constant during the time of gas injection. It is important that the gas flow attains steady-state conditions in a time short compared to the discharge time of the gun. The gas valve opened in 50 μsec, the flow became steady in 100 μsec. This was observed with a 6AH6 fast ionization gauge. The discharge lasted for 650 μsec.

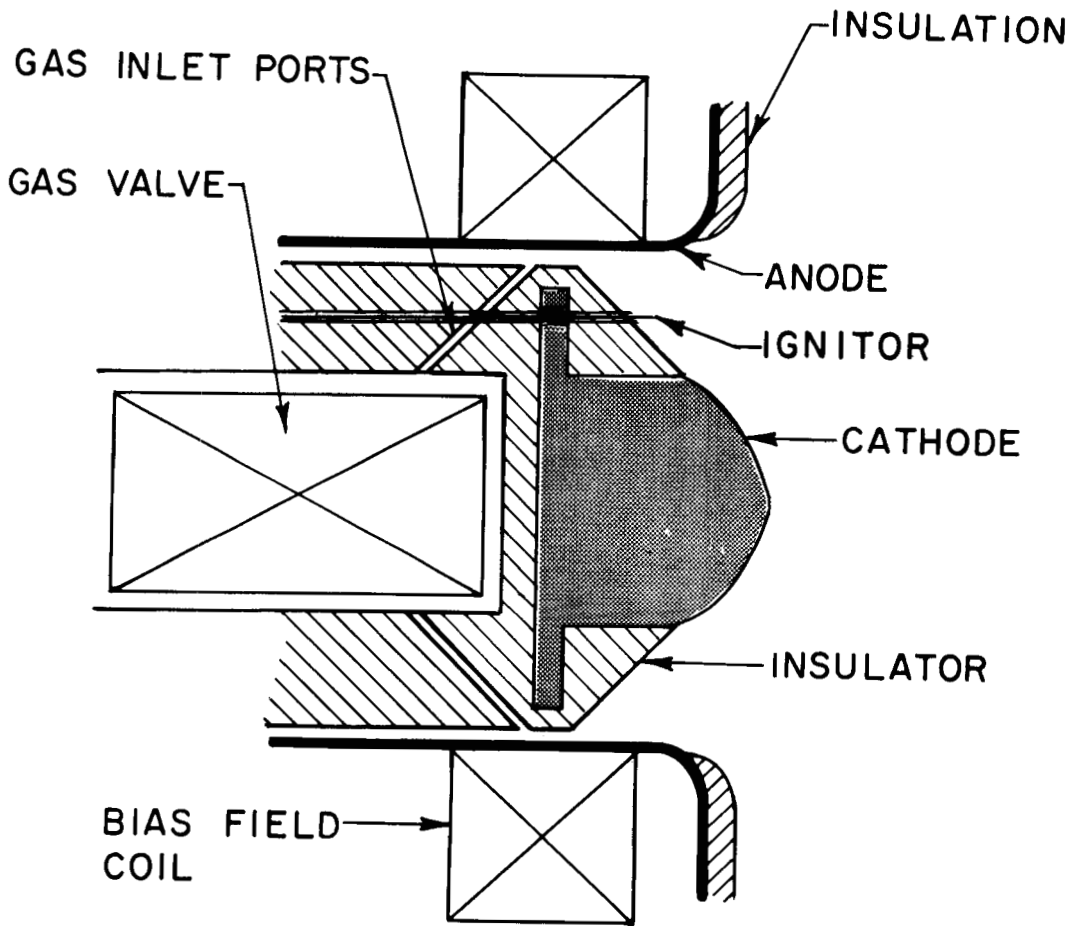

SCALE 1 : 1

FIG. 23 : SCHEMATIC OF THE PULSED ARC THRUSTOR

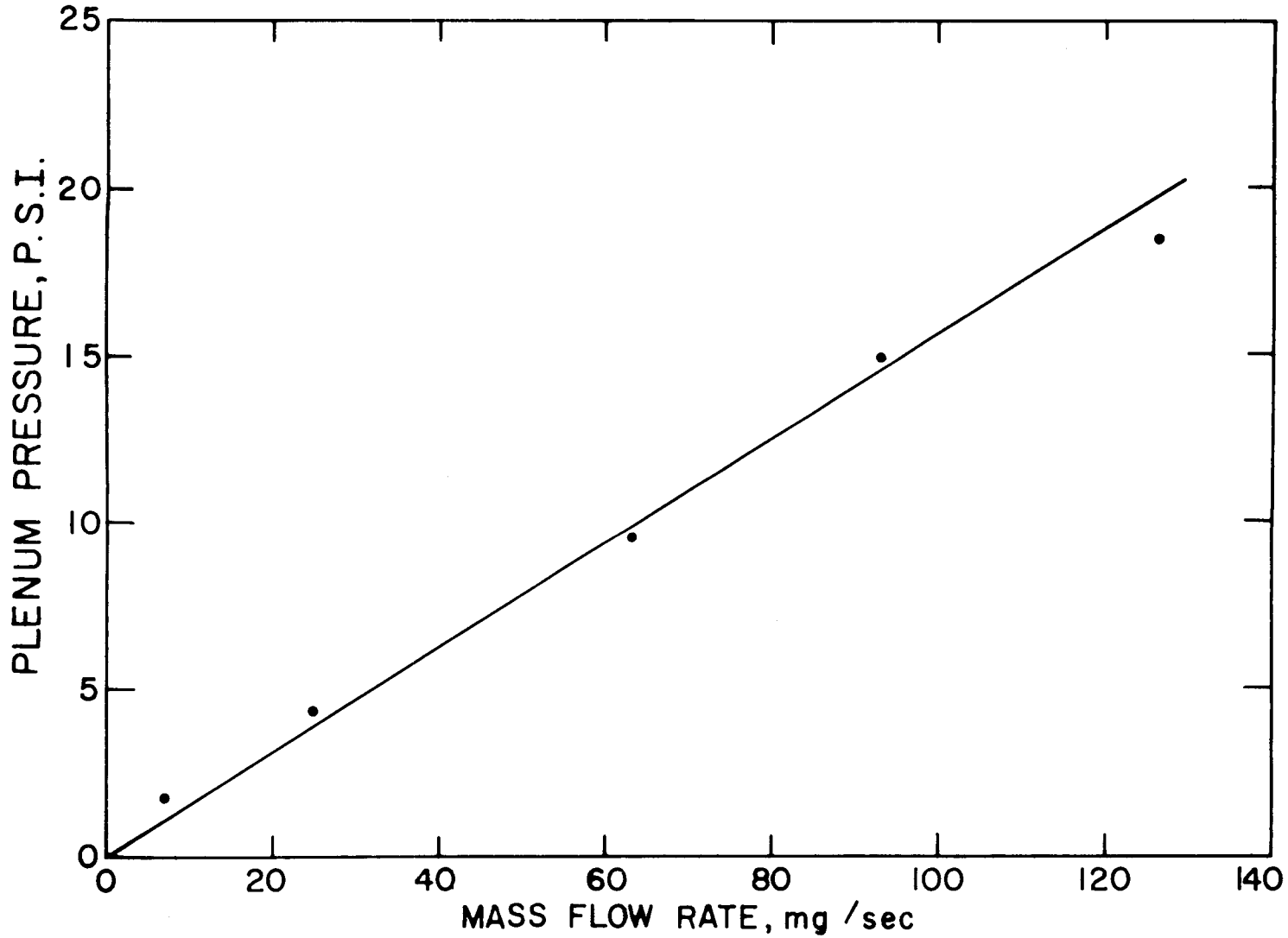

FIG. 24 : MASS FLOW RATE CALIBRATION, HELIUM PROPELLANT

In a series of experiments, the mass flow rate was varied between 30 mg/sec and 300 mg/sec, the bias field between 200 Gauss and 5 kGauss and the power level between 10 kW and 1.5 MW. Over this range of variation, the general behavior of the gun is as follows: A symmetric discharge could only be achieved if the gun impedance was below 1Ω. If this was fulfilled, the gun showed quasi-steady-state behavior; i.e., all measurements had a fairly constant value over the period of the discharge. Within these limits of operation, the voltage at the terminals of the gun stayed between 200 and 400 volts. At constant bias field and constant mass flow rate, the impedance always dropped with increasing arc power. The smallest impedance observed was 3 mΩ.

The high instantaneous power level of 1.5 Mwatt could be achieved without difficulties. The thrustor behaved well, and all the diagnostics gave reproducible signals. The cathode erosion was rather severe, however.

The set of measurements which is presented next was taken at a mass flow rate of 100 mg/sec, a gun voltage of 130 volts, and a power level of about 200 kwatts. The bias field in the region of the discharge was about 400 Gauss. The field pattern, measured with a Gauss-meter, is shown in Figure 25.

The value of current and voltage at the terminals of the gun is shown in Figure 26. The current stays constant for about 650 μsec. The voltage drops from the charging voltage of the capacitor bank to the gun voltage of about 130 V within 100 μsec. The quasi-steady-state behavior is a consequence of the pulse line power supply and the constant mass flow rate.

Figure 27 shows ion energy oscillograms taken in the exhaust with a retarding electric field analyzer[9] consisting of a grid and a collector plate. The lower trace is the grid current which is the same in all the oscillograms and shows the shot-to-shot reproducibility. The upper trace represents the ion current passing the region of retarding electric field. The ion collector signals are about constant up to 30 volt bias potential and drop down between 30 and 50 volts. Assuming single ionization, this indicates an ion energy of approximately 40 eV and a corresponding velocity of a little more than 4 cm/μsec. It was observed that the ion energy varied from about 40 to 150 volts as the power level was increased from 100 to 1500 kW. The ion energy was always less than the energy corresponding to the terminal voltage on the thrustor.

In addition, velocity measurements have been made with a newly developed tool which also could be applied to direct measurements in steady-state plasma thrustors. The development of this tool has not been a part of this NASA contract. But since the initial measurements with the velocity probe were performed on the pulsed arc thrustor under the above conditions, they will be included here.

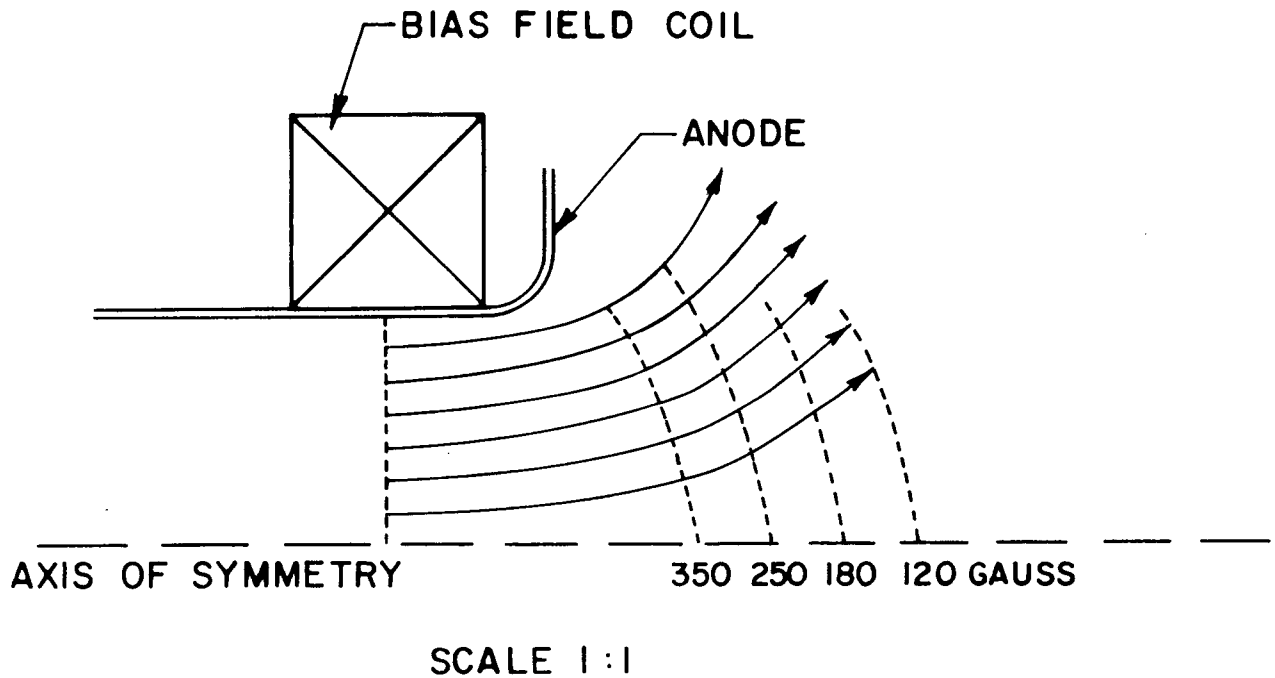

FIG. 25 : BIAS FIELD

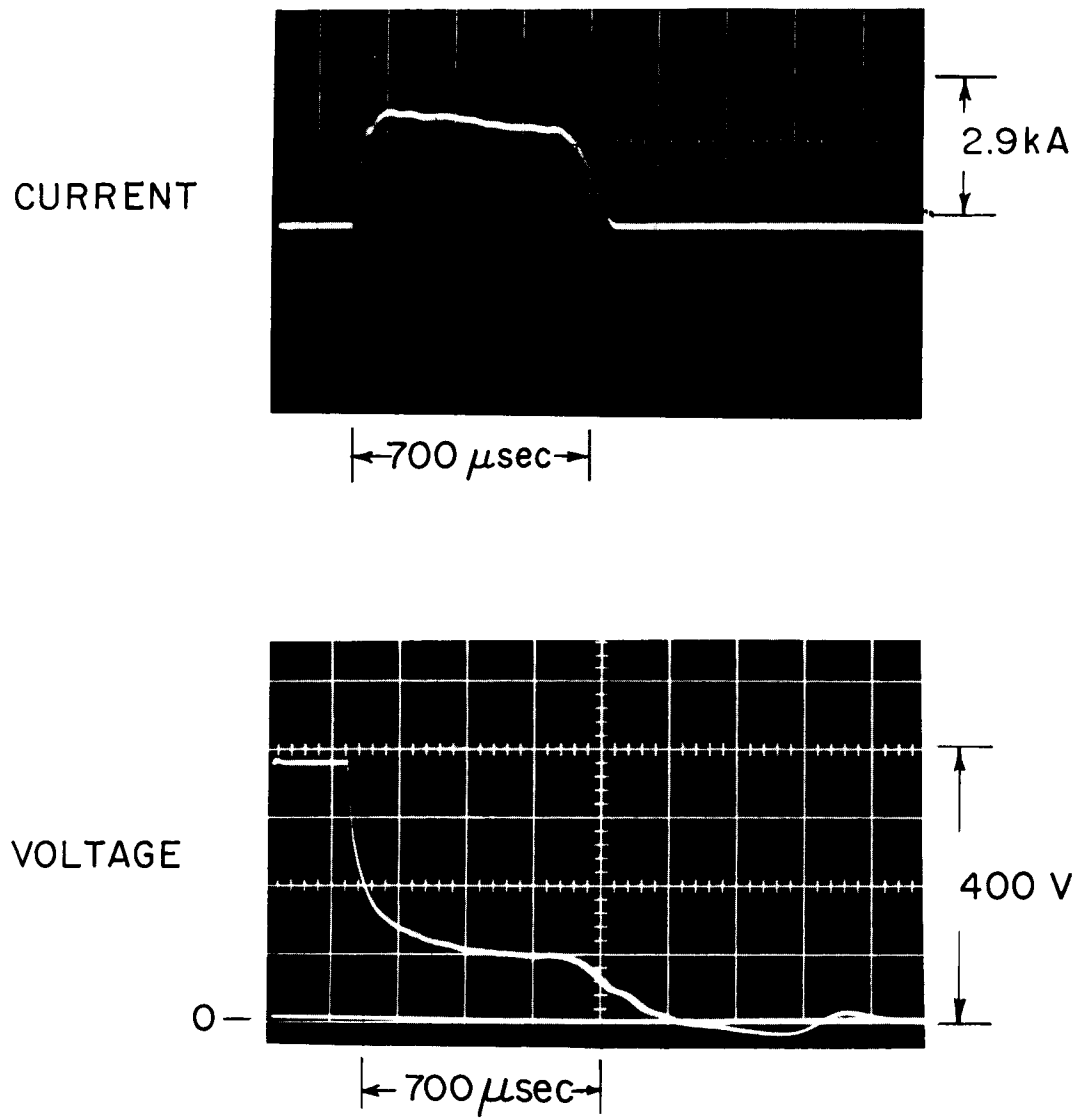

FIG. 26 : CURRENT AND VOLTAGE OSCILLOGRAMS FOR THE PULSED ARC THRUSTOR, HELIUM PROPELLANT 55 P.S.I. BANK VOLTAGE 400 VOLTS

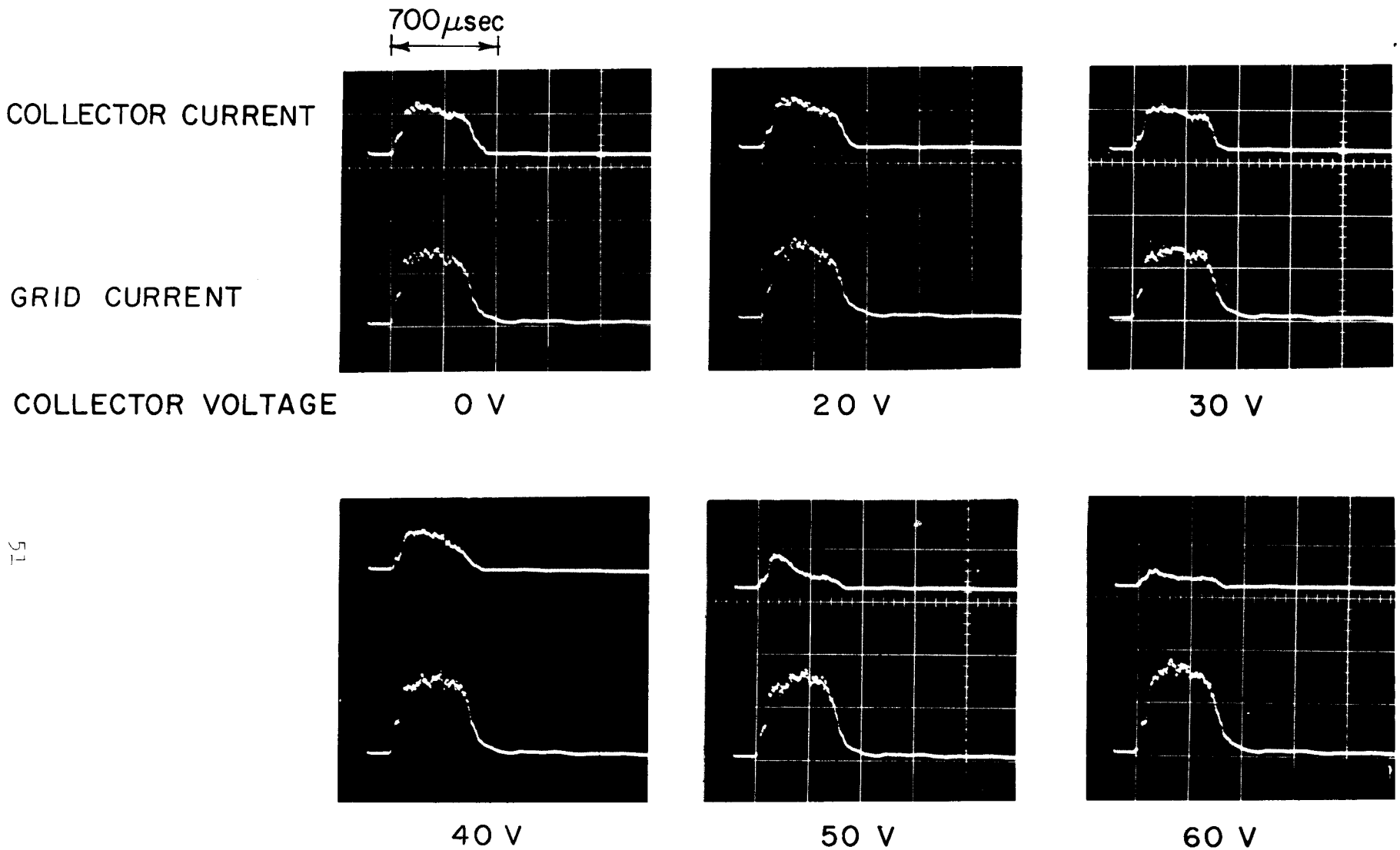

FIG. 27 : ENERGY ANALYZER OSCILLOGRAMS
HELIUM PROPELLANT

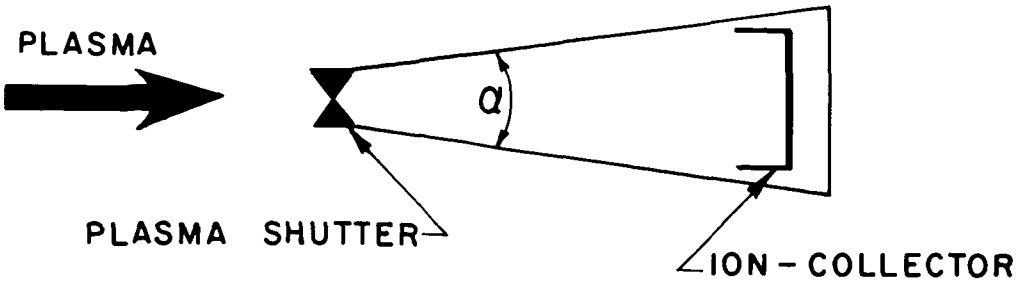

Above is a sketch of the essential features of the probe; the analysis of its operation is given in Section 8.4. The probe consists of a fast electric plasma shutter and an ion collector. The probe operates on the basis of a time-of-flight measurement. The capability of this probe is demonstrated in Figure 28. The lower traces show the open-closed state of the shutter; the upper traces show the ion current arriving at the collector. In the upper photograph the shutter remains open. The upper trace shows the quasi-steady-state ion pulse of the gun. The second photograph shows the effectiveness of the shutter in switching off the ion current. The last photograph shows the opening event of the shutter in a faster time sweep. The arrival rate of the ions at the collector allows us to determine the velocity distribution of the ions. A typical velocity distribution for the exhaust ions of the pulsed arc gun is shown in Figure 29. The measured distribution peaks near a velocity of 3 cm/μsec. Most of the ions have velocities somewhat less than indicated by the energy measurements, assuming a helium exhaust. The discrepancy is probably caused by eroded material. The erosion was considerable, as will be discussed later.

In order to derive the temperature of the ions in the exhaust, an improved velocity probe was employed. Also the terminal voltage of the gun was reduced to about 80 volts in order to minimize cathode erosion. For these measurements, the switch-off event of the shutter was used instead of the switch-on event as used in Figure 28. The signal obtained is shown in Figure 30. The upper beam shows the gun current on a time scale of 200 μsec/cm. The lower beam shows the collector signal (negative going with ion-current) on a time scale of 1 μsec/cm. The transient at the beginning of this signal is produced by the closing of the shutter and is used as a time-zero indication.

Again, the velocity distribution of the ions was determined from the profile of the collector current. This experimental curve is shown in Figure 31 as a solid line. For a comparison, theoretical curves were calculated for a Maxwellian ion gas with an average velocity taken

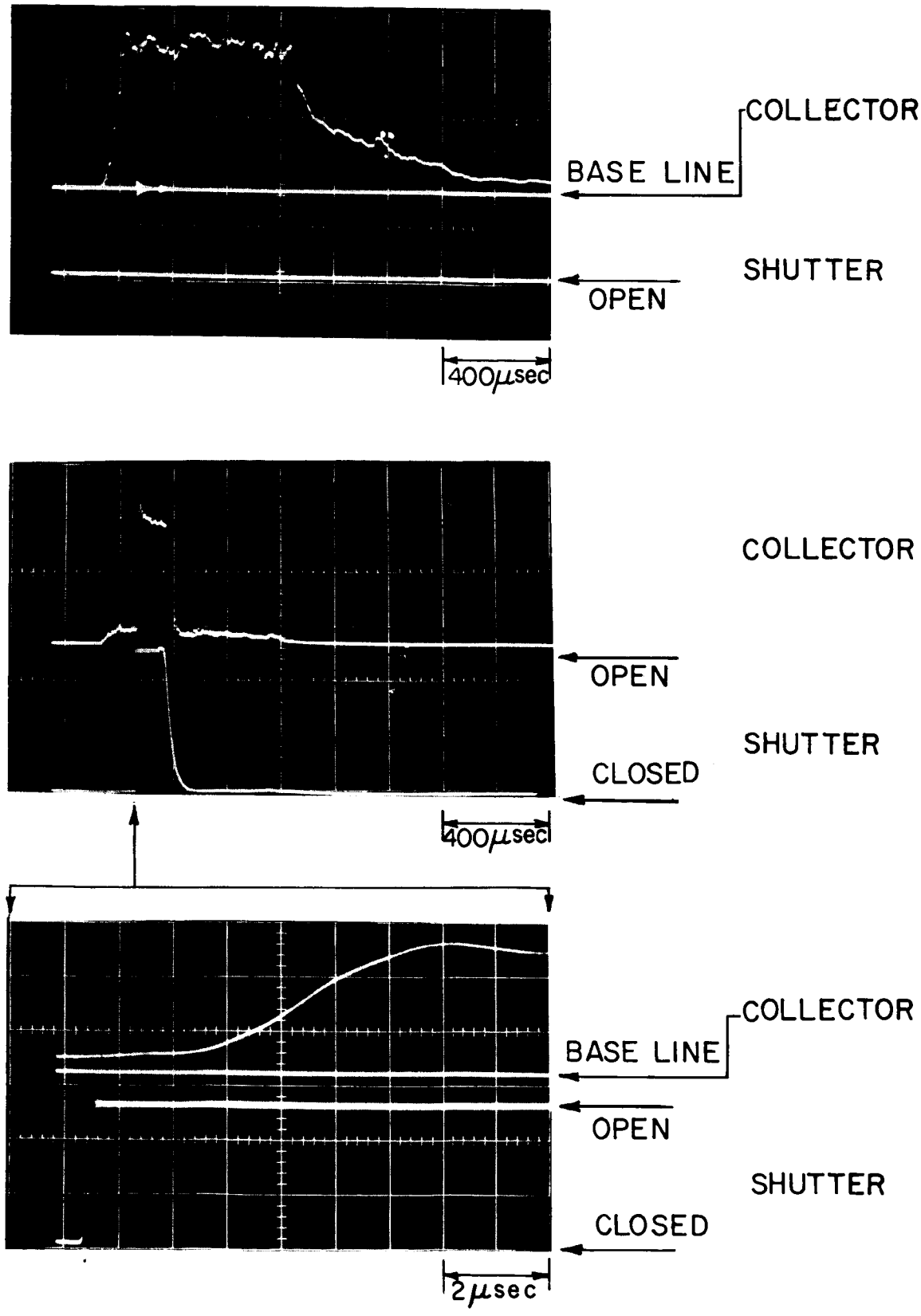

FIG. 28 : VELOCITY PROBE OSCILLOGRAMS

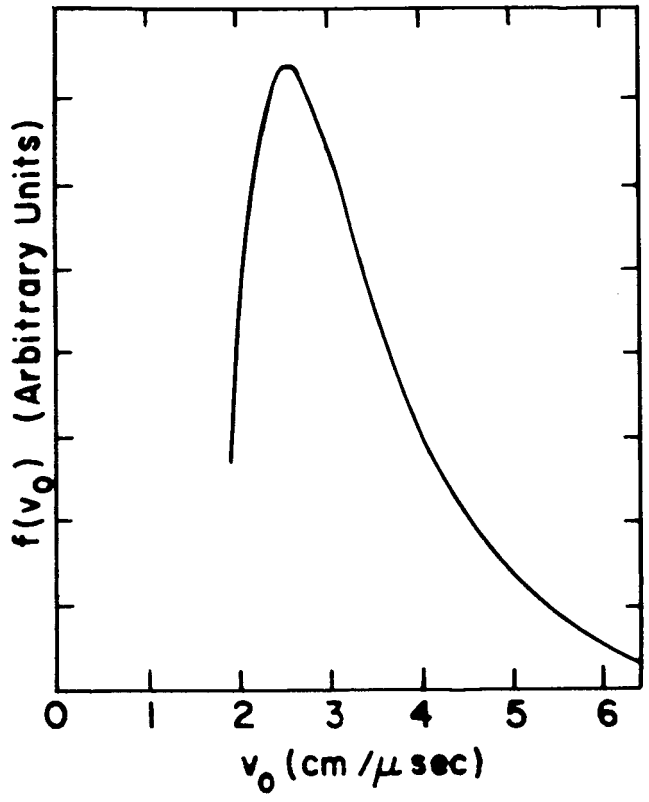

FIG. 29 : ION VELOCITY DISTRIBUTION DERIVED FROM VELOCITY PROBE DATA

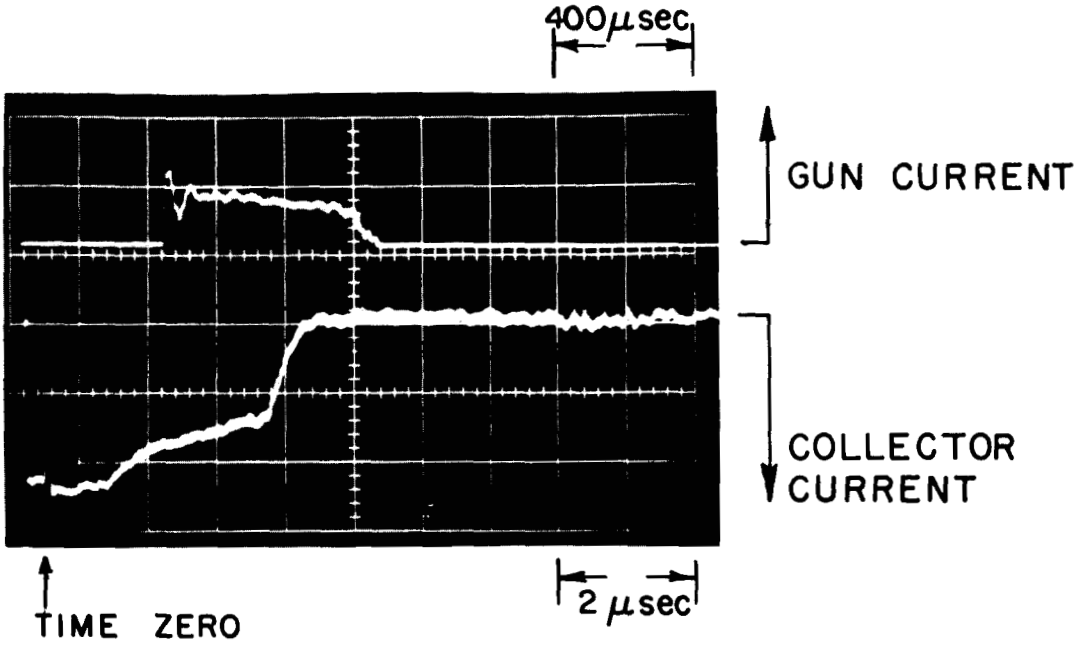

FIG. 30: VELOCITY PROBE OSCILLOGRAM

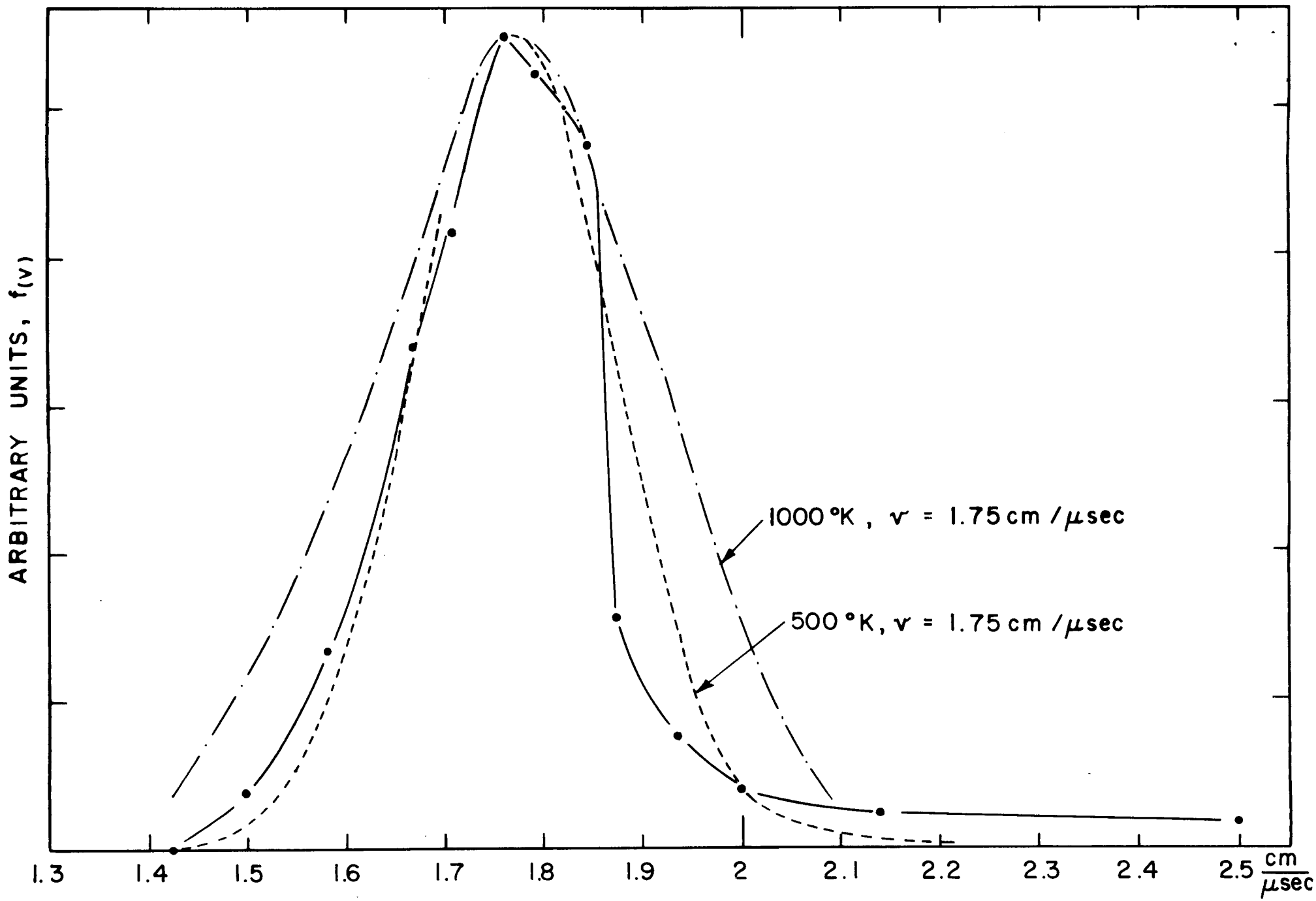

FIG. 31 : ION VELOCITY DISTRIBUTION

from the velocity measurements and with the temperature taken as the adjustable parameter. Two theoretical curves are shown in Figure 31 as dotted lines. The width of the peak characteristizes the temperature. The temperature of the helium ions in the arc gun exhaust seems to be rather low in the range of $500^{\circ}K$. These measurements have to be considered as preliminary though, because the complete absence of eroded cathode material still has to be verified.

A third set of measurements was taken with the main objectives being to determine the dominant axial electromagnetic forces and to estimate the Hall parameter $\omega_e \tau_e$ for the electrons. There are two components to the j x B force which provide axial acceleration, $j_r \times B_\theta$ and $j_\theta \times B_r$, and these have been measured. The power level of the gun was again 200 kW.

Two sets of magnetic field measurements are necessary. The unperturbed field of the bias coil without the gun operating was measured with a Hall effect probe. The self-field of the gun was measured with a conventional loop coil (B-probe). Figure 32 shows one position of the B-probe and also a Rogowski probe which was used to measure the current densities directly. Also shown are the azimuthal magnetic field and the azimuthal current density which were obtained by moving the probes downstream parallel to the axis.

The actual oscillograms of these measurements are shown in Figure 33. Consider the oscillograms at the top. The lower beam shows the Hall current density for the two polarities of the bias field. The Hall current reverses identically with the bias field. This shows that the measured current is indeed the Hall current. The upper beam presents the terminal gun current which proved to be independent of bias field polarity as expected. The lower oscillogram at the left compares the azimuthal current density with the radial current density at corresponding places near the insulator. Note that the scale for the upper beam is ten times larger than the scale for the lower. Therefore, j_θ is more than ten times larger than j_r. A more accurate determination of the radial current density was obtained by measuring the axial gradient of the azimuthal magnetic field. One oscillogram from the measurement of the azimuthal field is shown in the lower right-hand corner.

Total forces due to the cross products of j and B were estimated. The integral of $j_\theta B_r$ was calculated over the volume of the discharge. Since the signal-to-noise ratio on the j_r data is poor, the total force F due to $j_r \times B_\theta$ was estimated by the formula $F = L'I^2/2$, where L' is the inductance per unit length of the barrels and I is the total arc current. The total accelerating force produced by $j_\theta \times B_r$ was found to be about a factor of two greater than that produced by $j_r \times B_\theta$ with the reported geometry and bias field. These measurements are not sufficiently detailed to allow a theoretical analysis of the acceleration mechanism, however, they illustrate that the Hall current is important and that such measurements can successfully be made with the pulsed MPD arc.

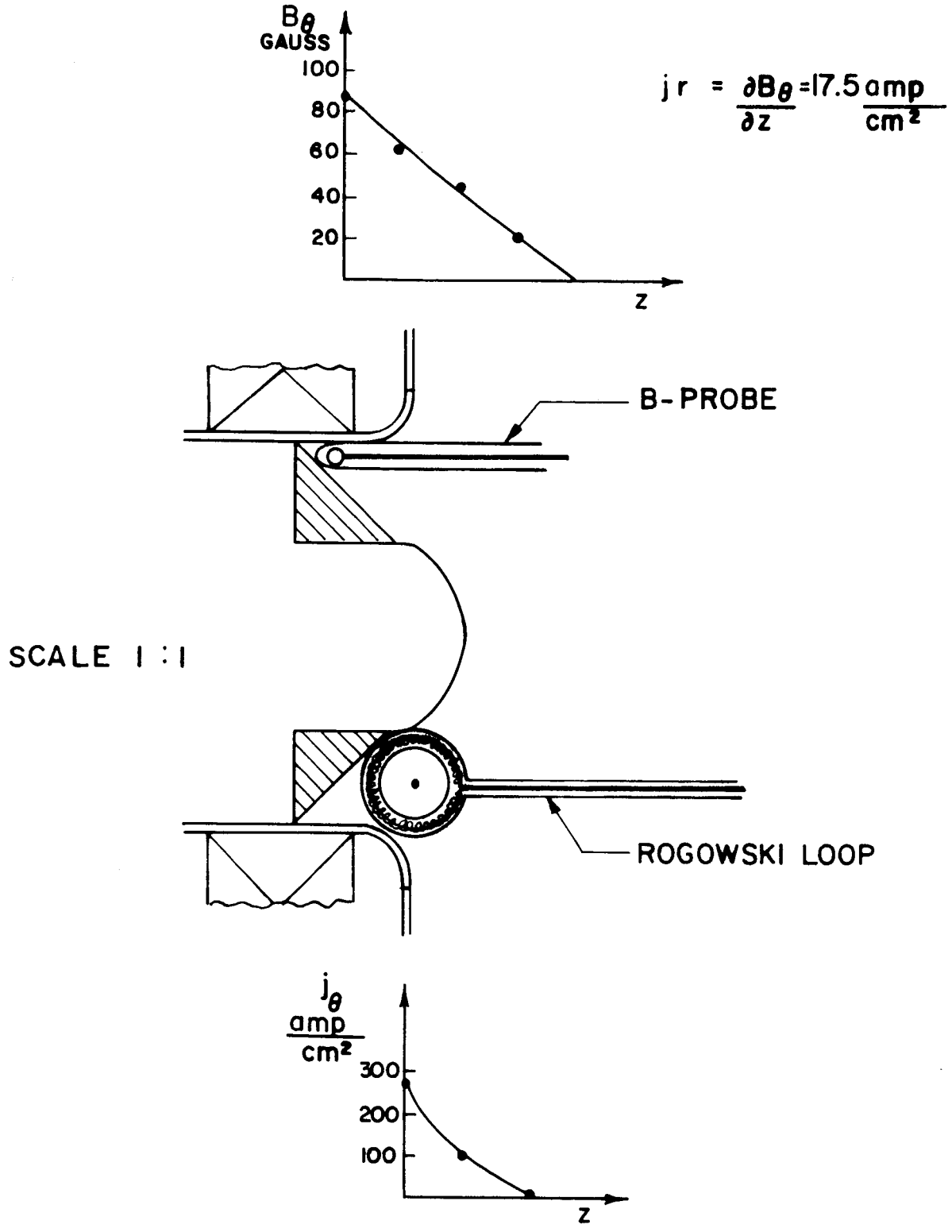

FIG. 32 : DIAGRAM SHOWING THE POSITION OF THE PROBES AND THE MEASUREMENTS OF B_θ AND j_θ

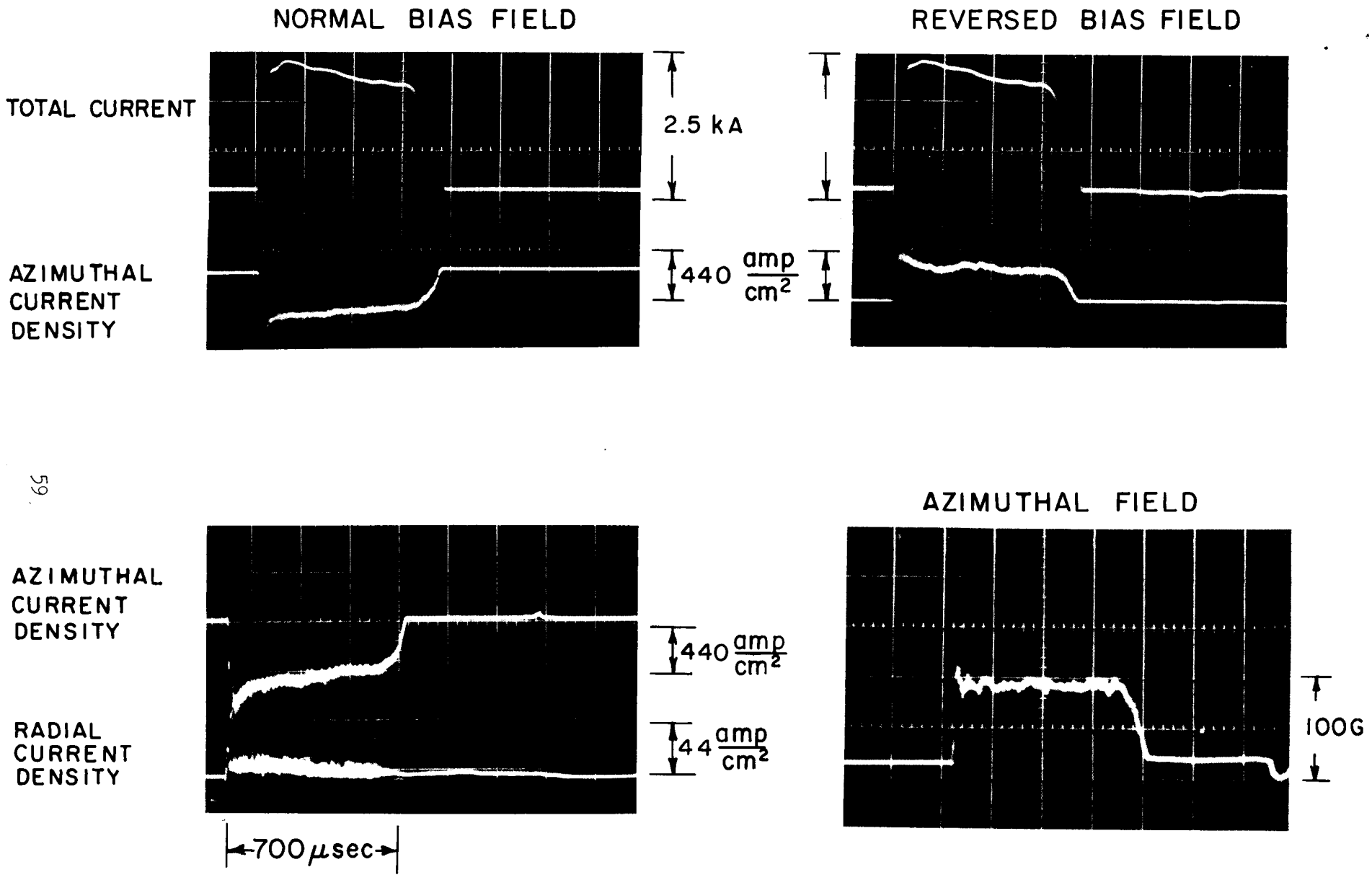

FIG. 33 : OSCILLOGRAMS OF ARC CURRENT, CURRENT DENSITY, AND MAGNETIC FIELD

The probe measurements between the electrodes also allow a good estimation of $\omega_e \tau_e$ for the electrons. Consider the generalized Ohm's law for a two-component plasma.

$$\vec{j} = \sigma \left\{ \vec{E} + \vec{V} \times \vec{B} - \frac{1}{en_e} \vec{j} \times \vec{B} + \frac{1}{en_e} \nabla P_e \right\}$$

Considering the θ component only, the electric field and the pressure-diffusion terms do not contribute because of the symmetry; therefore j_θ is given by

$$\vec{j}_\theta = -\omega_e \tau_e \frac{\vec{j}_e(r, z) \times \vec{B}(r, z)}{|B|}$$

where $\vec{j}_e(r, z)$ is the electron current in the r-z plane and $\vec{B}(r, z)$ is the magnetic field component in the r-z plane. We have measured B and the total current density. The electron current density has not been measured explicitly. If we assume that no ion current flows across the magnetic field lines, the average value of $\omega_e \tau_e$ inside the gun turns out to be near 5. This then is a lower limit for $\omega_e \tau_e$.

In a fourth set of experiments, a survey of the thrust efficiency has been made under various conditions of power, mass flow rate, and bias field.

A ballistic pendulum in the exhaust was used to determine the impulse produced by the thrustor. It is well known that erroneous results can be obtained with pendulums primarily as a result of the surface ablation; this effect is particularly severe in measurements with short-pulse thrustors. However, in pulsed arc thrustor measurements, the rate of energy deposition upon the surface is two orders of magnitude less. The main experimental observations here are not sensitive to such errors.

In what follows, sources of mass other than the neutral gas input are ignored. The thrust efficiency was measured in two ways. The first determination, based on the pendulum, the input power, and neutral gas flow measurements, gave an efficiency, $\eta = T^2/2\dot{m}P$, which increased with decreasing neutral gas flow. Since the thrust was insensitive to the neutral gas flow, values of η up to 100% could be obtained by decreasing $\dot{m}$, the neutral gas flow. The second determination, based on the pendulum, the power and the gridded analyzer measurements gave an efficiency, $\eta' = T\, v_e/2P$, which increased slightly with power but never exceeded 20%. The efficiency η' was also insensitive to the neutral gas flow rate.

The two thrust efficiency measurements are in serious disagreement. This indicates that the mass flow in the exhaust differs from that calculated from the rate of neutral gas input. This effect is well known in the MPD arc.

Some information on mass sources was obtained. Some measurements of weight loss in the cathode and the back insulator were made. It was found that the eroded mass was about proportional to the number of Coulombs of charge which had passed through the gun. The constant was of the order of $2 \times 10^{-4} \frac{g}{\text{Coulomb}}$.

At low injected mass flow rates the eroded mass per shot exceeded the injected mass. As expected in this case, the exhaust velocity was smaller than the apparent specific impulse. At high mass flow rates (30 mgm/sec) and moderate gun current (2 kA) the cathode contributed only 15% to the total $\dot{m}$.

5.3 Summary and Conclusions

The summary of the measurements may be made as follows:

1. The changes made in the electrode structure and bias field coil arrangement have not altered the behavior of the thrustor significantly.

2. Within a wide experimental range the discharge is symmetric, stable, and reproducible from shot-to-shot.

3. The random energy (ion temperature) in the exhaust is low compared to the directed energy.

4. The Hall current density has been found to be an order of magnitude larger than the radial current density. The $j_\theta \times B_r$ force is about a factor of two larger than the $j_r \times B_\theta$ force.

5. The true thrust efficiency of this thrustor with helium propellant at 200 kW and a specific impulse of 2000 sec is probably less than 20%. The obvious difference between the pulsed arc thrustor and the continuous MPD arc is the cathode temperature.

6. At moderate gun currents of about 2 kA and at high values of instantaneous mass flow rate, the cathode erosion constitutes a minor contribution to the propellant flow.

7. The thrustor has been operated successfully at power levels up to 1.5 MW.

These measurements demonstrate that the pulsed arc thrustor can be used to study MPD arc phenomena, and at very high power levels, if necessary.

Unique measurements have been performed which show the presence of a large Hall current in the discharge and a relatively low ion temperature in the exhaust. Cathode erosion remains a problem in the present arrangement. Yet, we see potential possibilities in using the cathode erosion as a production mechanism for metallic vapor propellant, if liquid metal is fed to the cathode surface. This is of particular interest in connection with the simple triggering mechanism described in Section 6.2.3.

6.0 PROPELLANT INJECTORS

Until this year, propellant injectors in our laboratory have been built only to effect a particular research purpose, and propellants such as nitrogen and xenon have been chosen for their handling convenience. During this contract, practical engineering problems such as energy consumption, reliability and simplicity of the injectors have been considered. A number of mechanical and non-mechanical injectors have been built, and preliminary experiments conducted on each. These injectors include types which are suitable for pulsed injection of metallic propellants. For the most part, the operating mode is for radial propellant injection.

6.1 Fast Gas Valves

The operation of very fast gas valves is almost invariably electromagnetic. The reasons are twofold: first, the driving force can be applied in extremely short times and with nearly perfect control as to the time of application, and second, the "fluid" which acts upon the moving material element in the valve has no limiting "sound speed" itself, short of the velocity of light.

In applications where speed of opening is of greatest importance, and where size or mass of the associated circuitry and energy supply is not an important constraint, it is usual to employ thin metallic diaphragms driven by very rapidly applied magnetic fields. During the time interval between switching on the field against one side of the diaphragm and the diffusion of the field through it, there is a strong flow of eddy currents in the metal; these interact with the field and result in a strong acceleration of the conductor away from the field. Extremely rapid acceleration can be achieved this way.

If, however, the quantity of energy necessary to operate the valve is itself an important consideration, the eddy-current valve appears much less favorable. The reason is simply that it is very difficult in such a device to deposit the majority of the magnetic energy where it is needed, i.e., in the immediate vicinity of the moving diaphragm surface. One may consider the use of "flux concentrators" to produce a more efficient field distribution; however, these do not seem to have been employed very effectively to date, if, indeed, they can be at all.

We have investigated three concepts for fast gas valves; one is based on the principle outlined above of an eddy current driven disk, in another a solenoid is utilized to compress a spring which is subsequently released to drive a lightweight hammer into impact with a valving element, and the third uses a ferromagnetic core. In all cases the energy required to open the valve is small compared with the energy delivered to the plasma. The experiments described below indicate that a gas valve need not limit the performance of pulsed plasma thrustors.

Two methods were used to measure the opening of the valves, first by photoelectric sensors, and secondly, by measuring, by means of a fast-ionization gauge, the gas emitted into the vacuum chamber.

Disk Valve Driven by Eddy Currents

The valve is shown schematically as follows:

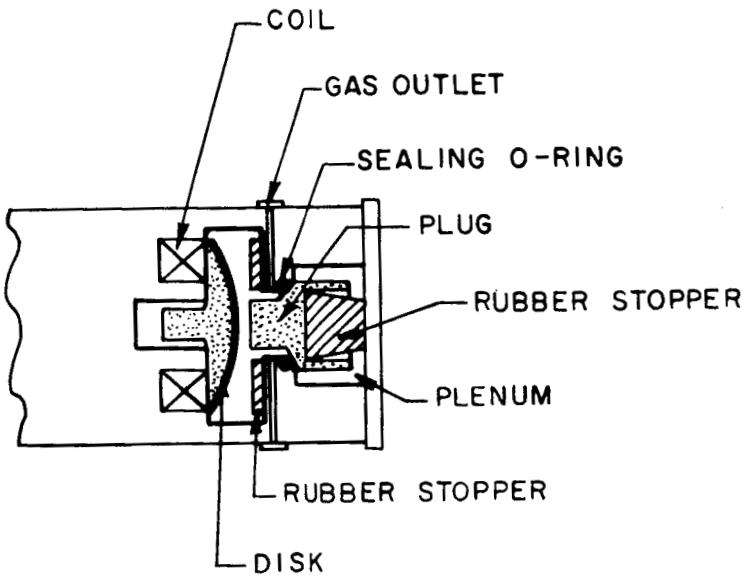

The disk is allowed to accelerate to its terminal velocity before impacting the sealing plug. This valve is in contrast to similar valves in which the disk itself opens a seal during its initial movement. The arrangement above allows a longer time for the magnetic forces to act and, thus, a relatively higher impedance for the force coil which can be matched to the energy storage capacitor.

This valve opens in less than 100 μsec, takes only 10 joules, and has survived 50,000 operations without damage. The basic losses are ohmic heating in the coil and in the disc.

Solenoid-Cocked, Spring-Actuated Valve

This valve employs a solenoid to compress a spring, then utilizes the spring energy for actuation. Since the solenoid plunger is used only for compressing the spring, the weight and velocity of the plunger do not limit the opening time of the valve. The mechanism, shown schematically in Figure 34, consists of a solenoid, (Guardian g-57458), a lightweight hammer, a permanent magnet, a sealing ball and a combination plenum chamber and ball seal. Three springs are required, the main energy storage spring,

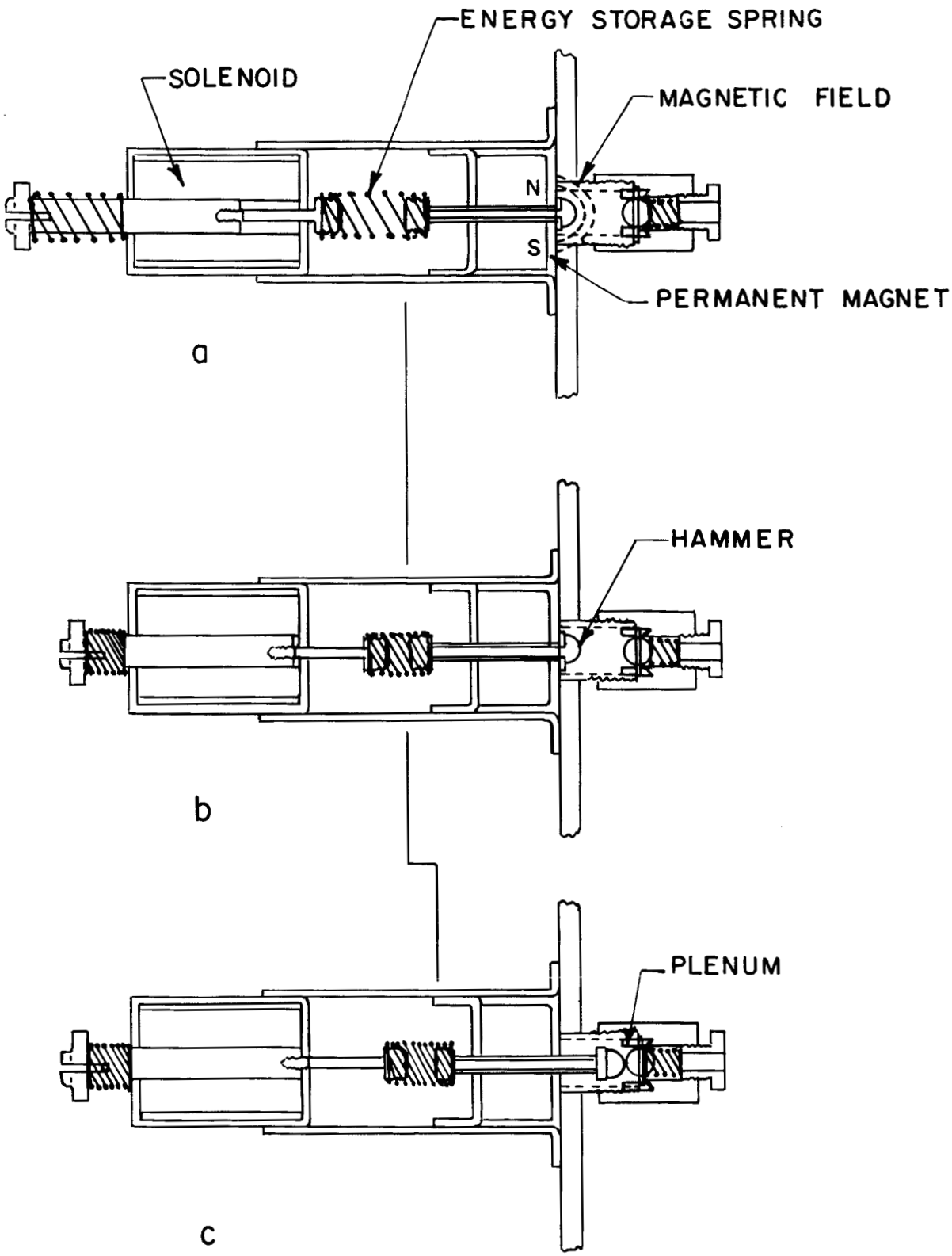

FIG. 34 : SOLENOID-COCKED, SPRING-ACTUATED VALVE

a ball seal spring, and a light spring for returning the solenoid plunger after each stroke. Referring to Figure 34(a), shows the valve in the normal standby condition prior to application of power. The hammer is held in position by the permanent magnet and the gas is sealed by the spring-loaded ball. Both the energy-storage spring and the solenoid plunger return spring are unstressed and in their free lengths. Actuation is initiated by discharging a capacitor through the solenoid. The solenoid armature is driven forward, compressing the energy-storage spring. During the compression stroke, Figure 34 (b), the hammer remains locked in position by the permanent magnet until impacted by the solenoid plunger. The impact unseats the hammer and transfers momentum from the plunger to the hammer. The hammer is then accelerated by the force exerted by the energy-storage spring, reaching maximum velocity at impact with the ball. During the final travel the hammer enters and seals the upstream end of the plenum chamber. The trapped gas is released upon impact of the hammer and ball as shown in Figure 34(c). The opening time of the valve is independent of valve closing time. The seal is closed by action of the valve seal spring before the energy-storage spring withdraws the hammer from its plenum seat. The solenoid plunger and hammer then return to their original positions shown in Figure 34(a).

The rise time of the gas pulse released by the valve and the effects of variation in spring constants and stroke were measured. Best performance obtained to date is a rise time of 125 μsec obtained with an energy input of 3 joules.

Potential reliability was demonstrated by the successful completion of 252,000 valve operations with no apparent degradation of the mechanism. The valve seal did, however, gradually deteriorate due to contaminants. After 150,000 operations the seal was restored by washing with alcohol. Thereafter, the contamination rate was observed to be less. After 252,000 operations the gas leakage was measured as approximately 1 lb per year if the seal is made against 0.1 atmosphere of nitrogen. The contamination rate should be appreciably less after selection of better materials.

Ferromagnetic Core Valve

The operating principles of the ferromagnetic core valve are given in Section 9.0. The first experimental mechanism is sketched below :

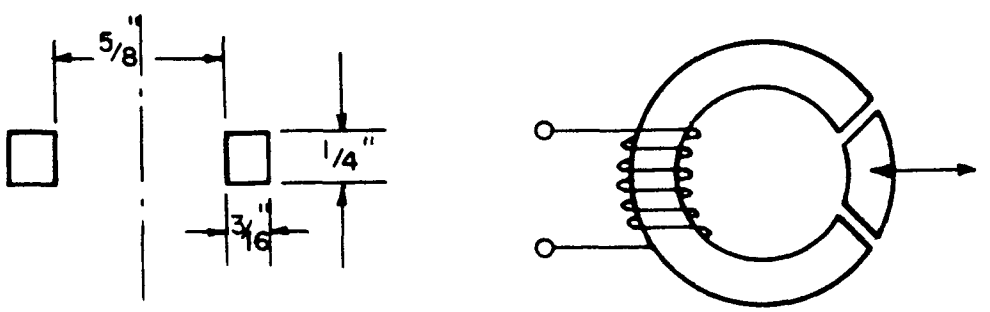

It is made from a toroidal core (Arnold T5651 L4V), with a 60° sector serving as the movable armature. The armature is held in place by a Be-Cu leaf spring which also provides the restoring force toward the null position. A 5 mm diameter hemisphere is attached to the armature: the ball, seated against an O-ring, forms the valve itself. Forty turns were wound on the core. It was fed from a 125 μfd electrolytic capacitor charged to voltages between 20 v and 150 v, and switched with a silicon controlled rectifier. Opening times of one to three hundred microseconds for fractional millimeter gaps have been obtained, and energies of about 40 millijoules are all that is required - typically, 25 volts on the 125 μfd capacitor. The total gas pulse duration was typically .5 to 1.0 millisecond.

As shown in Section 9.0, this design features economical use of the magnetic energy in the system. From experiments with the first prototype, it was determined that the theoretical estimates in Section 9.0 are fairly accurate and can be used for further design improvement. It is anticipated that with reasonably careful packaging, the entire valve, together with its energy-storage capacitor and switching electronics can probably be put into a single cubic inch. The 25-volt supply requirement also conforms nicely to available spacecraft voltages. The mechanical operation is simple: the parts should have good lifetime.

A new valve was designed for faster operation and packaged to suit the requirements of propellant injection in coaxial thrustor experiments. In Figure 14, it is shown in the position for radial gas injection at the gun insulator. In this design the gas pulse is shut off by the closing of the reservoir. The new valve operates on less than 0.1 joule. Nominally the gas pulse has a duration of 250 to 500 μsec. With careful adjustment of the parts, a gas pulse duration of less than 250 μsec can be obtained. The valve has been tested successfully to 28 million shots at 110 shots/sec without seal deterioration.

6.2 Metallic Vapor Injectors

6.2.1 Choice of Metal

The use of metals as propellants for the pulsed plasma gun has several possible advantages. The first is their relatively convenient storage during actual space flight missions. The low ionization potential of some metals may lead to an improved performance of the gun by minimizing frozen flow losses. In order to avoid the losses associated with secondary ionization, a large energy gap between the first and second ionization level is desirable. The metals with low molecular weight possess the larger energy gap. On the other hand, a high molecular weight is advantageous because the kinetic energy of the exhaust for a given specific impulse scales with the molecular weight, while the dominating losses from the plasma scale with the ion number density.

A low vapor pressure and a low melting point are desirable for the propellant metal. Sodium, potassium,cesium,gallium, mercury, indium, and tin are likely choices. By forming mixtures the melting point can be reduced below room temperature and the value of the surface tension can be changed. Since in a zero g environment the surface tension is a dominating force it can be used for pumping the propellant from storage to the thrustor. The following table gives some relevant properties of the metals being considered as a propellant.

	Molecular Weight	Ionization Potential I (eV)	Ionization Potential II (eV)	Melting Point (°C)	Boiling Point (°C) at 760 mm Hg	Vaporization (cal/g)	Surface Tension (dynes/cm) Near Melting Point
Li	6.9	5.4	75.3	186	1336	4680	394
Na	23.0	5.1	47.1	97.5	880	1005	200
K	39.1	4.3	31.7	62.3	760	496	86
Ga	69.7	6.0	20.4	29.8	1983	1014	735
In	114.8	5.8	18.8	156.4	2087	468	340
Sn	118.7	7.3	14.5	232	2270	573	526
Cs	134	3.9	23.4	28.5	670	146	40
Hg	200.6	10.4	18.7	-38.9	356.9	69.7	465

The choice of the liquid metal propellant represents a compromise between several different properties of the metal. Theoretical considerations alone are not sufficient because the physical mechanisms involved in the functioning of the gun are not yet completely understood. Thus a program of empirical variation is needed.

6.2.2 Injection Schemes

Continuous liquid metal feed systems have already been developed for the ion engines. These feed systems can be used to feed the metal propellant from storage tanks to the pulsed plasma accelerator. The problems to be solved are those of economical vaporization of the metal and proper deployment into the discharge region.

The requirements of optimum initial propellant distribution in the gun, precise timing and reliability make the development of such a pulsed injector a non-trivial task. There are several avenues of approach. We may consider first those schemes in which the metal is vaporized and driven into the discharge by the main current pulse itself. The metal can either be driven off the insulator or off the electrode surface.

The explosion of a thin metal film off the insulator requires that this film be replaced between shots. This has actually been accomplished,[16] but at the price of a complicated system of moving mechanical parts and a carefully adjusted vaporizing oven. Further, there is no apparent way to

embody such a scheme in a coaxial geometry.

Liquid metal propellant might be fed to the surface of the electrodes through capillary ducts in close array, or fed along narrow surface channels on the electrodes. The principal objection to this scheme is that in order for the propellant to get from the electrode surface and properly distribute itself in the interelectrode region, it must acquire transverse velocity of the same order as the axial velocity to which one wants to accelerate it. Consider the example of propellant evaporation from the center electrode (cathode) of a coaxial gun. In order that the mass be uniformly accelerated, (thus minimizing losses associated with axial velocity spread) the mass density, at the time of the shot, should vary as r^{-2}, as does $|\vec{j} \times \vec{B}|$. This is a less stringent requirement than uniform distribution, but it is still impossible to achieve with thermal evaporation speeds. Sodium vapor at 2000°K, for example, would expand only about 1 mm away from the surface in a microsecond.

The production of vapor by the main current pulse from localized liquid surfaces on the insulator also suffers from the lack of proper initial propellant distribution. Distributed liquid surfaces on the insulator might be used to overcome this objection but the feed systems and the actuation control tend to become complex. Furthermore, one could expect the main discharge energy to be distributed unevenly into the propellant.

We conclude, then, that the propellant must be introduced into the gun as a vapor prior to the main current flow. It appears here that two alternatives are possible. The first is to create the vapor in a steady-state way in an oven, for example, and to inject it with a pulsed control element. The engineering of a pulsed mechanical valve which is reliable in an alkali metal vapor atmosphere appears formidable, although perhaps not impossible. Another possibility is to control the output of the oven with supersonic bistable fluid elements. This scheme is simple, reliable, and admits unionized vapor to the barrels. In principle it is possible to build a device that meets our requirements of pulsing frequency, pulse length and amplitude. The principal objection is the propellant leakage in the "off" state. An advance in the fluid element technology would make the devices attractive for our purposes.

The second alternative for vapor injection is to vaporize the metal in bursts by electrical discharges, and to do it at the injection point. These evaporation schemes are much like the electrode or insulator evaporation method discussed earlier, except that the vapor is created by an energy source separate from the main bank, and at an earlier time than the main discharge. One such possibility is to incorporate an exploding wire into the inner barrel. The obvious disadvantage is the mechanical system which is needed to feed the wire.

The most attractive methods for vapor injection are the schemes which use liquid metals and which combine the technological principles of the exploding wire and of the arc cathode spot. Specific embodiments of

this approach have been built and tested.

One system, shown in Figure 35, consists of a tube containing the liquid metal propellant, and a second electrode, which in the accelerator application would be either an interior surface of the inner coaxial barrel, or a second liquid metal electrode, as in the figure. A small induction coil is wound tightly around the tube near its end. Normally, the propellant meniscus at the end of the tube and the second electrode surface are separated from each other; however, a current pulse in the induction coil "pinches" the liquid column, and forces it outward as a droplet so that a spark, energized by capacitor C, occurs. This spark establishes a cathode spot on the liquid metal which evaporates a portion of the droplet; the combination of vapor and electrodynamic forces is then observed to drive the metal slightly back into the tube, thus inhibiting "bridging" by the liquid across the gap.

The initial drive setup was quite inefficient, and required about 5 joules for operation. However, with a quite straightforward optimization of this circuit, only a small fraction of a joule should be required.

The energy requirements of the spark are not well known. However, initial estimates of the partitioning of this spark energy are encouraging.

Consider first the several channels into which the spark energy goes. They are:

(a) kinetic energy of the vaporized particles

(b) radiation from the vapor and cathode spot

(c) heat conductivity into the cold metal of the spark electrode

(d) heat of vaporization and ionization of electrode materials.

The energy loss associated with item (a), i.e., the random energy component of the vapor is entirely negligible, since experience indicates that 10^4 °K is a conservative upper limit to the spark temperature, and so, a loss of no more than 1 eV per atom is involved.

An upper limit to the radiative losses (b) would be obtained if we assume that the cathode spot is a blackbody at 10^4 °K. Assigning it an area of 10^{-2} cm^2, we obtain (for unity emissivity) a radiative power slightly less than one kilowatt, which for vaporization time of under a millisecond means less than one joule loss.

Conduction losses (c) can be estimated fairly well by simply using the thermal diffusivity of the base metal and an assumed 10^4 °K temperature

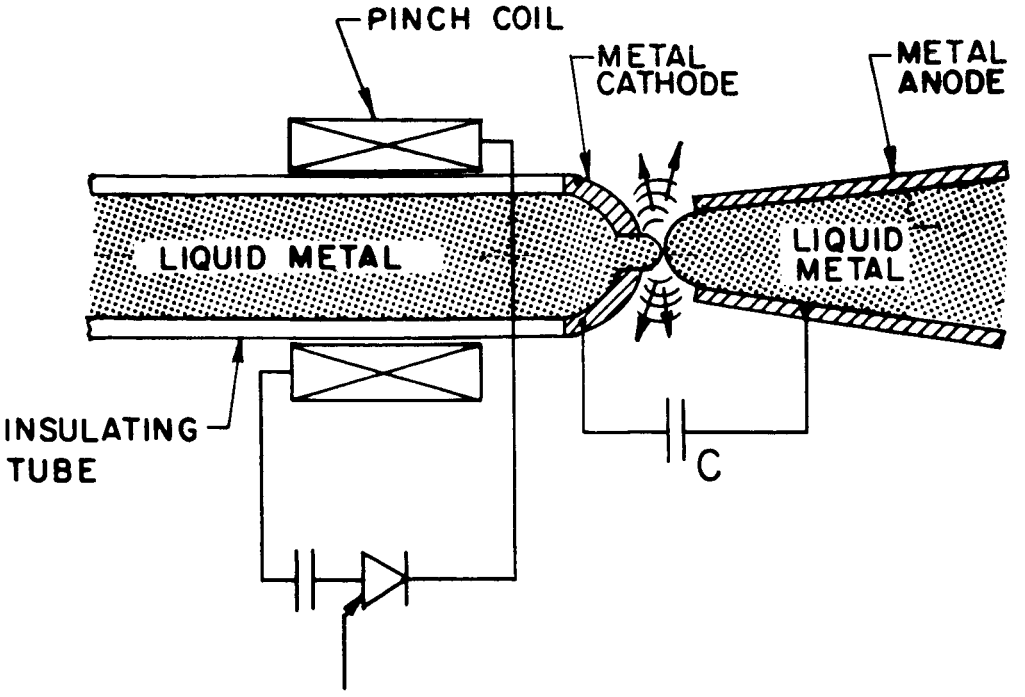

FIG. 35 : METAL PROPELLANT INJECTOR

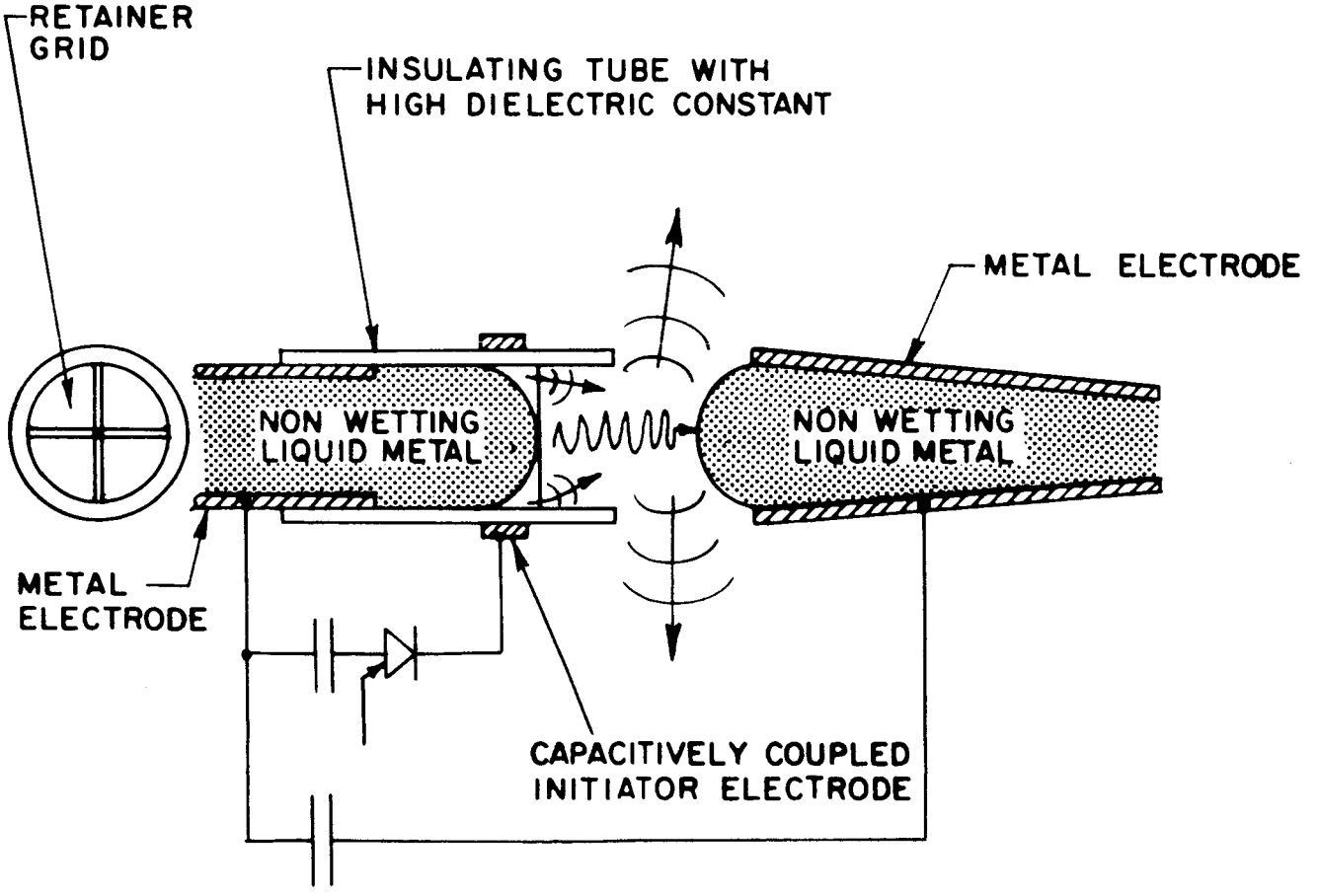

FIG. 36 : METAL PROPELLANT INJECTOR

in order to calculate the heat content of the metal at a given time after application of a temperature step. Even if we allow a conduction area of 1 cm^2, we find that in 10 msec, only 1 joule of heat energy has entered the electrodes.

We conclude from these admittedly rough estimates that the spark energy, if delivered in less than a millisecond, can be expected to go into channel (d) (vaporization) with fair efficiency, provided that more than a joule or so of energy is available.

One possible difficulty with this scheme is the formation of small droplets in addition to the vaporization. To prevent such formation, one would reduce the violence of the spark by investigating the minimum power level that need be used for successful operation. One could also use another design which is less prone to droplet formation.

Such a scheme which also probably allows faster operation is shown in Figure 36. The vapor generating discharge is initiated by a small capacitively coupled discharge. The non-wetting liquid metal is contained in an insulating tube with a high dielectric constant. An insulating grid prevents the metal from flowing out of the tube. When a fast-rising voltage pulse is applied to the initiator electrode, essentially all of the voltage will appear across the small free space between the liquid metal meniscus and the insulator wall. This will lead to breakdown and trigger the second discharge in the axial direction. (Ceramic insulators with relative dielectric constants of more than 10^4 are available. These are titanates, used for ceramic capacitors.) In the laboratory this scheme has shown its feasibility. The technical application is a question of choosing the right materials since there exists the danger of high voltage breakdown. Similar glass coated and capacitively coupled electrodes have been used for a long time for triggering commercial mercury rectifiers.[17] This scheme should be very efficient because most of the energy goes into vaporization and ionization. In the present density and temperature regime most of this energy can be transported into the gun barrels if a suitable geometry is chosen.

Another way of evaporating the propellant is given by a direct application of the ignitron starter principle. Here a thin rod of an electrically conducting and non-wetting material is dipped into the liquid metal, and a current pulse is applied. The resulting small discharge establishes an arc spot which evaporates the metal. Along this line we have conducted a series of experiments which shall be described later.

The advantages of the above schemes are obvious:

1. No erosion or ablation of surfaces from which the propellant is fed.

2. High repetition rates, high power operation of the thrustor.

3. Possibility of controlling the amount of vaporized material

by changing the electrical parameters of the vaporization circuit.

4. Low-energy consumption.

5. Simplicity and potential reliability.

6.2.3 Experiments

Exploratory work has been done on three types of metallic vapor injectors based on the principles which were chosen in the preceeding section. First, lithium vapor was injected radially into the coaxial gun, as a result of a wire explosion on axis, and the gun performance and discharge characteristics were determined. Secondly, a mercury propellant injector was assembled to be suitable for gun experiments with axial propellant injection. The mercury propellant distribution emitting from the injector was measured. Third, vacuum sparks between solid electrodes were investigated as a source of propellant.

Diagnostics

Straightforward measurements of the propellant distribution are possible, using the fast-acting ionization technique,[2] for the experiments in which non-condensable, unionized gases are used. For the complete description of the distribution of the partially ionized metallic vapor, no method is readily available. For our exploratory experiments with metallic vapors, simple pendulums,[6] Faraday cups,[9] and plates upon which the propellant is collected, were used to measure the beam impulse, ion flux and velocity, beam spread, and mass ejected per shot. The neutral atom density is not measured explicitly, and the pendulum and beam collector plates are known to have inaccuracies of perhaps a factor 2 due to surface effects. The problems are further complicated in measurements on mercury because of the high vapor pressure. Thus one can only achieve a gross description of the propellant distribution.

Exploding Lithium Wire

As a starting point in the investigation of metal propellants a laboratory system was fabricated to extrude lithium wire into the electrode structure of a coaxial thrustor and to vaporize the lithium by the exploded wire technique. The device, shown in Figures 37 and 38, consists of a motor driven piston, an extrusion cylinder and an orifice. Lithium is introduced into the extrusion cylinder in the form of a 3.2 mm rod and continuously extruded in the form of a 0.064 mm wire. The extruding nozzle, made of molybdenum, serves as one electrode for exploding the wire. The nozzle is supported by an insulator rod within the inner barrel of the thrustor. The inner barrel serves as the other electrode for exploding the wire. Mechanical motion of the wire tip across a 0.125 mm gap triggers the explosion. The explosion is fed by a capacitor separate from the main capacitor of the thrustor. Lithium vapor enters the interbarrel region of the thrustor and discharges the thrustor capacitor.

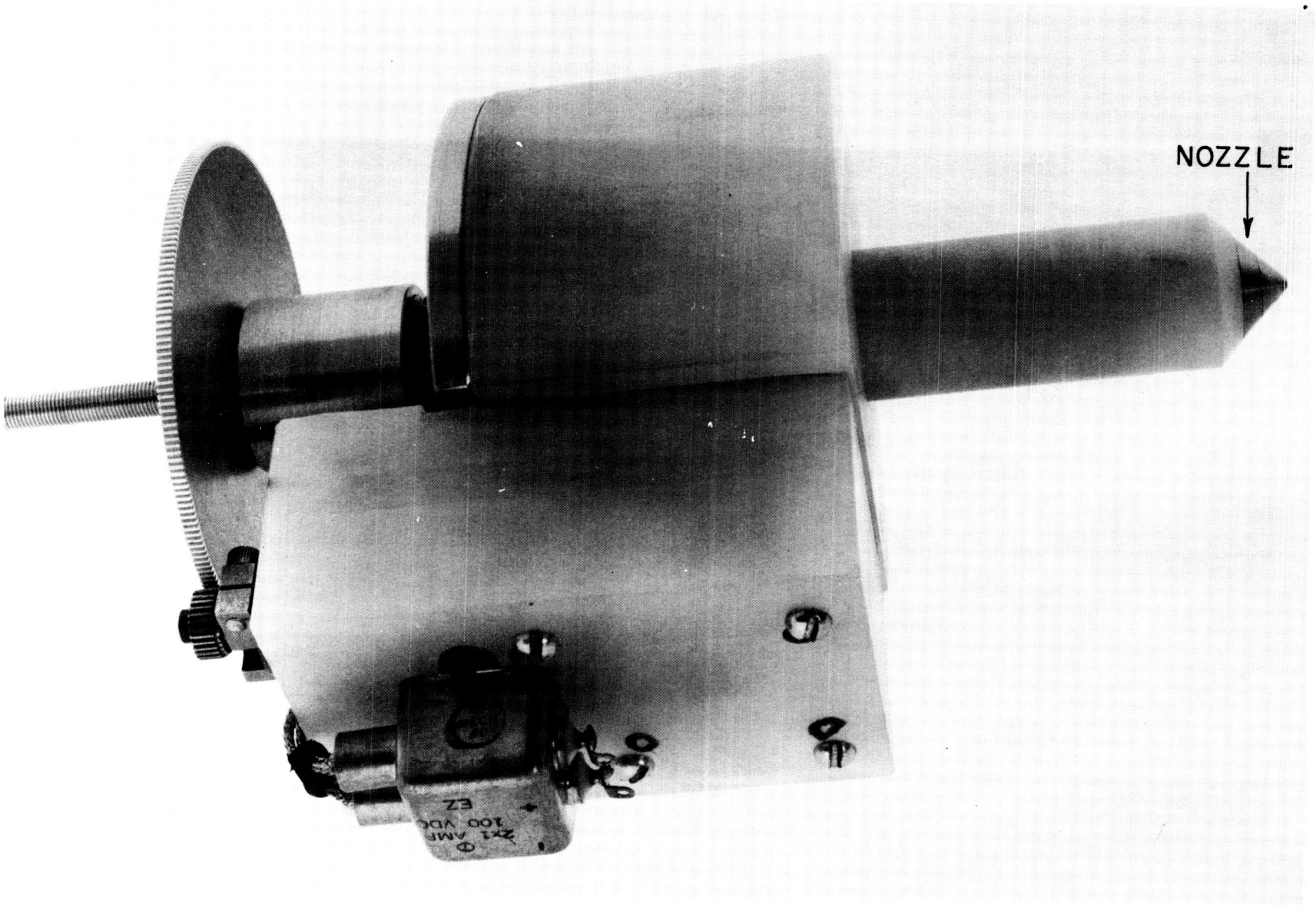

FIG. 37 : LITHIUM WIRE EXTRUDER

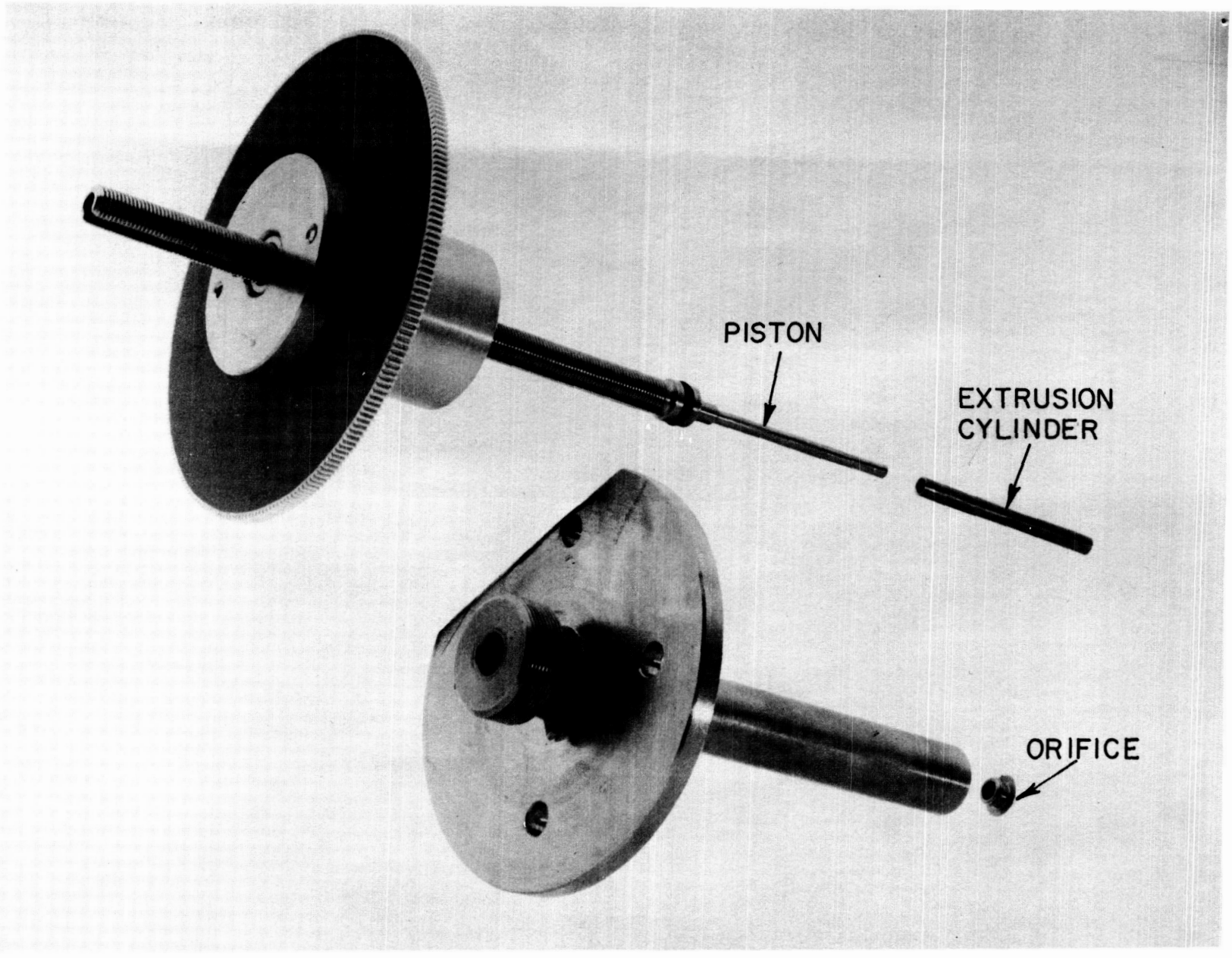

FIG. 38 : DETAILS OF LITHIUM WIRE EXTRUDER

For preliminary tests, the feed system was incorporated into a coaxial barrel assembly with barrels of 15 cm length and diameters of 7.8 and 3.9 cm. The lithium wire explosion took place on axis, about 7 cm from the insulator. The Mark IX-pulse line (22 μF, 17 mΩ, .75 μsec) charged to 5 kV was used as the thrustor capacitor and a 20 μF capacitor charged to 2.5 kV was used for the storage of the explosion energy. The initial results are: (1) successful repetitive wire explosions can be produced, (2) the thrustor discharges into lithium vapor in a stable, axisymmetric manner, (3) the exhaust consists of Li^+ ions with kinetic energies of about 100 eV, (4) some lithium is found on the electrodes, (5) the amount of energy used in the propellant feed system is about one-fourth the amount used in the accelerator, (6) the gun fires early in the wire explosion process, (7) the period of the current which vaporizes the lithium is four times the thrustor pulse-line period.

The behavior of the thrustor discharge seems encouraging, but obviously the energy and mass utilizations have to be improved.

Mercury Injector

The device constructed specifically for the injection of mercury is shown in Figure 39.

A puddle of propellant metal forms the cathode inside a glass enclosure. The anode is ringshaped surrounding the exit of the enclosure. Ignition of the vacuum spark is achieved by a separate trigger electrode which is coupled to the anode by a 1 μF capacitor. The energy stored in the 108 μF capacitor then is discharged in a time of about 40 μsec between cathode and anode. The generated plasma protrudes through the hole in the anode and expands in the form of a fast-moving jet into the vacuum. It was found that for low enough background pressure ($p < 10$ mm Hg), a reliable ignition could be obtained for capacitor charging voltages exceeding 200 V, where the cathode consisted of either mercury, a liquid mixture of gallium, indium, and tin or a solid mixture of tin and indium. The ignitor electrodes consisted either of carbon which showed some erosion or boron carbide which showed negligible erosion after a few thousand discharges.

The mass ejected per discharge was determined by weight measurements of the injector and also of the deposits collected on a plate at liquid nitrogen temperature. It was carefully secured that steady evaporation from the free mercury surface had only a small effect on the weight measurements. The measurements yielded a value of $3.1 \cdot 10^{-4}$ g ejected per discharge for a charging voltage of 400 volts on the 108 μF capacitor. This corresponds to a specific evaporation rate of $8.1 \cdot 10^{-3}$ g per Coulomb.

The spreading of the ejected mercury jet, shown in Figure 40, was determined from the diameter of the circular condensation pattern on the cryogenically cooled plate mounted at varied distance in front of the

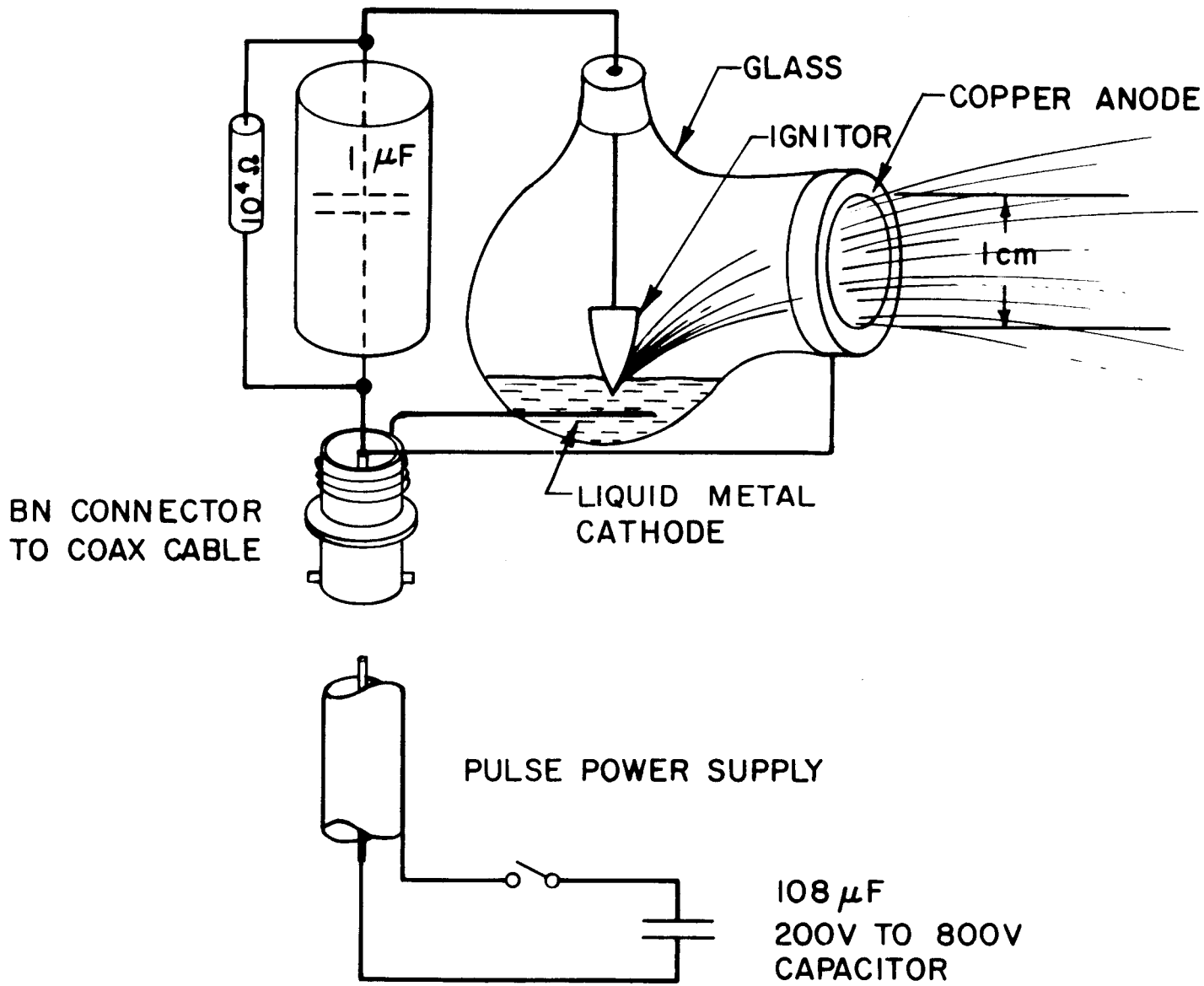

FIG. 39 : MERCURY INJECTOR

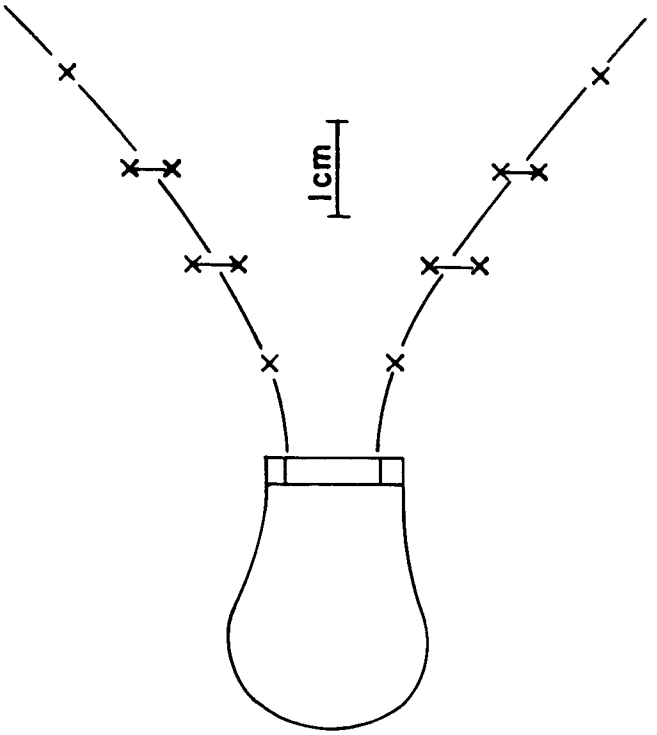

FIG. 40 : SPREADING OF THE EJECTED MERCURY JET (AS DETERMINED BY CRYOGENIC CONDENSATION)

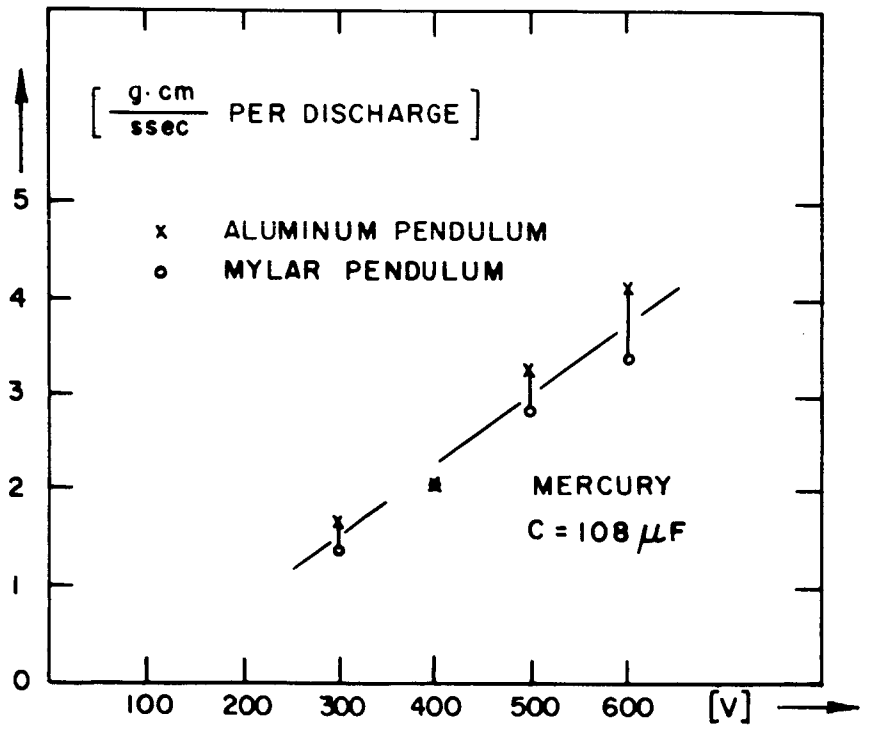

FIG. 41 : MOMENTUM TRANSFERRED FROM PLASMA JET TO BALLISTIC PENDULUM AS FUNCTION OF CAPACITOR CHARGING VOLTAGE

anode hole. The radial distribution seemed to be uniform with a well defined edge of the jet. The spread was also measured 35 cm from the source by traversing the beam with a Faraday cup. At 40° off the axis the value of the ion current density has dropped to only about 1/3 of the value of the centerline.

Knowing the directed velocity of the ions and the ion current density, the number density of the ions can be determined. Single ionization is assumed for this purpose. The ion density in the plasma jet about 1 m downstream from the source turns out to be in the range from $1 \cdot 10^{10}$ to $4 \cdot 10^{10}$ cm^{-3}. Integrating in a rough way the measured ion flux density over the cross section of the exhaust and over the duration of the ion pulse yields the total mass of the ions that are emitted per pulse. This value is about 1% of the total emitted mass.

The total momentum in the plasma jet as measured by two pendula made from aluminum and mylar is shown in Figure 41. The slightly different behavior of the two pendulum materials points to an influence of particle evaporation off the pendulum. These momentum measurements are probably correct within a factor of two.

Some typical results of the measurements with negatively biased ion collecting probes[9] are shown in Figure 42. Part (a) shows a typical oscillogram where 3 traces of the ion current density and of the discharge current are superimposed. The current and the arrival time of the ions are very repeatable while the amplitude of the ion flux density shows some jitter. From oscillogram (b) we see, using another ejector, that the arrival time of the ions does not markedly depend on the magnitude of the discharge current. The amplitude of the ion current density in the ejected plasma jet grows about linearly with the magnitude of the discharge current. Oscillogram (c) shows three values of arrival time for varied distance between the plasma source and the ion collecting probe. Oscillograms like this one were used for a determination of the ion velocity according to a time of flight consideration. The ion velocity determined from Figure 42(c) has a value of about $2.5 \cdot 10^{6}$ cm/sec. The ion velocity is influenced by the type of cathode material. For mercury, ion velocities in the range from $1.2 \cdot 10^{6}$ cm/sec to $4.2 \cdot 10^{6}$ cm/sec have been measured for discharge vessels of different dimensions.

For the mercury injector, from the momentum and mass measurements, one calculates an average exhaust velocity 2 to 3 orders of magnitude below the measured ion velocity. This seems unlikely and could be explained if, immediately following the discharge, the "impulsive" evaporation rate from the mercury surface is abnormally high. Such a process would neither be revealed by the pendulum, nor by the "steady" evaporation control experiments because of the time scales involved. Another explanation would involve the emission of small, slow moving droplets. Although no evidence for this was visible, droplets of micron size are known to exist in mercury puddle rectifiers.

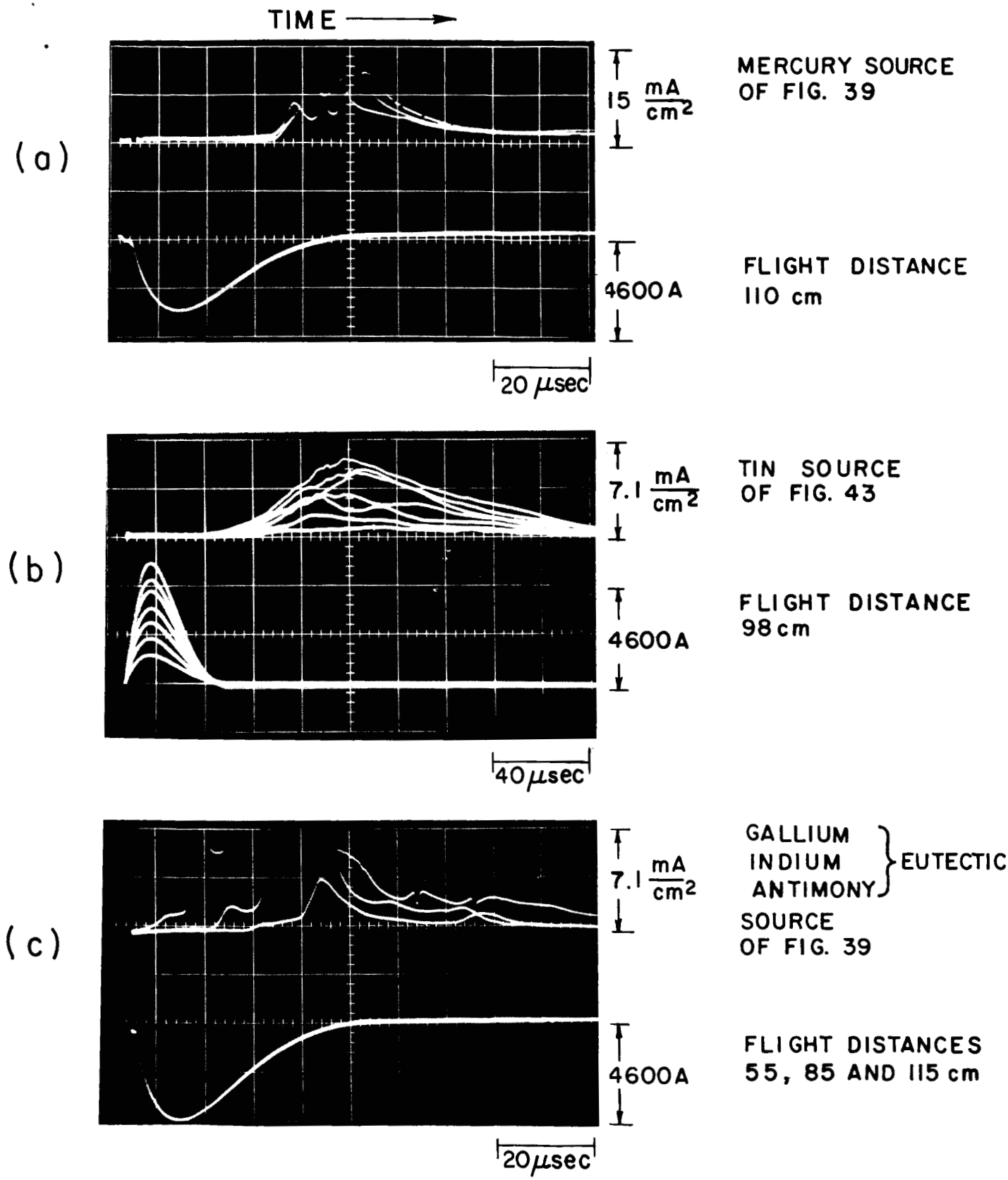

FIG. 42 : OSCILLOGRAMS OF CURRENT DENSITY : UPPER BEAM AND CAPACITOR DISCHARGE CURRENT : LOWER BEAM

If, as suggested by the ion flux measurements over the exhaust cross-section, the pendulum is sensitive to about 10^{-6} g of mass travelling about 10^{6} cm/sec, then the measurements with the mercury injector become internally consistent. The measurements are then also consistent with the experiments in the next section which are less subject to the phenomena discussed above.

Vacuum Spark Injector with Solid Electrodes

A coaxial discharge geometry, shown in Figure 43, also was used for testing various metals in solid form as the eroding cathode material. Initially the discharge was triggered by a small trigger electrode in the anode which was pulsed with 6 kV. Starting with clean surfaces, it was found that after a couple of discharges, the trigger pulse no longer was needed. Simply closing the switch which connects the discharge element to the pulse capacitor fires the discharge. For all the materials listed in Table V, this self-starting of the pulsed discharge was found to occur. It was obvious that this self-starting was easier to obtain with metals of a low melting point. It seems that this process of igniting the discharge potentially has a high reliability. For example, with lead as the propellant, the device showed no failure in a short endurance test of 12,000 self-triggered discharges. All materials were tested for more than 10^{3} discharges. Failures to ignite the discharge were occasionally encountered for high-melting point materials if the mechanical tolerance between cathode, glass insulator and anode was not kept tight enough.

It appears that the discharge is ignited by the explosion of a thin metal film which is deposited on the glass insulator surface by the preceeding discharges. The resistance of this film is in the range of 10^{4} Ω. When the capacitor voltage is set so low that a full discharge does not occur, one can observe the formation of some small bright spots at the cathode glass interface. These obviously develop into arc spots when the discharge takes place. When used in connection with a low vapor pressure, liquid metal cathode, this scheme of igniting a discharge can simplify the operation of a pulsed metal feed system.

In a series of measurements with various cathode materials the mass and momentum transferred by the pulsed discharge were measured. The momentum was measured by a pendulum while the mass was determined by weighing the accumulated deposits formed by about 2,000 discharges on a glass plate. It was checked for the case of lead that about 80% of the mass in the exhaust was collected on the glass plate. The results of these measurements are shown in Table V.

As is reasonable, a strong correlation exists between the ejected mass and the physical properties of the propellant, specifically, the energy per gram required for vaporization from room temperature. From this correlation, mercury would be expected to be a good emitter as indeed the mercury experiments showed.

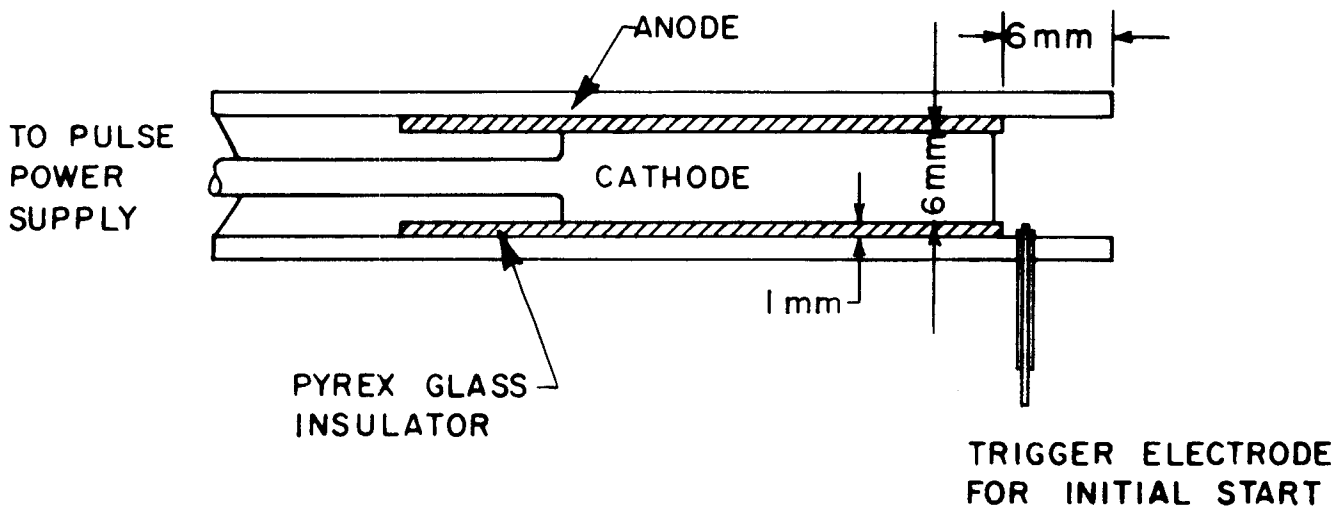

FIG. 43 : COAXIAL SOURCE OF METAL PLASMA BURSTS

TABLE V

EXPERIMENTAL RESULTS WITH VACUUM SPARK INJECTOR

SECTION 6.2.3

Cathode Material	Mass ejected per discharge (g) C = 148 μF, U = 600V	Momentum transferred to a pendulum (dyne sec)	Average velocity computed from measured values of ejected mass and momentum (cm/sec)
Bi	$1.9 \cdot 10^{-5}$	2.1	$1.1 \cdot 10^{5}$
Pb	$1.2 \cdot 10^{-5}$	17.0	$1.4 \cdot 10^{6}$
Sb	$1.0 \cdot 10^{-5}$	6.0	$6.0 \cdot 10^{5}$
Cd	$7.8 \cdot 10^{-6}$	6.4	$8.2 \cdot 10^{4}$
Sn	$6.1 \cdot 10^{-6}$	2.5	$4.1 \cdot 10^{5}$
Zn	$5.4 \cdot 10^{-6}$	5.3	$9.8 \cdot 10^{5}$
In	$4.4 \cdot 10^{-6}$	4.8	$1.1 \cdot 10^{6}$
Al	$3.6 \cdot 10^{-6}$	3.6	$1.0 \cdot 10^{6}$
Ag	$2.8 \cdot 10^{-6}$	4.8	$1.7 \cdot 10^{6}$
Fe	$1.8 \cdot 10^{-6}$	3.7	$2.1 \cdot 10^{6}$
Cr	$1.4 \cdot 10^{-6}$	5.3	$3.8 \cdot 10^{6}$
Ti	$1.3 \cdot 10^{-6}$	3.3	$2.5 \cdot 10^{6}$
Mg	$1.0 \cdot 10^{-6}$	3.3	$3.3 \cdot 10^{6}$
Cu	$9.0 \cdot 10^{-7}$	4.8	$5.3 \cdot 10^{6}$

Summary and Conclusions

A variety of metals are desirable as propellants for the pulsed plasma gun. It is concluded that the propellant must be introduced into the gun as a vapor prior to the main current flow. Various schemes are discussed. It seems most attractive to generate small metal plasma bursts by a small secondary discharge. An experimental program was started to investigate these so-called vacuum sparks. It was found that the magnitude of propellant ejected per burst could be of suitable magnitude for use in the pulsed plasma gun. The ejected plasma has a directed velocity in the order of 10^6 cm/sec. A simple self-triggered mechanism exists for metal propellants in a suitable discharge geometry. The propellant injector can be operated simply by connecting it to a charged capacitor. This scheme uses a thin metallic film coated out on an insulator by the preceeding discharges.

7.0 POWER

7.1 Introduction

In the last quarter, a prelimimary study of power conditioning and control systems suitable for our devices was accomplished. Three prime electrical power sources were considered; solar photovoltaic, nuclear turboelectric, and nuclear thermionic. Source characteristics were examined to the extent that they affect the choice of particular conversion schemes. Power conditioning and control systems to match plasma device characteristics to those of the sources were considered. Particular details and problems of the power conditioning subsystems were studied.

Although the potential power capability of the sources considered is greater, the power level chosen for this study is 10 kW. The more immediate prospective missions dictate this and it is felt that higher power levels may be accommodated by paralleling proposed 10 kW systems. In view of the state-of-the-art in thrustors and semi-conductor devices it is not considered possible to operate a single thrustor at say, 1 MW nor is it practical for spaceflight to condition and control 1 MW with an individual power conditioning unit. These power levels will be obtained with multiples of thrustors and power conditioning modules. This is desirable from a reliability standpoint.

Operation of the plasma thrustor system at 1 kV and a frequency of 150 pulses per second with a 140 μF capacitor corresponds to a 10.5 kW power level. The major portion of the power (99.8%) is supplied by the power conditioning at a nominal 1 kV to charge the capacitor. The remaining control power (~ 50 W) is supplied at 28 VDC. From our development experience we feel that reasonable weights for the 10 kW thrustor system components are: 10 lbs for thrustor electrodes, propellant injector and gun trigger assembly, 30 lbs for the capacitor and 3 lbs for the control, timing and valve pulse circuitry. This amounts to a 4.0 lbs/kW thrustor specific weight exclusive of cooling structure and the propellant storage system. Cooling penalties have been estimated to be about 7.5 to 11 lbs/(kW rejected).[18,19] Given the achievement of the performance goal of 70% efficiency for the thrustor, the thrustor system specific weight, including cooling structure, would be about 7 lbs/kW. The power conditioning modules will be discussed later.

A conceptual plasma thrustor system is illustrated in Figure 44 A particular system would involve sufficient redundancy and switched interfaces to provide maximum flexibility and reliability at the expense of increased weight penalties. Provision for the operation of any combination of thrustors and power conditioning modules is desirable to meet various power levels and to accommodate for degradation of individual units. We are considering here a system for prime propulsion. With a nuclear turboelectric or thermionic power source the thrust vector would probably

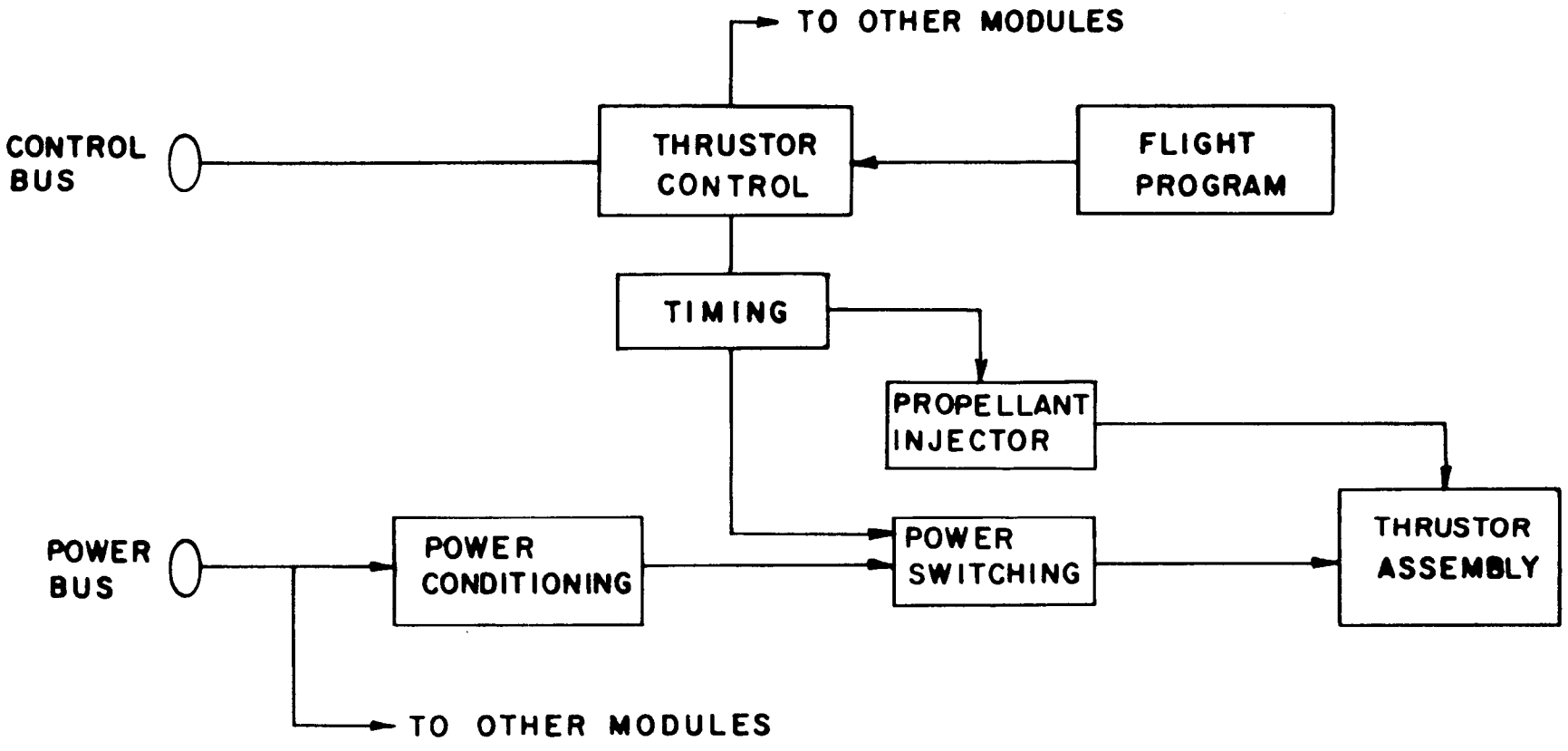

FIG. 44 : CONCEPTUAL PROPULSION SYSTEM

be fixed relative to the spacecraft with attitude control accomplished by an auxiliary system, whereas with a solar array there may be the necessity for independent orientation control of the array and of the thrustors.[19,20]

7.2 Power Sources

Solar Photovoltaic

The state of the solar panel technology has been advancing rapidly. In use now are the Mariner-type systems with specific weights of 100 lbs/kW. A system operating at about 50 lbs/kW is a practical design constraint today,[20,21] and more advanced systems at 37 lbs/kW are being studied. Particular missions may require more or less panel regulation and protection circuitry and sufficient provision for radiation, micrometeorite, and trajectory degradation of panel power output. Without such provisions panel output characteristics will vary greatly with time. For a scientific payload a fairly well defined output characteristic is desirable, while the requirements for electric propulsion are less stringent. With this in mind one might obtain mission advantages from a two section array with one section designed for gross power (propulsion), the other for lower power systems requiring closer control of input power.

Arrays may be designed with output voltages ranging from about 30 to 500 volts dc although the high voltage output represents a greater reliability problem. For the purpose of an electrically propelled scientific payload a two-level output is desirable. One bus is at a nominal 28 VDC to supply conventional control and instrumentation circuitry and the other at 100 to 500 VDC as input to power conditioning for the plasma device. 100 to 500 V output is within the rating of modern semiconductors and permits utilization of the higher efficiency, lower weight characteristics of proposed power conditioning circuits operating at these higher voltages.[18]

Nuclear Thermionic

Nuclear thermionic power sources will have specific weights of 5-10 lbs/kW depending upon shielding and power level. The cesium diodes produce about 100 W of power each at .6-.8 VDC. A typical diode module will produce 10-15 kW at about 100 VDC.[22,23] Again it is possible to design a two-bus system, a low voltage bus for control and instrumentation and a high voltage bus (100-500 V) for prime propulsion.

Nuclear Turboelectric

The reactor-powered turbo-alternator concept, SNAP 50/SPUR,[22,23] is to produce .3 - 1 MWe of 3 phase, 120/208 VAC power at 2.4 kHz to 3.2 kHz with a specific weight of 10-20 lbs/kW depending upon shielding requirements. An alternative output voltage level considered possible is 1,500/2,600 VAC.[24] It is also feasible that a multi-stage generator

could provide a number of specific directly usable power levels, ac as well as dc.

7.3 Power Conditioning

Power conditioning for a pulsed plasma thrustor involves problems distinctly different from other systems. Much work has been done on high efficiency power supplies for ion engines using the conventional Jensen and Royer converters, or voltage or current fed SCR inverters. A difficulty arises in trying to use these power supplies to charge the capacitor of a plasma thrustor directly because they cannot be more than 50% efficient in such an application. Therefore, a fundamentally different circuit concept is needed. Two concepts are discussed in this section.

It is well known that a RLC series resonant circuit can provide an efficient ($\eta > 90\%$) means for capacitor charging. With this scheme, the final charge voltage on the capacitor is twice the source voltage, if charging is terminated after the first half cycle of current. In that case, the source must be "stiff", i.e., of low impedance and adequate surge capability.

To use a resonant charging scheme with a solar array having an output of 500 volts, thus giving a 1 kV capacitor charge voltage, a large filter capacitor bank is necessary to buffer the array against the thrustor capacitor charging current surge. A typical system is shown in Figure 45(a). This prevents the source voltage from decreasing by an appreciable amount, thereby achieving an efficient resonant charge and reducing the inefficiencies associated with charging the buffer bank itself which are proportional to the incremental charge in buffer bank voltage. The buffer bank capacitance must be approximately ten times the thrustor capacitance or about 1 to 2 millifarads. For this electrolytics are to be used because of their high specific capacity. Their construction requires that they be enclosed in a hermetic container at atmospheric pressure if used in a space environment. Silicon controlled rectifiers are suited for use as a combination switching and commutating element and are available with the necessary voltage and current ratings. The inductor is chosen so that the charge period is less than the minimum thrustor repetition period, and need only be large enough to limit peak charging currents to acceptable levels. Estimated weights for the basic system components shown in Figure 45(a) are tabulated below.

Component	Weight (lb)
5 400 μF - 550 V electrolytic capacitors	4.5
hermetic case	3.0
charging inductor	7.5
2 silicon controlled rectifiers	1.0
	16.0 lbs
	1.6 lbs/kW

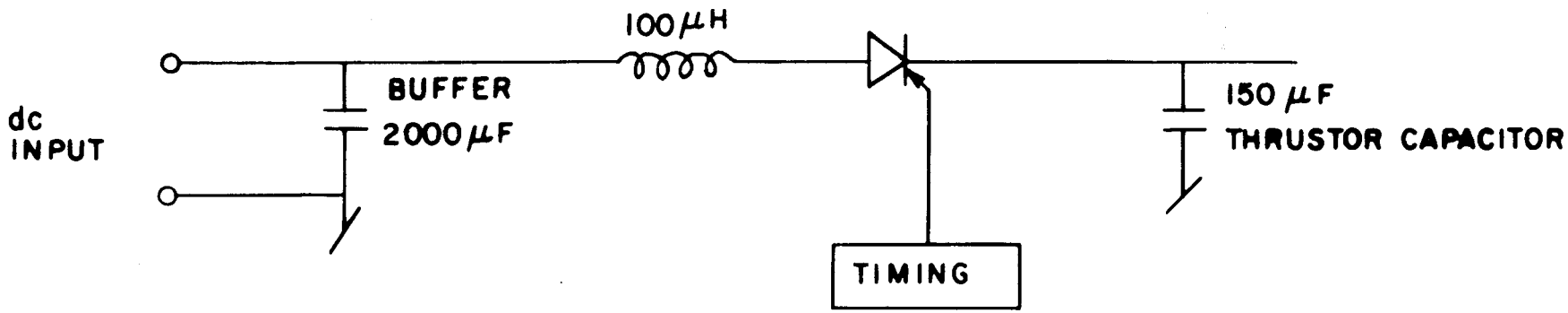

(a)

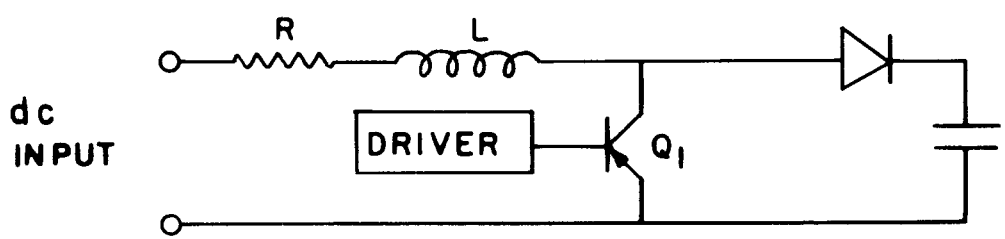

(b)

FIG. 45 : CAPACITOR CHARGING SCHEMES

The most common failure mode of the electrolytic capacitors is by a short-circuit dielectric breakdown. Reliability in the filter capacitor bank may be obtained by redundancy and by connecting the capacitors with fusible links so that failure of one capacitor will result in clearing it from the circuit by the action of all others which discharge into it. The most common failure mode of an SCR is by breakdown of its blocking characteristic, i.e., anode to cathode short. To increase reliability in the switching circuit one may place two or more SCRs in series, each rated for the maximum voltage and current. Obviously if one were to run the thrustor in a self-resonant mode,[1] the need for a switching element is eliminated.

The low impedance, high current characteristics of a nuclear thermionic source permit the possibility of resonant charging with reduced requirements for the buffer bank. The constraints are, first, the peak surge current limitations in the thermionic diodes, and secondly, the standby loading requirements of the diodes between the periods of capacitor charging.

Resonant charging may also be used with a nuclear turbo-electric source. A number of variations are possible depending upon the alternator output characteristics. For a low voltage ac output one may transform and then rectify to charge a buffer bank or if dc power is available, charge the buffer bank directly. One might also utilize the output reactance of the alternator and resonant charge directly or through a transformer at a submultiple of the alternator frequency.

Another efficient means of charging a capacitor is the method illustrated schematically in Figure 45(b). If we close the switching element, Q_1, a current begins to flow, storing energy in the inductor L. For times less than the L/R time constant of the circuit a favorable energy balance exists between energy stored in L and dissipated in R. If Q_1 is opened rapidly, the diode D_1 becomes forward-biased and C is charged efficiently. The final charge voltage being determined by the Q_1 turn-off time.

Conversion modules which produce 10 kW of power at 1 kV using this concept have been designed by ITT Space Power Components Division. By using SCR's as switching elements an efficiency of 82% with a specific weight of 13.5 lbs/kW has been obtained. A transistorized circuit is 87% efficient @ 11.5 lbs/kW. The SCR unit is less efficient due to commutation losses. These units may be used as 10 kW building blocks to condition a plasma thrustor to any of the previously mentioned sources. By optimizing input voltages, filtering, and by using modern semiconductors, efficiencies of 90% appear to be possible. The SCR unit is more efficient at lower power levels because of decreased commutation losses. Both circuits could be used in a highly redundant and reliable matrix type of power conditioning, if load sharing problems can be solved.

8.0 DIAGNOSTICS

8.1 Thrust Stand

8.1.1 Description

A schematic of the thrust stand system is shown in Figure 46. The thrust stand consists of a closed-loop servo-controlled system. The stand proper, upon which the plasma thrustor is mounted, is supported as an inertial platform above a reference platform by four flexures. The flexures are critically loaded to remove mechanical restoring forces.

The advantages of using a four-flexure support rather than load cells or other devices were described in a previous report[4] and by Hyman and Conner.[25] A displacement of the stand relative to the reference platform is sensed by a non-mechanically coupled transducer. When the thrustor fires, the servo circuitry cancels the momentum given to the stand. The servo forces are electromagnetically coupled to the stand by the servo coil and magnet assembly. The servo circuitry consists of two closed loops, one for position control, the x-loop, and one for rate damping, the $\dot{x}$ loop. Each servo coil assembly consists of a many turn solenoid immersed in a homogeneous radial B field as shown below.

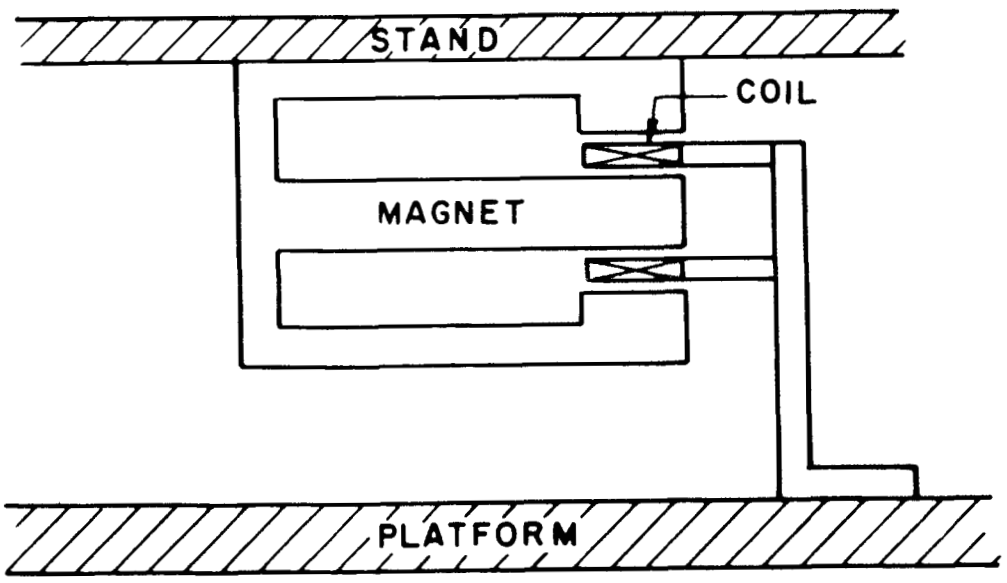

The magnet is attached to the stand and the coil to the platform. The servo

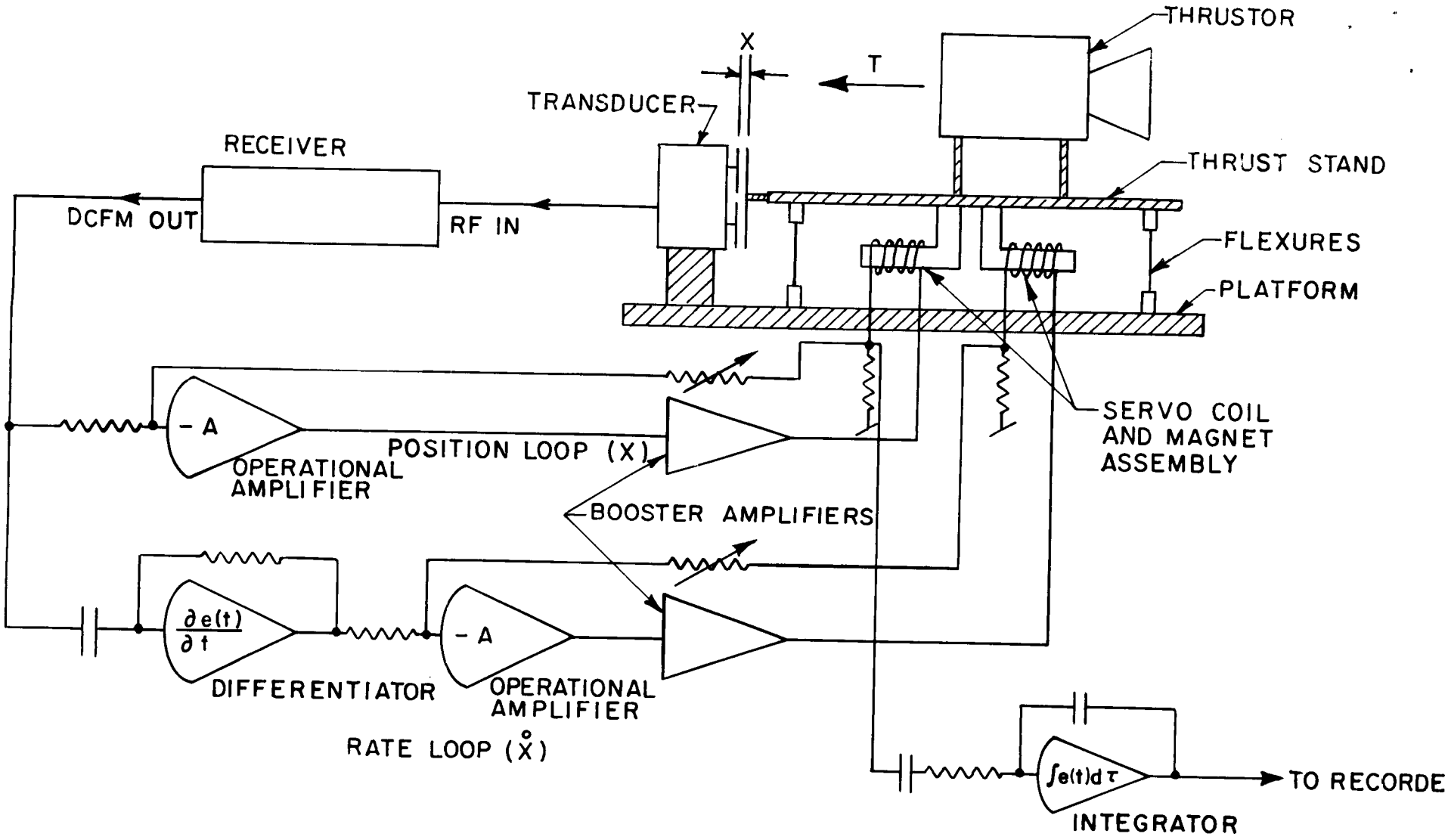

FIG. 46 : SCHEMATIC OF THE THRUST STAND SYSTEM

force is proportional to the coil current and can be calibrated by applying known forces or impulses to the stand.

The stand can be used in two ways: at high thrustor repetition rates or on a single shot basis. At high repetition rates (i.e., pulse repetition period less than system response time) a net balance between the accelerator thrust and the x-loop position force is obtained on a static basis. On a single shot basis, the accelerator impulse is measured by integrating the servo forces over time. It is required that the initial and final momentum of the stand be the same, i.e., the sum of all impulses delivered to the stand be zero. Thus,

$$\int F_a \, dt = \int F_p \, dt + \int F_r \, dt$$

where the first term is the impulse from the accelerator, the second and third terms are the impulses from the position and rate servo forces, respectively. It has been assumed that no other restoring forces are operating. If, as above, the net impulse to the stand is zero, it then follows that the accelerator impulse is measured correctly even if electronic transients were to cause a temporary malfunction in the servo circuitry. The electronic component recovery times are orders of magnitude less than the overall system response time.

As a specific example of the general expression above, let the servo forces be linear in position and velocity, i.e.

$$F_p = k_p x \quad \text{and} \quad F_r = k_r \dot{x}$$

where k_p and k_r are constants. Also let the stand be returned to its null position, i.e.

$$\int \dot{x} dt = \Delta x = 0 \; ; \; \Delta \dot{x} = 0 \; .$$

Then the accelerator impulse, I, is given by

$$I \equiv \int F_a dt = k_p \int x dt \; .$$

The impulse is proportional to the time integral of the displacement. If the output of the position transducer is proportional to displacement, then the impulse is proportional to the integral of the transducer output signal. Our thrust stand system meets all the above requirements.

The thrust stand can also be used as a free ballistic seismic pendulum where the only restoring forces are those due to the stand flexures. The flexures are not critically loaded and the servo coils are disconnected. The position transducer and receiver are used only to monitor displacement from the null position. The peak displacement is calibrated by application of a known impulse. For accuracy and economy it is convenient to have: the force constant of the flexures be linear

over the range of motion; the response of the transducer-receiver system be linear over the range of operation; and the time constant for the decay of the oscillatory motion be greater than the oscillation period. These criteria have been met in our thrust stand. By using known impulses, response over a wide range was checked and found to scale linearly.

The initial design of the thrust stand is given in the last final report.[4] Much of the initial system has been modified to obtain higher sensitivity, stability and signal-to-noise ratio. Tektronix operational amplifiers, type "O", are now used in the servo loop. These units have better characteristics and more flexibility than the previous amplifiers. Booster amplifiers are used to obtain the power gain necessary to drive the servo mechanisms directly. The new transducer is a simple FM system. A modified Colpitts oscillator is the basic frequency determining element and is mounted in such a way that the capacitance of the oscillator tank circuit varies with displacement of the stand, thereby varying the output frequency. The oscillator output is fed into an FM receiver and demodulated. System null frequency is 31.5 MHz and bandwidth is 600 kHz. Displacement of the stand results in a DC output from the discriminator at the rate of 24 mV/μ. The discriminator output is the signal fed to the servo circuit. The previous transducer system was a Sanborn linear differential transformer and bridge circuit. Its drawbacks were: an incomplete demodulation of the 2.4 kHz carrier, the necessity of extracting the signal from a 350v offset, and an inherent phase shift in the overall system.

8.1.2 Typical Operation

In the thrustor performance measurements of Section 4, the thrust balance was operated as a free ballistic seismic pendulum with the stand flexures providing the only restoring force. The displacement from the null position was monitored directly from the output of the transducer receiver.

It was established that no electrical transients or nonlinear elements in the mechanics of the thrust stand produced erroneous measurements. The gun was fired into an insulated bucket which was fastened to the gun, in order to cancel net momentum transfer, and it was observed that the thrust stand reading dropped to less than 6% of the reading corresponding to the thrust measurement. The current to the tank walls was measured with different Rogowski coils and found to be less than 5% of the total gun current. No corona was visible around the total system.

The thrust balance was calibrated by transferring a known impulse to the stand through an inelastic collision of the bob of an adjustable simple pendulum. Since the calibration impulse bit was transferred to the thrust stand at a different place than the gun impulse, there existed a possibility of a different response of the thrust stand if the flexures are not perfect. We examined this potential error by the following experiment.

In addition to the calibration pendulum (1) another pendulum (2) was installed which transferred its momentum to the cathode of the gun. If the bobs have the same tank mount, and if they fall through the same angle, then the thrust stand readings T are related as follows:

$$\frac{T_2}{T_1} = \frac{m_2}{m_1}\sqrt{\frac{\ell_2}{\ell_1}}$$

where m and ℓ are the mass and the length of the pendulums. The agreement of the measurements was within 3%.

A typical calibration run is shown in Figure 47: it shows the linearity of the response of the stand. A typical thrustor run is shown in Figure 48. When the propellant injector alone is operated, without firing the gun, no stand response is observed.

8.2 Mass Flow Apparatus

The measurement of the mass flow per shot is made with the apparatus drawn schematically below. It is similar to a displacement

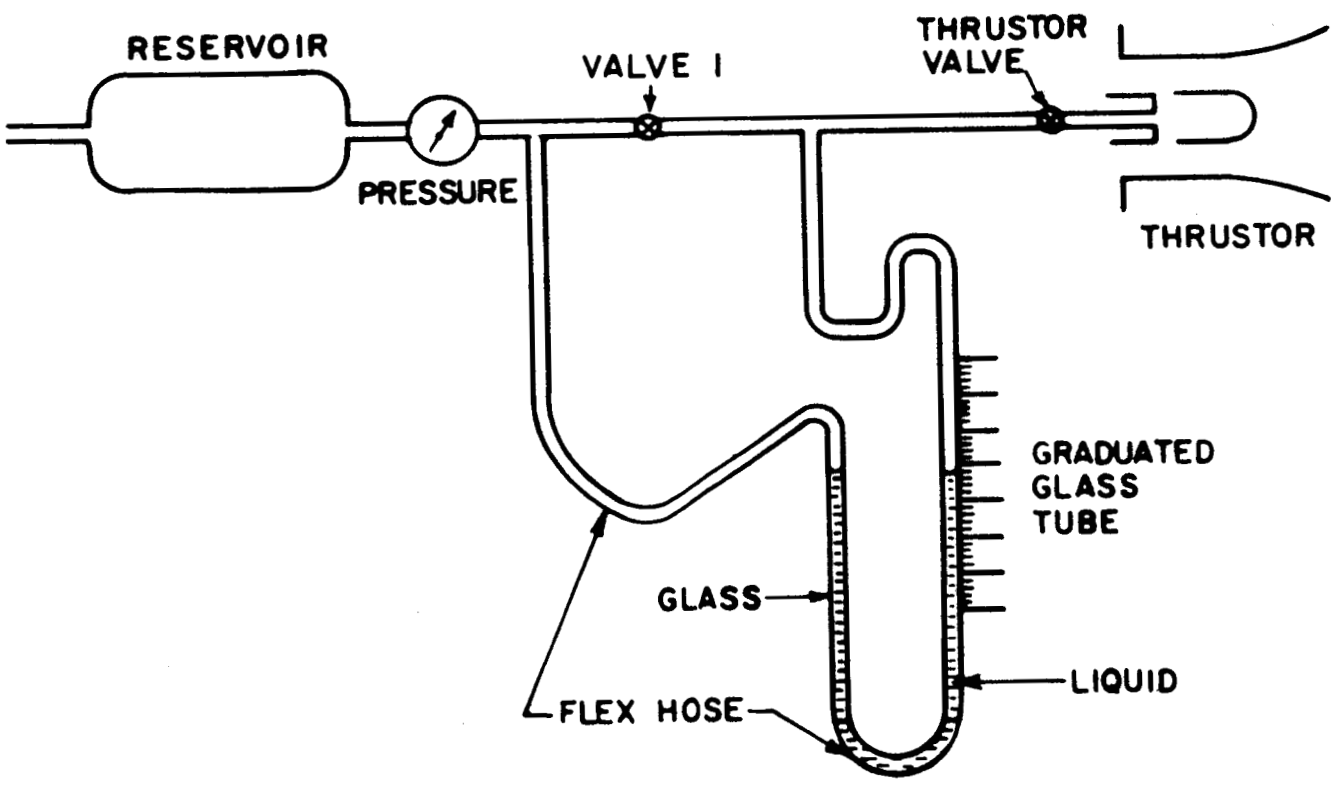

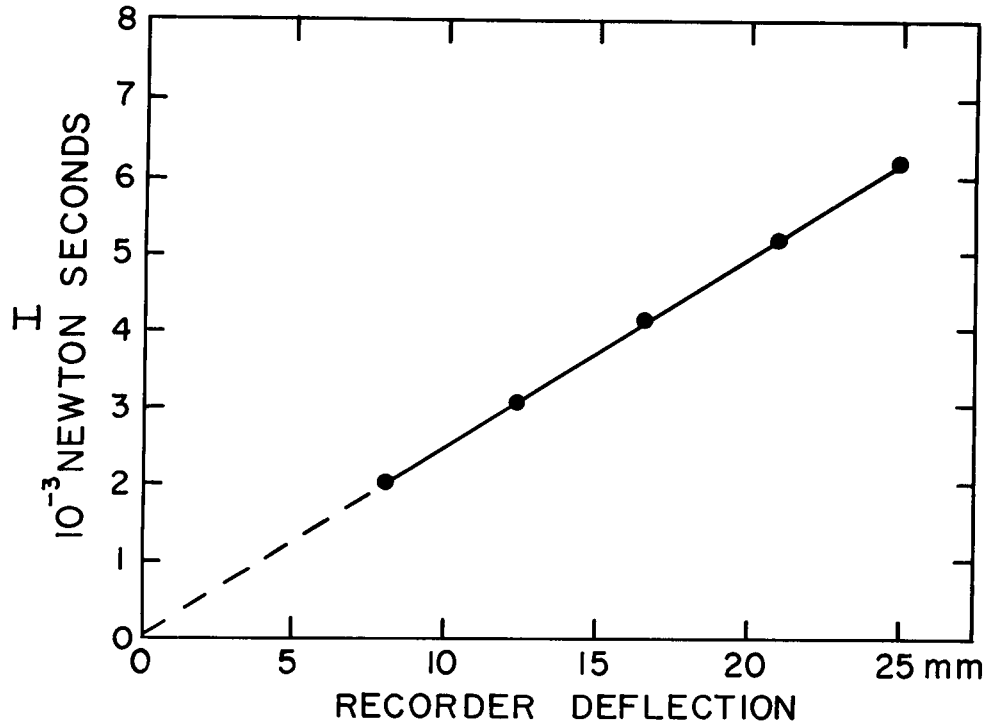

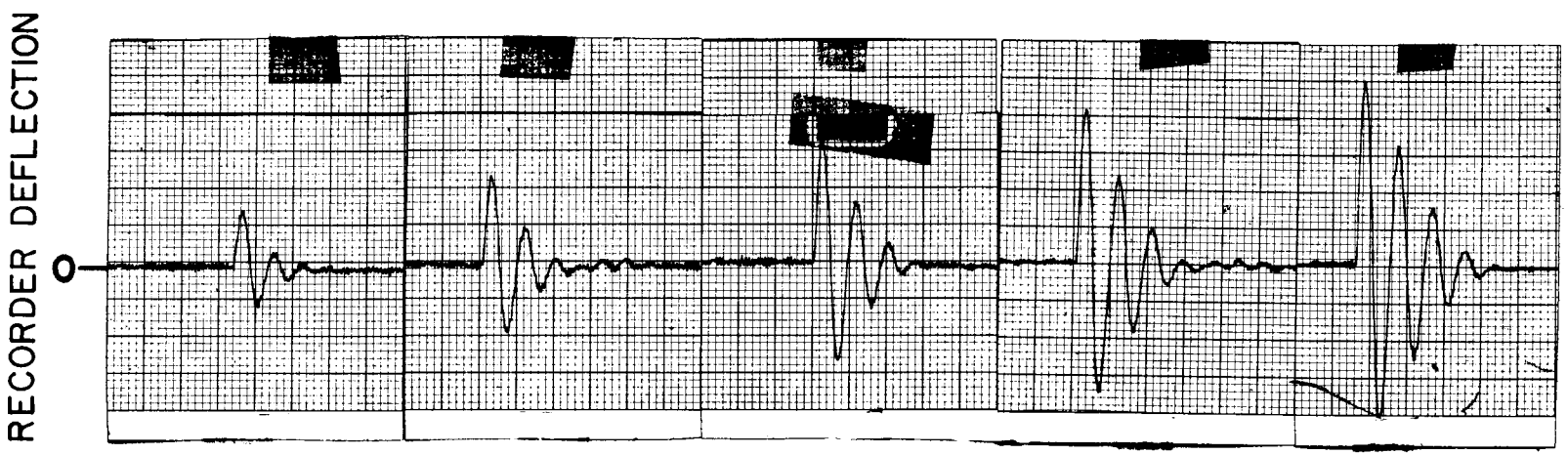

FIG. 47 : THRUST BALANCE CALIBRATION

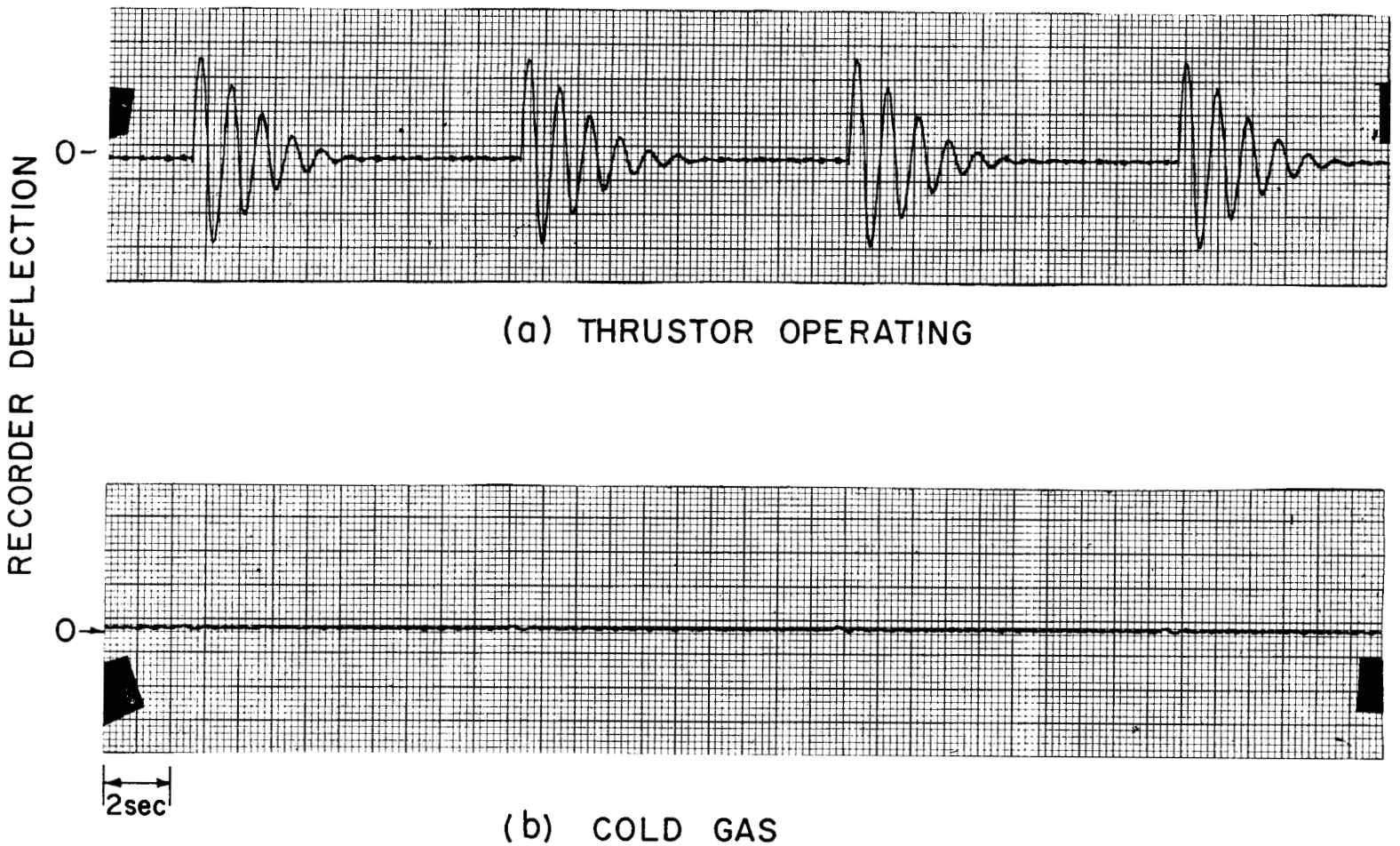

FIG. 48 : TYPICAL IMPULSE RECORDS

type manometer. To make the measurement, valve 1 is closed and the thrustor is fired. The mass flow displaces the levels of the liquid columns. The columns are brought to the same level again by adjusting the flexible hose. The releveling of the columns eliminates differential pressure effects. The change in gas volume to the right of valve 1 is noted, and the reservoir pressure is measured. With these measurements, the mass flow per shot may be calculated from the equation of state for the gaseous propellant.

For good sensitivity of the device, the measured gas volume has to be comparable with the tube volume existing between the two valves and the liquid surface. Also, the vapor pressure of the liquid must be small compared to the gas pressure.

8.3 A Fast-Acting Calorimeter

A new calorimeter has been developed to measure the exhaust energy from a single shot of the plasma thrustor. It has a fast time response and only one measurement is required to determine the total energy incident on the calorimeter. The calibration is simple and direct and radiation losses can be determined easily. The calorimeter consists of a long narrow ribbon of metal foil wound continuously around a glass frame to form a re-entrant cavity. It is illustrated schematically below.

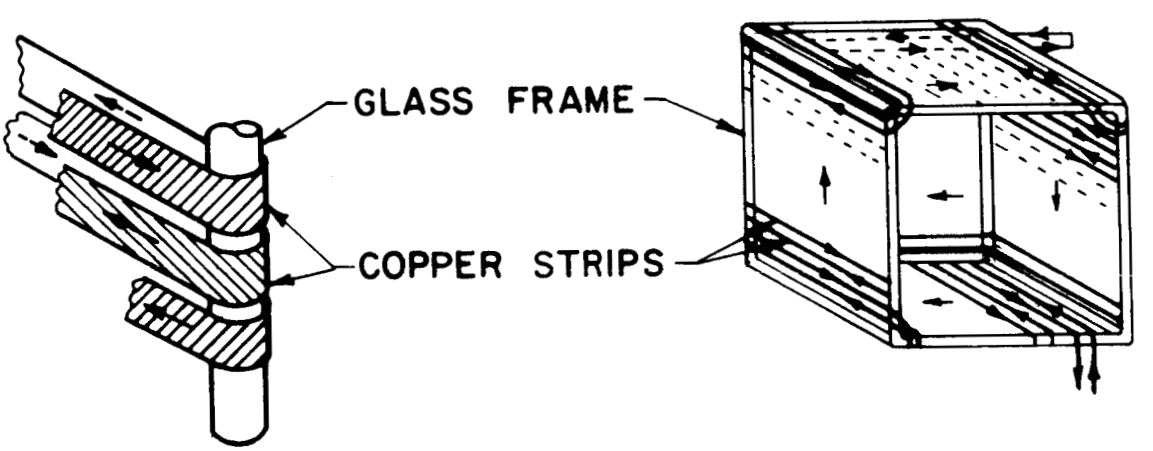

The plasma heats the ribbon and changes its resistance. It will be shown that the total resistance change depends only on the total energy deposited in the ribbon and is independent of the local energy density. Consequently, the total resistance change can be used to monitor the total

energy input to the calorimeter. The calorimeter can be made in sections if local energy density measurements are required. The resistance change, typically of the order of 10^{-2} ohms per joule, is measured with a Wheatstone bridge circuit. The time resolution of this type of calorimeter is determined primarily by the thickness of the ribbon, and is of the order of tens of microseconds. Consequently, the measurement can be made before significant radiation losses can occur.

The resistance change can be calculated as follows. Let an element of ribbon length, $\Delta\ell$, undergo a resistance change, Δr, due to a change in temperature, ΔT. Then

$$\Delta r = \frac{\alpha \, \Delta\ell \, \Delta T}{\sigma A}$$

where α is the temperature coefficient of resistance, σ is the conductivity, and A is the area of the ribbon cross section. The energy deposited, $\Delta\epsilon$, which causes the temperature change is

$$\Delta\epsilon = \beta \, \rho \, A \, \Delta\ell \, \Delta T$$

where β is the specific heat and ρ is the mass density. Eliminating the product $\Delta\ell \, \Delta T$ and summing over the ribbon elements we get for the total resistance change

$$\Delta R = \frac{\alpha}{\sigma \, \beta \, \rho \, A^2} \Delta E \, .$$

The total resistance change depends on the total energy deposited and not on the local energy density.

The calorimeter is calibrated by feeding electrical power into the ribbon and observing the temperature rise after a known time. The procedure is illustrated in the oscillogram shown in Figure 49(a). The beginning of the trace shows the first resistance reading R_1; the calorimeter is heating up during the measurement because of the power input from the measuring circuit. The measuring circuit is then disconnected, and simultaneously, a known power is fed into the ribbon. The power is shut off and a second resistance measurement is made. The second reading R_2 illustrates the resistance change due to the known power input. The third reading R_3 taken a few seconds later establishes the radiation losses. No electrical power is fed into the ribbon between the second and third readings.

Figure 49(b) shows a measurement taken with a pulsed arc plasma thrustor. The procedure is the same except that the thrustor is fired at the end of the first resistance reading R_1.

8.4 Velocity Probe

The essential features of the velocity probe, and its usage, have been described in Section 5.2. In this section formulas are given which link the probe signals to the velocity distribution and the temperature of the ions.

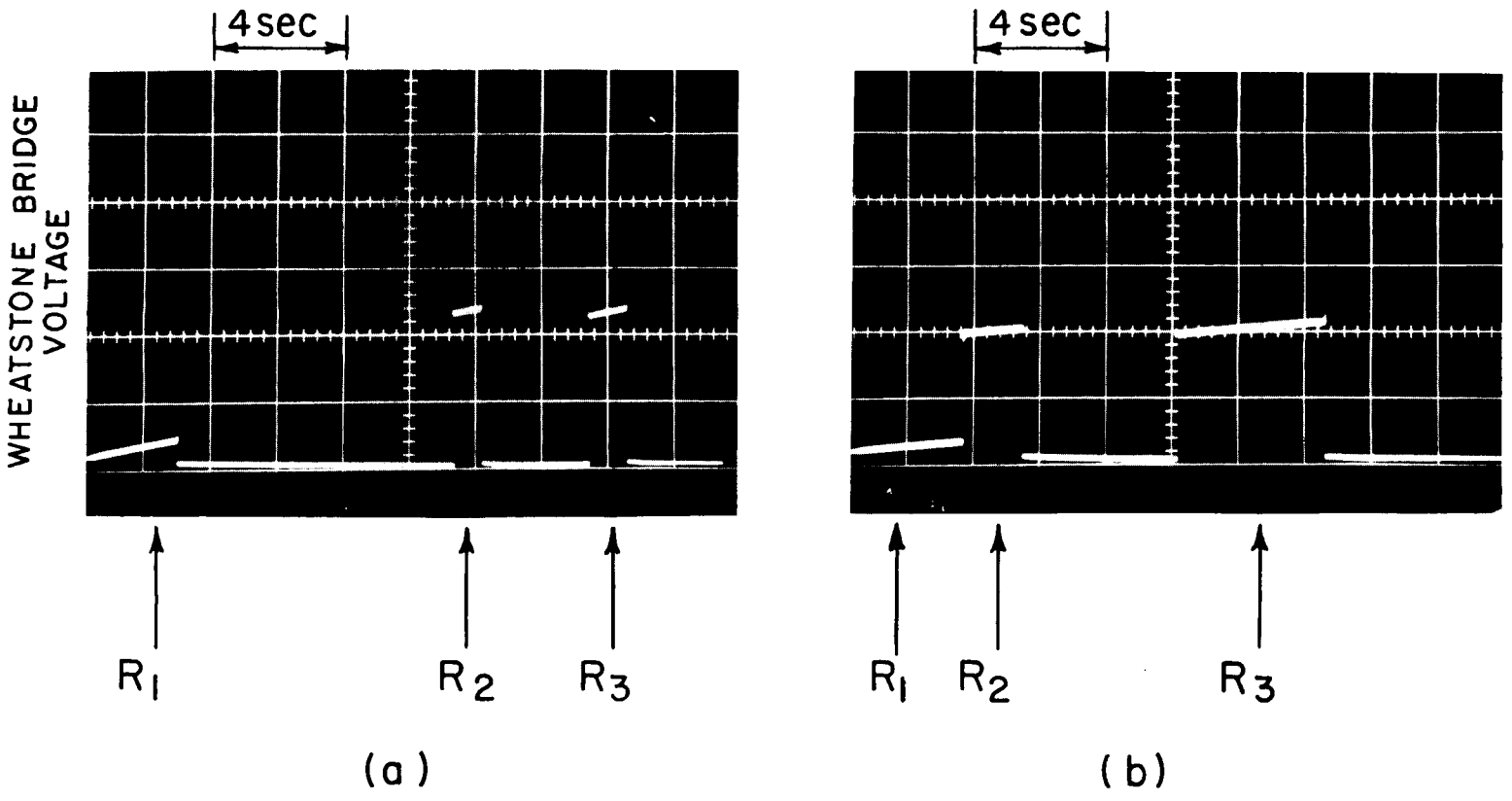

FIG. 49 : FAST-ACTING CALORIMETER OSCILLOGRAMS
(a) CALIBRATION (b) WITH THRUSTOR

Consider that the probe is intercepting a steady-state plasma flow. Let the plasma shutter be nominally shut. Assume that the shutter is opened instantaneously. The fast ions arrive first at the collector. The ion current will increase to its steady-state value as the slower ions arrive. If the time is measured from the opening of the shutter, the ion current is related to the velocity distribution function of the particles in front of the probe by means of Equation (1).

$$I(t) = c \int_{v_o}^{\infty} f(v)\ v\ dv \tag{1}$$

where

c = a constant describing the degree of ionization and the area of the entrance hole,

$f(v)$ = the number distribution of ions with the axial velocity component v,

t = the time after shutter opening,

d = the distance between the shutter and collector,

$v_o = d/t$.

Taking the derivation of Equation 1 with respect to v gives

$$- c\ f(v_o)\ v_o = \frac{dI(t)}{dv_o} = \frac{dI(t)}{dt}\frac{dt}{dv_o} \tag{2}$$

from which results an expression for $f(v_o)$

$$f(v_o) = \frac{d}{c\ v_o^3}\frac{dI(t)}{dt}\Bigg|_{(t = d/v_o)} . \tag{3}$$

Let us next consider the case in which the ions in the plasma are characterized by a Maxwellian velocity distribution superimposed on an average plasma velocity, U. Observed in the laboratory frame the distribution is given by Equation (4). The motion of the plasma is assumed to be in the x-direction.

$$dn \approx e^{-\frac{m}{2kT}[(v_x - U)^2 + v_y^2 + v_z^2]}\ dv_x\ dv_y\ dv_z \tag{4}$$

n = number density of ions with velocity v_x, v_y, v_z

m = particle mass

k = Boltzmann constant

Equation 4 represents all the ions of the plasma in front of the probe. Only part of them, however, can reach the collector because of the probe geometry. The necessary condition for collection is that the velocity vector be contained in the opening angle α of the probe (Equation 5).

$$\sqrt{v_y^2 + v_z^2} \leq v_x \quad tg \frac{\alpha}{2} \tag{5}$$

The number of particles n_x with the axial velocity component v_x which will reach the collector, is obtained by integrating Equation (4) with respect to v_y and v_z, observing the integration limits given in Equation (5). This integration then gives:

$$dn_x \approx \left(e^{-\frac{m}{2kT}(v_x - U)^2} \int_{r_o}^{r_1} e^{-\frac{m}{2kT} r^2} r\, dr\right) dv_x \tag{6}$$

with $r_o = 0$

$$r_1 = v_x \quad tg \frac{\alpha}{2}$$

or

$$dn_x \approx e^{-\frac{m}{2kT}(v_x - U)^2} - e^{-\frac{m}{2kT}\left[(v_x - U)^2 + v_x^2 \, tg^2 \frac{\alpha}{2}\right]} dv_x \tag{7}$$

This expression contains the velocity distribution function f(v) for the axial velocity component v as it will be observed by the probe. The temperature and the plasma velocity are independent constants.

$$f(v) \approx e^{-\frac{m}{2kT}(v - U)^2} - e^{-\frac{m}{2kT}\left[(v - U)^2 + v^2 \, tg^2 \frac{\alpha}{2}\right]} \tag{8}$$

Equation (3) and (8) are the relations which have been used in Section 5.2.

9.0 APPENDIX

OPERATING PRINCIPLES OF THE FERROMAGNETIC CORE VALVE

Consider the following geometry:

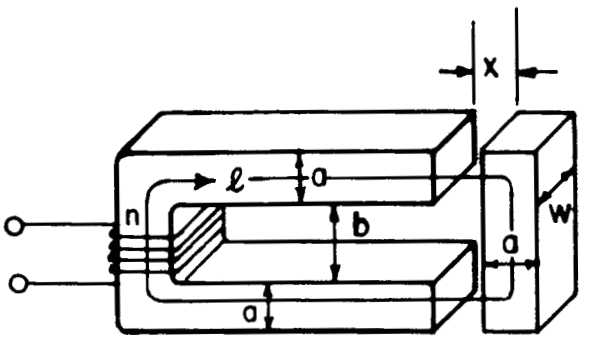

The moving armature at the right is designed to open the valve; we assume that it contains the majority of the moving mass.

The inductance of this circuit as seen at the coil terminals is

$$L = \frac{\mu_o \, awn^2}{\frac{\ell}{\mu} + 2x} ,$$

where μ is the incremental permeability at whatever flux exists in the circuit. For high-μ core materials, even a very small gap x will establish the inequality

$$x \gg \ell/\mu \; ;$$

we will assume this to hold, and so,

$$L = \frac{\mu_o}{2} \frac{awn^2}{x} .$$

The gap alone then sets the inductance, and furthermore, nearly the entire magnetic energy in the system exists in the gap. This is easily verified if one recalls (1) that the energy density is

$$W_m = \frac{B^2}{2\mu} ,$$

and (2) that B is continuous from the core into the gap.

The force which acts to close the gap is, for a given current I

$$F_x = \frac{1}{2} I^2 \frac{\partial L}{\partial x} = \frac{\mu_o aw}{4} \left(\frac{nI}{x}\right)^2$$

neglecting the sign.

(For best economy of design in terms of core weight and acceleration, we assume that both the armature and the rest of the core are run near saturation; they will both be given the same cross-section area aw.)

The mass of the armature is

$$m = \rho\ aw(2a+b)\ , \qquad \rho = \text{mass density}$$

and so its acceleration is

$$\ddot{x} = \frac{F_x}{m} = \frac{\mu_o}{4\rho(2a+b)} \left(\frac{nI}{x}\right)^2 .$$

But now,

$$nI = H_{core}\ \ell + H_{gap}\ 2x$$

$$= \frac{B}{\mu_o} \left[\frac{\ell}{\mu} + 2x\right] .$$

Since we assume that $x \gg \frac{\ell}{\mu}$, this becomes

$$\frac{nI}{x} = \frac{2B}{\mu_o} ,$$

and so,

$$\ddot{x} = \frac{B^2}{\mu_o \rho(2a+b)} .$$

This says that as long as the coil current is large enough to keep the core saturated, the acceleration is determined only by the saturated B, and by the length and mass density of the armature. It must be kept in mind, however, that three assumptions are involved here. They are: (1) that $x \gg \ell/\mu$, (2) that the cross sections of the armature and core are identical and (3) that the armature is significantly heavier than anything which may be attached to it.

Let us substitute some typical numbers into the expression for $\ddot{x}$.

Let

$$B = 1.7 \text{ Tesla}$$

$$\rho = 8 \times 10^3 \text{ kg/m}^3$$

$$2a+b = 1.5 \times 10^{-2} \text{ m} .$$

Then,

$$\ddot{x} = 1.9 \times 10^4 \text{ m/sec}^2$$

A displacement of 1 mm will then occur in a time

$$t = \sqrt{\frac{2x}{\ddot{x}}} = 300 \ \mu\text{sec} ,$$

and a 1/4 mm opening, which is sufficient in some instances, occurs in 150 μsec.

The magnetic field energy which must be established in the gaps is dependent on w while the acceleration is not; if we set w = a and take a = 5 mm as typical, then for, say $x_o = 0.5$ mm,

$$\text{Field Energy} = \frac{B^2}{2\mu_o} \cdot 2a^2 x_o$$

$$= 2.9 \times 10^{-2} \text{ joules} .$$

In contrast, many joules are needed to run any eddy-current valve.

10.0 REFERENCES

1. Lovberg, R. H., Hayworth, B. R., and Gooding, T. J., "The Use of a Coaxial Gun for Plasma Propulsion," Final Report, Contract NAS 5-1139, GD/Astronautics Report No. AE 62-0678, dated May 1962.

2. Gooding, T. J., Hayworth, B. R., and Lovberg, R. H., "Development of a Coaxial Plasma Gun for Space Propulsion," Final Report, Contract NAS 3-2501, GD/Astronautics Report GDA 63-0454, dated May 1963.

3. Gooding, T. J., Hayworth, B. R., Larson, A. V., and Ashby, D. E. T. F., "Development of a Coaxial Plasma Gun for Space Propulsion," Final Report, Contract NAS 3-2594, NASA Report No. CR 54149, GD/Astronautics Report No. GDA-DBE 64-051, dated June 1954.

4. Gooding, T. J., Larson, A. V., Hayworth, B. R., and Ashby, D. E. T. F., "Development of a Coaxial Plasma Gun for Space Propulsion," Final Report, Contract NAS 3-5759, NASA Report No. CR 54245, GD/Convair Report No. GDA-DBE 64-052-4, dated April 1965.

5. Lovberg, R., Phys. Fluids 7, Part 2-Supplement, S57 (1964).

6. Gooding, T. J., Lovberg, R. H., and Hayworth, B., ARS J., Oct. (1962) p. 1599.

7. Gooding, T. J., Hayworth, B., and Lovberg, R. H., AIAA J. 1, 1289 (1963).

8. Fleischmann, H. H., Ashby, D. E. T. F., Larson, A. V., Nuclear Fusion 5, 349 (1965).

9. Ashby, D. E. T. F., Gooding, T. J., Hayworth, B. R., and Larson, A. V., AIAA J. 3, 1140 (1965); also AIAA Reprint 64-704 (1964).

9a. Lovberg, R. H., AIAA J. 4, 1215 (1966).

9b. Larson, A. V., Gooding, T. J., Hayworth, B. R., and Ashby, D. E. T. F., AIAA J. 3, 977 (1965).

10. Ashby, D. E. T. F., AIAA J. 3, 1045 (1965).

11. Ashby, D. E. T. F., Liebing, L., Larson, A. V., and Gooding, T. J., AIAA J. 4, 831 (1966).

12. Hayworth, B. R., Miller, A. R., and White, C. W., AIAA Paper No. 65-337, San Francisco, July 1965.

13. Black, N. A. and Jahn, R. G., AIAA J. 3, 1209 (1965).

14. Michels, C. J., Heighway, J. E., Johansen, A. E., "Analytical and Experimental Performance of Capacitor Powered Coaxial Plasma Guns," AIAA Paper No. 65-340, San Francisco, July 1965.

15. Gorowitz, Gloersen, Karras, Summary Report 214-220, NASA CR-54846, for Contract NASw-1044, March 1966.

16. Rosebrock, T. L., Clingman, D. L., and Gubbins, D. G., "Pulsed Electromagnetic Acceleration of Metal Plasmas," AIAA J. Vol. 2, No. 2, p. 328 Feb. 1964.

17. Germeshausen, K. J., "A New Form of Band Igniter for Mercury-Pool Tubes," Phys. Rev. Vol. 55, Jan. 1939, p. 228.

18. Space Electric Power Systems Study, Vol. 5, NASA Contract No. NAS 5-1234, 1963.

19. "A 20kW Solar Powered Pulsed Plasma System Concept," Gorowitz, B., Gloersen, P., Karras, T., AIAA Paper No. 66-114.

20. "Solar Powered Electric Propulsion Study," Hughes Final Report, JPL Contract No. A51144/Dec. 65/SS050094R.

21 "An 850 lb, 20 kW Solar Array," AIAA Paper No. 65-471.

22. Szego, G. C., Jour. Spacecraft and Rockets 2, Sept.-Oct. (1965).

23 "Power Generating Techniques," General Dynamics/Convair Report No. GDA-ERR-AN-556, Dec. 1964.

24. "Design and Analysis of Power Conditioning for Ion Propulsion Systems," AIAA Paper No. 66-215.

25. Conner, R. F. and Hyman, J., Jr., ARS Report 2180-61, ARS Space Flight Report to the Nation, New York, October 1961.

11.0 ACKNOWLEDGEMENTS

The authors wish to express their appreciation to Professor R. H. Lovberg, University of California, La Jolla, for his continuing support as consultant. Credit is given to Dr. Lovberg, in particular, for contributions toward the thrust balance system and for the concept and development of the ferromagnetic core valve.

E. H. Wrench, Engineering Staff Specialist, has contributed valuably through his work on the mechanical propellant feed system. A. R. Miller is responsible for Section 7.

The skill and careful craftmanship of O. J. Neller and J. P. Tinkham, Test Engineers, give a sound base to the laboratory program. We are thankful to Mrs. J. E. Keaton for her administrative assistance and efficient secretarial services.

12.0 DISTRIBUTION LIST

Addressee	Number of Copies
1. NASA-Lewis Research Center	
21000 Brookpark Road	
Cleveland, Ohio	
Attn: Spacecraft Technology Procurement Section (M.S. 54-2)	
John R. Eski	1
Attn: Technology Utilization Office (M.S. 3-19)	
John Weber	1
Don Vargo	1
Attn: Spacecraft Technology Division (M.S. 54-1)	
C. C. Conger	2
Dr. H. G. Kosmahl	1
P. Ramins	4
Attn: Electro-Magnetic Propulsion Division (M.S. 301-1)	
W. Moeckel	1
E. Callaghan	1
G. Seikel	1
C. J. Michels	1
2. NASA Headquarters	
FOB-10B	
600 Independence Avenue, S. W.	
Washington, D. C. 20546	
Attn: J. Lazar (RNT)	1
J. Mullin	1
3. NASA Scientific and Technical Information Facility	
P. O. Box 33	
College Park, Maryland 20740	
Attn: NASA Represetnative RQT-2448	6
4. NASA-Marshall Space Flight Center	
Huntsville, Alabama 35812	
Attn: Ernest Stuhlinger (M-RP-DIR)	1
5. NASA-Langley Research Center	
Langley Station	
Hampton, Virginia 23365	
Attn: M. Ellis	1
6. NASA-Ames Research Center	
Moffett Field, California 94035	
Attn: Dr. Glen Goodwin	1
7. Jet Propulsion Laboratory	
Pasadena, California	
Attn: J. J. Paulson	1

Addressee	Number of Copies
8. General Electric Company Valley Forge Space Technology Center P. O. Box 8555 Philadelphia 1, Pennsylvania Attn: Dr. P. Gloersen	2
9. Electro-Optical Systems, Inc. 300 North Halstead Street Pasadena, California	1
Attn: Dr. T. M. Teem	1
10. The Marquardt Corporation 16555 Saticoy Street Van Nuys, California 91408 Attn: A. N. Thomas	1
11. Aerospace Corporation P. O. Box 95085 Los Angeles, California 90045 Attn: Dr. H. Mirels	1
12. Westinghouse Astronuclear Laboratories Pittsburgh, Pennsylvania 15224 Attn: H. W. Szymanowski, Manager Electrical Propulsion Laboratory	1
13. AFWL Kirtland AFB, New Mexico Attn: Capt. C. F. Ellis/WLPC	1
14. AVCO-Everett Research Laboratory A Division of AVCO Corporation 2385 Revere Beach Parkway Everett 49, Massachusetts Attn: Dr. A. R. Kantrowitz	1
Dr. R. M. Patrick	1
15. Aeronutronics - Ford Motor Company Newport Beach, California Attn: Dr. S. R. Byron	1
16. Space Sciences, Inc. Natrick, Massachusetts Attn: J. Proud	1
17. Graduate School of Aeronautical Engineering Cornell University Ithaca, New York Attn: Prof. E. L. Resler, Jr.	1

Addressee	Number of Copies
18. Case Institute of Technology 10900 Euclid Avenue Cleveland, Ohio 44106 Attn: Prof. O. K. Mawardi	1
19. Massachusetts Institute of Technology Naval Supersonic Laboratory Cambridge, Massachusetts Attn: T. K. Kerrebrock and E. E. Covert	1
20. Rensselaer Polytechnic Institute Troy, New York Attn: Dr. E. H. Holt	1
21. General Technology Corporation 3510 Torrance, Boulevard Torrance, California Attn: Dr. M. Clauser	1
22. Lockheed Missile Systems Division Palo Alto, California Attn: D. Bershader	1
23. United Aircraft Corporation Research Laboratories East Hartford 8, Connecticut Attn: R. G. Meyerand	1
24. Radio Corporation of America Astro-Electronics Division Princeton, New Jersey Attn: T. T. Rebaul	1
25. Litton Systems, Inc. Beverly Hills, California Attn: A. S. Penfold	1
26. Allison Division, GMC Indianapolis, Indiana Attn: T. L. Rosebrock	1
27. Electro-Optical Systems, Inc. 125 North Vinedo Avenue Pasadena, California Attn: Mr. Gordon Cann	1
28. University of California San Diego, California Attn: Prof. R. H. Lovberg	1

Addressee	Number of Copies
29. Aeronautical Research Associates of Princeton Princeton, New Jersey Attn: R. G. Jahn	1
30. Commander Aeronautical Systems Division Wright-Patterson AFB, Ohio Attn: ASRMPE/R. Rivir	1
31. TRW Space Technology Laboratories Thompson Ramo Wooldridge, Inc. One Space Park Redondo Beach, California Attn: Dr. C. L. Dailey	1
32. TAPCO Division Thompson Ramo Wooldridge, Inc. 7209 Platt Avenue Cleveland, Ohio 44107 Attn: R. T. Craig	1
33. Magnetohydrodynamics, Inc. P. O. Box 1815 Newport Beach, California Attn: Dr. V. Blackman	1
34. NASA Headquarters FOB-10B 600 Independence Avenue, S. W. Washington, D. C. Attn: RRP/Dr. K. H. Thom	1
35. Aerospace Corporation P. O. Box 95085 Los Angeles, California 90045 Attn: Library Technical Documents Group	1
36. Naval Research Laboratory Washington, D. C. 20025 Attn: A. C. Kolb	1
37. Stevens Institute of Technology Hoboken, New Jersey Attention: W. H. Bostick	1
38. AVCO Corporation Research and Advanced Development Division 201 Lowell Street Wilmington, Massachusetts Attn: Dr. R. John	1

Addressee	Number of Copies
39. Giannini Scientific Corporation 3839 South Main Street Santa Ana, California Attn: Adriano Ducati	1
40. Los Alamos Scientific Laboratories Los Alamos, California Attn: Dr. Stratton	
41. Aerospace Corporation Propulsion Department P. O. Box 95085 Los Angeles, California 90045 Attn: Mr. H. Crouch	1

GENERAL DYNAMICS

Convair Division